Université de Lomé

Universität Rostock

DRP-CCDRM

INTERNATIONAL MASTER PROGRAMME IN ENERGY AND GREEN HYDROGEN

SPECIALITY: Bioenergy, Biofuels, and Green Hydrogen Technology

MASTER THESIS

Subject/Topic:

AGRO-FORESTRY AND AGRI-PV TECHNOLOGIES USING BAMBOO, SUNFLOWER AND INDIAN MUSTARD TO REGENERATE NATURE IN POST-MINING AREAS ASSOCIATED WITH ASPEN PLUS SIMULATION OF HYDROGEN PRODUCTION

2023-2025

Presented on September 30, 2025

by:

Ndeye Ngoné SARR

Exam Committee members:

Chair: Oudjaniyobi SIMALOU, Associate Professor, Université de Lomé - Togo
Examiner/judge: Damgou MANI KONGNINE, Associate Professor, Université de Lomé - Togo
Main Supervisor: Kosi Mawuéna NOVIDZRO, Associate Professor, Université de Lomé - Togo
Co-Supervisor: Satyanarayana NARRA, Professor, University of Rostock - Germany

WASCAL West African Science Service Centre on Climate Change and Adapted Land Use

Federal Ministry of Research, Technology and Space

Dedication

This thesis is dedicated to my dear family. To the memory of my beloved father Tamsir SARR, whose absence I feel deeply, may his soul rest in peace. His values, sacrifices, and quiet strength continue to inspire me every day.

To my mother Amy DIOP, thank you for your endless love and unwavering support. To my brothers and sisters, your presence and encouragement have meant more than words can express.

Acknowledgements

First and foremost, I give thanks to Almighty God for His grace, guidance, and strength, not only throughout my academic journey but throughout my entire life. Without His divine support, none of this would have been possible. I also send blessings and peace upon His noble Messenger, Prophet Muhammad (peace be upon him), whose teachings continue to illuminate my path.

My sincerest thanks go to the German Federal Ministry of Research, Technology, and Space (BMFTR) and the West African Science Service Centre on Climate Change and Adapted Land Use (WASCAL) for granting me this scholarship and for all the knowledge and experiences gained throughout my studies.

My heartfelt appreciation goes to the President of the University of Abdou Moumouni, Niamey, for their unwavering support throughout the first and second semesters, as well as for their continued commitment to academic excellence and institutional growth.

I also extend my sincere thanks to the Vice Chancellor of the University of Lomé, Prof. KPODAR, for providing a conducive academic environment during my third semester.

My stay in Germany was beneficial to both my research and personal development. I am deeply thankful to the Vice Chancellor of the University of Rostock for offering such a valuable opportunity.

I wish to acknowledge Prof. Adamou Rabbani, WASCAL Director at the University of Abdou Moumouni, for the quality of the teaching he provided us during our 1st and 2nd semester training years.

My sincerest thanks go to Dr Komi Agboka, WASCAL Director, University of Lomé, for his mentorship and guidance, which have played a vital role in shaping my academic path.

I would also like to express my truthful thanks to Dr Komi Begedou, the Deputy Director of WASCAL, University of Lomé, for his unfailing support and advice, which made this program very successful for us.

I would also like to express my sincere thanks to Dr Damgou Mani Kongnine, the coordinator of the Green Hydrogen Programme, University of Lomé, and Dr Mouhamed Idrissou, the scientific coordinator, for their unfailing support and advice.

My deepest gratitude goes to my major supervisor, Dr Kosi Mawuéna Novidzro, for his involvement and support throughout. I would like to offer him my sincere gratitude for his constant technical support, academic guidance, motivation, encouragement and pertinent feedback throughout my work. His patience and immense experience noticeably contributed to the impact of this work.

My deepest and sincerest gratitude goes to my Co-Supervisors, Prof. Dr Habil Satyanarayana Narra, and MSc Fatou Balleh JOBE, for constantly guiding, supporting, motivating, and encouraging me, and for believing in me from the beginning to the end of this study. I greatly appreciate their hard work, responsiveness, leadership and respect. Their constant encouragement and mentoring enabled me to complete this thesis.

I am also thankful to the esteemed members of the jury for their time, feedback, and expertise during my defence, which greatly contributed to the enhancement of my work.

I extend special thanks to the Director and the research team of the Department of Waste and Agriculture at the University of Rostock for providing a nurturing and collaborative learning environment.

Furthermore, I appreciate all the team members from Niger who collaborated with us during the first and second semesters; your contributions significantly enriched our learning experience.

I would also like to sincerely thank all my Senegalese brothers and sisters who are in the same program with me for their support, camaraderie, and encouragement throughout this journey.

Additionally, I could not end without thanking my cherished friends Léontine Nelly MANGA and Mame Haicha FAYE, whose support, motivation, and companionship have meant so much to me.

Finally, but not least, I would like to offer my sincere thanks to my colleagues, friends, and everyone who had contributed to this work in one way or another.

Abstract

The management of soil contaminated with heavy metals, especially that of abandoned mining sites, represents a major challenge for environmental protection. Among the possible solutions, phytoremediation offers promising prospects for post-mining restoration. However, this option is limited by the need for long-term monitoring and the considerable potential of inedible biomass. This study aimed to combine agroforestry and Agri-PV systems to regenerate degraded land while producing green hydrogen from solar energy and biohydrogen from harvested biomass.

To achieve this, a one-hectare copper mining site in Zambia was divided into two plots: one for agroforestry and the other for Agri-PV. Moreover, three plants, sunflower, Indian mustard and bamboo, were theoretically evaluated for their phytoextraction and phytostabilisation efficiency. Thereby, Aspen Plus was used to simulate the production of green hydrogen by alkaline water electrolysis from surplus electricity from the Agri-PV system, after meeting irrigation needs. In addition, biohydrogen production was modelled with the same software from biomass harvested at the contaminated site, using downflow gasification with enhanced tar and char cracking.

The results revealed that sunflower is the most suitable for phytoextraction, thanks to its high translocation of metals to the aerial parts (TF > 1). On the other hand, mustard and bamboo showed better phytostabilisation capacity, with greater accumulation in the roots. Bamboo stood out for its high efficiency in absorbing and removing heavy metals. After one season, all metals were reduced to acceptable levels, except for copper and cobalt, which would require an additional two and nine years, respectively, to be completely remediated. Energy simulations yielded 7,923.3 kg of green H_2/year and 284.3 kg of bio H_2/year, for a total of 8,207.5 kg of H_2/year for the two systems combined.

The theoretical model designed for the restoration of abandoned mining sites shows particular promise for the ecological rehabilitation of soils contaminated with heavy metals. However, experimental validation remains an essential step in confirming its effectiveness and demonstrating its practical relevance, paving the way for its actual application in the field.

Keywords: Mining, phytoremediation, Agroforestry, Agri-PV, hydrogen

Résumé

La gestion des sols contaminés par les métaux lourds, surtout celle des sites miniers abandonnés, représente un défi majeur pour la protection de l'environnement. Parmi les solutions envisageables, la phytoremédiation offre des perspectives prometteuses pour la restauration post-minière. Cependant, cette option est limitée par un suivi à long terme et un potentiel considérable de production de biomasse non comestible. Cette étude visait à combiner les systèmes d'agroforesterie et d'agri-PV pour la régénérescence des terres dégradées tout en produisant de l'hydrogène vert issu de l'énergie solaire et de biohydrogène grâce à une production optimale de la biomasse.

Pour ce faire, un site minier de cuivre d'un hectare en Zambie a été partagé en deux : une parcelle pour l'Agroforesterie et l'autre pour l'Agri-PV. Les trois plantes telles que le tournesol, la moutarde indienne et le bambou ont été théoriquement évaluées pour leur efficacité en phytoextraction et phytostabilisation. Aspen Plus a été utilisé pour simuler la production d'hydrogène vert par électrolyse alcaline de l'eau à partir de l'électricité excédentaire du système Agri-PV, après avoir satisfait aux besoins en irrigation. En outre, la production de biohydrogène a été modélisée avec le même logiciel à partir de biomasse récoltée sur le site contaminé, par gazéification à courant descendant avec des mécanismes améliorés de craquage du goudron et du charbon.

Les résultats ont révélé que le tournesol est le plus adapté à la phytoextraction, grâce à sa forte translocation des métaux vers les parties aériennes (TF > 1). En revanche, la moutarde et le bambou ont montré une meilleure capacité de phytostabilisation, avec une accumulation plus importante dans les racines. Le bambou s'est distingué par sa grande efficacité d'absorption et d'élimination des métaux lourds. Après une saison, tous les métaux ont été réduits à des niveaux acceptables, sauf le cuivre et le cobalt, qui nécessiteraient respectivement deux et neuf années supplémentaires avant d'être entièrement assainis. Les simulations énergétiques ont donné 7923,3 kg $H_{2\ vert}$/an et 284,3 kg $H_{2\ bio}$/an, soit un total de 8207,5 kg H_2/an pour les deux systèmes combinés.

Le modèle théorique conçu pour la restauration des sites miniers abandonnés se révèle particulièrement prometteur pour la réhabilitation écologique des sols contaminés par les métaux lourds. Toutefois, la validation expérimentale demeure une étape incontournable afin de confirmer son efficacité et d'en démontrer la pertinence pratique, ouvrant ainsi la voie à son application réelle sur le terrain.

Mots-clés : Exploitation minière, phytoremédiation, agroforesterie, agri-PV, hydrogène

Acronyms and abbreviations

Agri-PV: Agrivoltaics

AWE: Alkaline water electrolysis

CRF: Char Reactivity Factor

ER: Equivalent ratio

Eq: Equation

FAO: Food and Agriculture Organisation of the United Nations

HM: Heavy metal

MW: Megawatt

OM: Organic matter

OB: Overburden

PV: Photovoltaics

PSA: Pressure Swing Adsorption

SBR: Steam to biomass ratio

SCW: Super critical water

List of tables

List of figures

Table of Contents

Introduction

Background

Human development in the last century was tied to fossil fuels, due to their abundance and affordability. Using fossil fuels has irrefutably led to significant technological advancement quickly. One of the major downsides of this technological progress was increasing pollution on such a scale that the Earth could not withstand any more without considering the disastrous consequences [1]. Human activities have led to excessive emission of greenhouse gases into the atmosphere. These gases trap heat above the surface of Earth and then radiate it back to the planet, contributing to global warming. Most of these emissions originate from fossil fuel consumption, industrial processes, deforestation, inappropriate land use, and changes in land utilisation.

Mining, an essential industry for extracting valuable minerals and resources, has significant environmental implications. The typical ecological damage caused by mining is multifaceted and can have lasting impacts on ecosystems. One of the most immediate and visible impacts of mining is land degradation, habitat destruction, and pollution effects caused by industrial waste on the environment. This process also leaves altered landscapes, such as open pits and unexpected waste deposits. Soil degradation is another significant concern caused by mining, resulting in erosion, compaction, and contamination from heavy metals and chemicals, all of which harm soil health and inhibit post-mining vegetation regrowth [2]. Compaction, low or high pH, low water-holding capacity, gullies, bulk density, and deficiencies of micro- and macronutrients are the major factors limiting the productivity of mine wastelands [3]. Presently, these negative effects are visible in many forms, the most notable ones being connected to climate change, land degradation, ecosystem functionality, urban development, or renewable energy drivers, etc., depending on the regional needs and capacities. However, rehabilitation has been a viable way of reducing the negative impacts of abandoned mine lands and ensuring productive and efficient utilization of mine wastelands. To restore this area to its natural state, heavy equipment such as cranes, graders, bulldozers, and excavators, as well as hand processing techniques like planting trees and other vegetation, are involved. To address the issue of poor soil quality in the reclamation of mining wasteland, experiments were conducted to improve compost and green manure [4]. Islam et al. [2] discussed restoration methodologies like soil remediation, reforestation, and water purification. Damptey et al. [5] reported the use of the composition of tree species and crop diversification. Damptey et al. [6] recommended the use of fertile soil to fill the mine-out pits, followed by the planting of potted seedlings of some selected tree species. A forestry reclamation approach is supplanting a grassland reclamation approach, where forests are the logical post-mining land use. As a result, restored forests have developed into distinct ecosystems, with natural succession occurring slowly [7]. However, the recovery of damaged land in mining areas is

very slow, and in the process of land remediation and utilization of mining wasteland, improving the reclaimed soil, enhancing the quality of mining soil, and restoring land productivity is one of the key issues in land reclamation of mining wasteland [4]. Achieving suitable vegetation cover may take over a century, emphasizing the need for ongoing intervention and management [7]. One of the land management strategies that could contribute to combating land degradation and simultaneously provide carbon sequestration is the establishment of bioenergy crops (plants grown for energy production), namely perennial grasses and short-rotation woody crops [8]. Biomass improvement technology could improve the fertility level of mine reclamation soil in a short time [4].

Cultivating local biomass and fast-growing energy crops on degraded or abandoned mining land can be a sustainable approach to land restoration and energy security, thanks to its benefits such as carbon sequestration, biodiversity support, and the provision of other ecosystem services. Thus, biofuel plantations have recently garnered considerable attention due to several advantages they present. Bioenergy crops can aid in land restoration by increasing soil fertility, growing in stress conditions, and leading to the production of fuels through their various parts, yielding biofuel as a product, and enhancing soil fertility and health for further sustainable agricultural practices [9]. Biomass production on different categories of marginal or degraded lands is variable. It depends on the characteristics of a particular site, the applied land management practice, and the selection of suitable plant species for this purpose. It is important to consider various factors when deciding which crop to grow for bioenergy purposes. The yield and lifetime of the crop are important, but it is also important to consider whether the crop can meet other aims, such as promoting nature restoration and biodiversity. Planting fibre-producing plants such as bamboo (*Bambusa vulgaris* L.), mustard (*Brassica juncea*), and sunflower (*Helianthus annuus*) on mine land as agroforestry is looking very positive. Not only do these plants rehabilitate the land through selectively absorbing metals from the soil, attracting insects, and fixing nitrogen, but they could also spur the development of bioenergy plants. Moreover, another way to optimise land use and reduce conflicts over land access and risk of erosion and drought, to meet the increasing demand for agricultural products and energy resulting from rapid population growth, is to have a combination of solar panels and crops, so-called Agri-PV [10]. It creates a microclimate that protects crops from extreme weather, such as hail, heavy rain, and intense sunlight. Therefore, the energy from the sun and the resulting biomass from the plants can be explored as a potential feedstock for bioenergy purposes, helping to reduce reliance on fossil fuels.

As the world undergoes an energy transition, energy storage plays a crucial role in supporting this shift. Hydrogen technology, with its many advances, was recognised as the most promising choice. It is an important and promising energy carrier that could play a significant role in the reduction of greenhouse gas emissions [1]. Hydrogen (H_2), a low-carbon fuel, has

emerged as the most promising future energy carrier as it is renewable, has a high energy content (122 kJ/g, which is 2.75 times higher than fossil fuels), and produces only water upon consumption [11]. Hydrogen is the most promising clean energy for future energy carriers, which has the advantages of high energy density and extensive availability. It can be used as an alternative fuel for internal combustion engines and gas turbines, which can operate at high efficiency and ultra-low pollution in these applications [12]. Hydrogen can be generated from both fossil fuels and renewable energy sources. Regarding hydrogen from renewable sources, there are two main types: green hydrogen and biohydrogen.

Green hydrogen refers to hydrogen that is produced from water electrolysis powered by renewable energy sources without releasing greenhouse gases into the atmosphere. Some established technologies, such as alkaline, polymer electrolyte membranes, and solid oxide electrolysers, are being used [13]. Water electrolysis based on electricity derived from solar, geothermal, hydro, and wind that do not emit greenhouse gases, such as carbon dioxide and others, is the most environmentally friendly process. This attractive method for green hydrogen generation is a well-established and mature technology [14]. Additionally, biohydrogen can be produced from biomass using biological and thermochemical methods. Biological methods include dark fermentation, photo-fermentation, bio-photolysis, and microbial electrolysis. In contrast, thermochemical methods involve gasification, pyrolysis, and steam methane reforming [15]. Biomass gasification is a promising technology to displace the use of fossil fuels and to reduce CO_2 emissions. It is the most effective thermochemical conversion route for producing enriched bio-hydrogen from various biowaste feedstocks [16]. It is the earliest and most economical method to produce hydrogen [17].

Problem statement

Despite its promise for post-mining restoration, phytoremediation remains constrained by two critical gaps: the lack of long-term monitoring frameworks and the underutilization of contaminant-rich biomass. A study of [18] notes that current models fail to integrate agronomic practices and native plants, resulting in uncertainty when predicting remediation performance across time and scales. Similarly, to the study of [19], it emphasises that without systematic long-term monitoring, phytoremediation outcomes cannot reliably inform management strategies for co-contaminated soils. In parallel, there is a significant underutilization of the biomass generated during phytoremediation, which represents a lost opportunity to close material and energy cycles. Research on bamboo as a phytoremediator [20], illustrates that while bamboo offers high productivity and valuable biomass, little progress has been made to systematically valorise its contaminant-rich residues, despite clear potential for transformation into biochar or biofuel. More broadly, Edgar et al. [21] underscores that phytoremediation biomass is often treated as waste, although it could serve as feedstock for advanced energy carriers such as hydrogen, as well as high-value products through biorefinery approaches.

To address these gaps, this study proposes the integration of agroforestry and Agri-photovoltaic (Agri-PV) systems with phytoremediation as a dual strategy for ecological regeneration and clean energy production in post-mining landscapes. Specifically, it explores the cultivation of fast-growing plants and solar arrays installation beneath crops, evaluates pathways for biomass conversion into hydrogen, and assesses ecosystem resilience following reclamation. By systematically quantifying biomass availability, linking it to valorisation technologies, and embedding long-term monitoring into management practices, this research aims to transform post-mining remediation into a model of circular bioeconomy that reduces fossil fuel dependency, supports hydrogen production, and enhances sustainable land restoration.

Significance of the study

The integration of agroforestry and Agri-PV technologies presents a promising solution to address these challenges while contributing to sustainable energy production. Agroforestry enhances soil fertility, promotes biodiversity, and improves land resilience [22], while Agri-PV reduces the land use, protects crops from extreme heat, and enables the simultaneous production of food and energy, providing undeniable economic benefits for farmers, with additional potential synergistic effects [23]. By scientifically combining these two approaches, we can optimize land use, restore soil health and fertility while produce biomass that can be converted into biohydrogen, and generate renewable electricity for green hydrogen production.

Objectives

Main Objective

To maximise biomass production by rehabilitating the mining area for high-yield hydrogen production.

Specific Objectives

- To structure a system of agroforestry and Agri-PV for soil improvement
- To estimate the available biomass potential after remediation for bio-hydrogen production
- To evaluate the water required and the energy generated from the solar panel for green hydrogen production
- To optimise the potential green and bio-hydrogen production from mixed technologies using Aspen Plus software.

Research questions

This research work is motivated by the following questions:

- What would be the impact of combining agroforestry and Agri-PV in the post-mining area?

- How can biomass be harvested and evaluated for biohydrogen production?
- What is the potential green and biohydrogen yield of gasification and electrolysis of water?

Research hypotheses

- Biomass derived from land reclamation exhibits high lignocellulosic content suitable for biohydrogen generation by the gasification process.
- Utilizing solar energy from Agri-PV systems for water electrolysis produces green hydrogen with a lower carbon footprint compared to conventional energy sources.
- Replacing fossil fuels with green and biohydrogen produced in post-mining areas significantly reduces greenhouse gas emissions.

Thesis statement

The study is divided into five parts. In this section, which is the Introduction, the context of the study and the problem are presented. The objectives, research questions, and hypotheses are also defined. Chapter I will include a literature review of previous knowledge related to the topic of this work. Chapter II will cover the materials and methods used in this study. Following that, Chapter III will present the results along with interpretation, discussion, and conclusions. Finally, the work concludes with a summary of the key findings and some recommendations.

Chapter 1: Mining extraction: Advantages, Impacts and Soil Remediation

Mining supplies essential materials for technology and economic growth, but it can also lead to significant environmental and social challenges, such as land degradation, pollution, and community disruptions. This literature review explores the dual role of mining, its contributions to technological and societal advancement, alongside its environmental and ecosystem impacts. It highlights sustainable practices, including mine restoration through agroforestry and agrivoltaics systems.

1.1 Mining

Mining involves extracting valuable minerals, ores, or other geological materials from the Earth's crust. These resources, which include metals, coal, gemstones, and industrial minerals, are acquired through various methods [24] such as open-pit, underground, placer, and in-situ mining, where the two main types are underground and surface mining or open-pit. Mining activities play a central role in enabling modern technologies, particularly those driving the global energy transition. Critical minerals such as lithium, cobalt, nickel, and graphite extracted through mining are indispensable for producing lithium-ion batteries, which power electric vehicles, renewable energy storage, and portable electronics [25]. Similarly, copper mining is vital for expanding electricity infrastructure, as copper's high conductivity and durability make it essential in power grids, electric motors, and charging stations [26]. The availability of these materials also drives technological innovation, since stable mineral supplies encourage investment in advanced battery chemistries, energy storage systems, and motor technologies [27].

Beyond direct technological benefits, mining contributes to broader economic and social development. It strengthens supply chains by reducing dependence on a few exporting countries, thereby enhancing resilience and energy security [28]. Moreover, mining supports the scaling of clean technologies, as without access to critical minerals, it would be impossible to expand electric vehicles, wind turbines, and solar storage at the required pace [29]. Mining also creates jobs, infrastructure, and tax revenues that attract downstream industries like refining and battery manufacturing [30]. Finally, resources such as copper and lithium are fundamental to low-carbon technologies, helping societies shift away from fossil fuels toward more sustainable energy systems [31].

Nevertheless, the expansion of mining to satisfy technological needs brings a variety of environmental, ecosystem, and social issues.

1.1.1 Impacts

The most significant impact of mining is the alteration of landforms caused by clearing vegetation, removing topsoil, and disposing of large amounts of waste [32]. It is a significant

source of heavy metal pollution, disrupting soil microbial communities and nutrient cycles [33]. Surface mining or open-pit mining, which creates tailings dams, has the greatest impact on the surrounding areas due to the relatively large volumes of material moved [32, 34]. These mine tailings and waste dumps persist as long-term sources of contamination [35]. In addition, the Open-cast mining generates waste material consisting of rock, soil, and various minerals. This waste material is often referred to as overburden (OB). It is reported that the amount of OB is greater in open-cast mining than in underground mining processes [36]. Moreover, mining disrupts topography, vegetation, and biodiversity, causing soil erosion [37], pollution [38], désertification [39], and land collapses [40], see *Figure 1.1*. It reduces arable land, biodiversity, and ecosystem stability [41, 42], and affects water quality by reducing the pH and increasing contamination with heavy metals, contributing to off-site contamination via aeolian dispersion and water erosion of mine wastes [32]. Furthermore, the waste dumps contribute to landslides and mudslides [43], and prevent the natural succession of plant growth [36]. On a global scale, between 5 and 7 billion tons of tailings are created annually [32]. Islam et al. [36] found that the OB of coal are composed of silicate minerals and clay minerals, had low moisture contents (0.36-3.36%), volatile matters (5.48-14.6%), and high ash content (72.2-92.9%) and are dominantly sandstones, as also correlated by their high SiO_2 (58-71 wt%), total alkalies (1.3-4.4 wt%), and Al_2O_3 (15-22 wt%) content as major oxides.

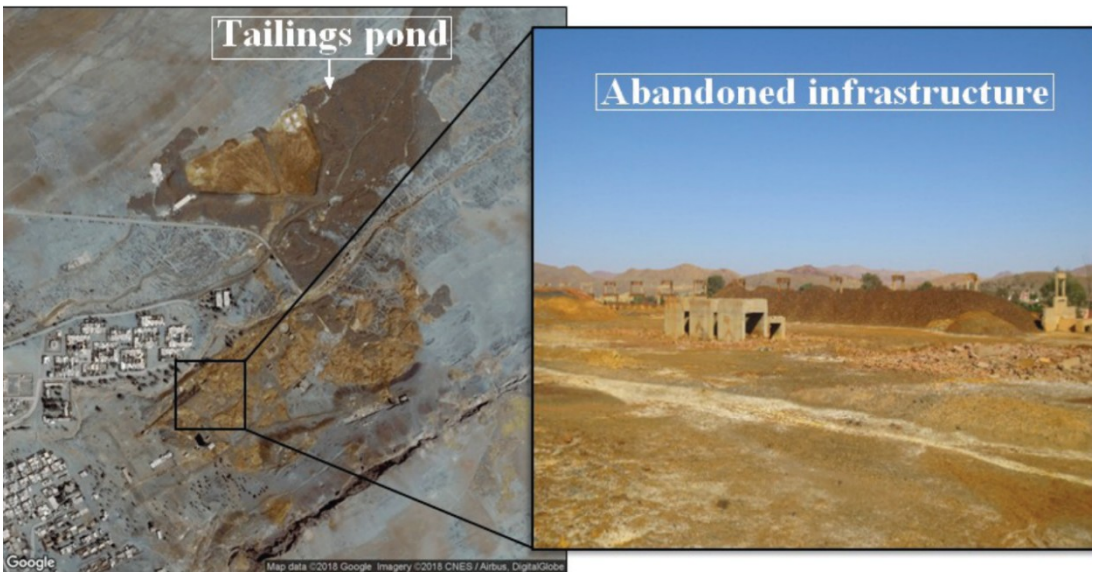

Figure 1.1: Mining Impact on the Landscape. Source [35].

During mining, waste sulphides, chromium, lead, mercury, and other toxic and hazardous substances enter the soil through the leaching effect of long-term rainwater. Soil contaminated with mercury will adversely affect the photosynthesis of plants; With the increase of lead concentration, the enzyme activity gradually decreases, etc. [36]. The major environmental issues associated with abandoned mine sites are acidification and the associated metal toxicities [37]. Under strongly acidifying conditions, the pH of the mine soils can be lowered rapidly, and metal ions, including Pb, Zn, Cu, Cd, Fe, Mn, and Al, will be released at

extremely phytotoxic levels. In general, acidification and heavy metal toxicity act synergistically under natural conditions, which collectively deteriorate the physicochemical properties of mine soils and pose potential hazards to the surrounding natural ecosystems [44]. As a result, the recent 2 decades have witnessed a global surge in research on post-mining landscape restoration, yielding a suite of techniques and combinations [32].

1.1.2 Strategies for Mine Soil Restoration

Due to the great economic and social importance of mining, new mines inevitably disrupt natural ecosystems. For this reason, the development and establishment of methods and techniques able to minimize initial negative effects and, after mining, to restore the original functions and services of the ecosystems, becomes a research priority [45]. Soil reconstruction is key to mine remediation by improving soil stability, moisture content, and nutrients to support revegetation [46]. Restoration technologies include physical (soil replacement, irrigation), chemical (biochar, phosphate, limestone), and biological (mycorrhizal symbiosis, native plants) methods [45, 46, 47].

The physical method for restoring mine surface soil includes topsoil transfer backfill, guest soil filling, isolation, and electrodynamic techniques [48]. Soils on tailings dams are often nutrient-poor, acidic/alkaline, and of very poor quality; hence, adding topsoil can be a solution to improve the soil quality [32]. This approach is costly, and salvaged topsoil that has been stockpiled for long periods can have low nutrient and biological quality. Adegbite; Worlanyo & Jiangfeng [3, 49] report that amending soils with organic residues to improve the quality is an effective method. The use of vegetative compost can increase microbial activity and protect against erosion as the compost decreases the concentration of contamination within the soil and creates a more suitable growing environment for plants. However, not all organic materials are equally good for the manufacture of technosols [32]. Studies of [3] and [32] found that biochar has gained increasing attention recently as a soil amendment. Besides being a carbon source, biochar also contains high proportions of essential plant nutrients: nitrogen, phosphorus, potassium, calcium, magnesium, iron, and zinc that are bioavailable for plant growth but can also increase the pH and enhance the physical properties of soil by raising its porosity and thereby its water holding capacity.

Chemical restoration technology is a method that improves soil structure and quality by adding chemical substances to mitigate heavy metal toxicity, inhibit modified solidification, and soil drenching [48]. Soil pH can be raised by adding fertilizers such as dolomite (limestone) and by applying biological amendments such as organic waste [32]. The solubility and bioavailability of heavy metals can be improved by adding synthetic chelators such as ethylene diamine tetraeacetic acid (EDTA) [32], which can remove 25-75% of Cu, Zn, and Pb [48]. This method is limited by high cost for chemical reagents and machines, the need for

skilled technicians, and the potential to pollute groundwater and adversely affect soil quality in the event of excessive application [32].

The biological method, or phytoremediation, involves the use of plants, especially fast-growing plants, microorganisms such as fungi and bacteria, soil animals such as earthworms (vermiremediation), and other biological systems for clean-up [49]. These plants are characterized by their robust growth capacity, drought tolerance, strong root systems, effective absorption and enrichment capabilities, and the ability to prevent soil erosion and nutrient loss. Moreover, their nitrogen fixation enhances soil fertility and supports animal survival. Additionally, plant root systems also help in remedying heavy metal pollution [48]. This method is cheap, of low-technology demand, low re-contamination potential, and is applicable on a large scale. It also renders agricultural soil productive and aesthetically appealing [49]. Studies of contaminated sites have proven that trees that are either pioneers or legumes show higher survival. However, revegetation could improve the fertility of degraded mined lands, but it requires longer periods to restore the fertility to approximations of the original levels [32]. Consequently, single restoration techniques have limitations; so, integrated methods are needed for effective rehabilitation [50]. Native herbs and shrubs with adaptability, drought resistance, and fast growth should be prioritized for revegetation [51].

1.2 Agroforestry

1.2.1 Definition and principles

Agroforestry integrates trees or woody perennials with crops or livestock to enhance food security, restore degraded lands, and address climate change, blending ancient agricultural practices with modern techniques [52]. It optimizes land use through sustainable resource management, rural development, and environmental preservation (*Figure 1.3).* Key practices, including alley cropping, silvoarable systems, riparian buffer strips, and silvopasture, improve biodiversity, soil fertility, and carbon sequestration [53]. Covering 1.6 billion hectares globally, with 78% in tropical regions, agroforestry benefits communities through social, community, and farm forestry [52, 53]. Regardless of the land use, post-mining land must be replanted with fast-growing pioneer plants suited to the local climate.

1.2.2 Advantages for regeneration:

Agroforestry enhances soil fertility and ecosystem resilience through various mechanisms, such as improving soil nutrient levels via rainfall, nitrogen fixation, and fertilizers, while reducing nutrient losses from erosion, leaching, and volatilization [54, 55]. By increasing soil organic matter, agroforestry boosts moisture retention, nitrogen mineralization, and carbon sequestration, aiding climate change mitigation [56]. Tree roots enhance water absorption, nutrient uptake, and phytoremediation, helping soil restoration [56, 57] by acting as "nutrient pumps" *(Figure 1.2***)** [58], redistributing nutrients from deeper soil layers via litter fall, and enhancing organic fertilizer potential [55, 59]. For instance, agroforestry systems in Denmark

showed improved nitrogen mineralization, and the rotational woodlots of Tanzania successfully produced firewood [60, 61].

(a)

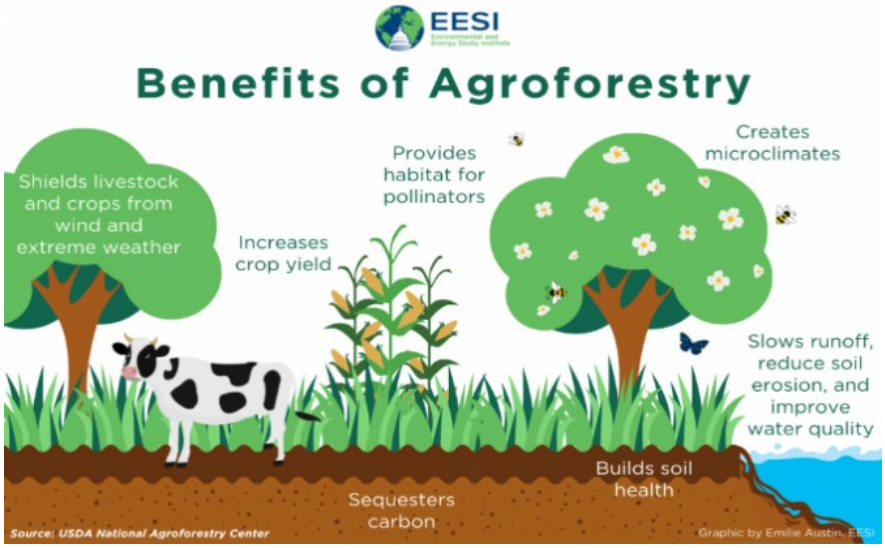

(b)

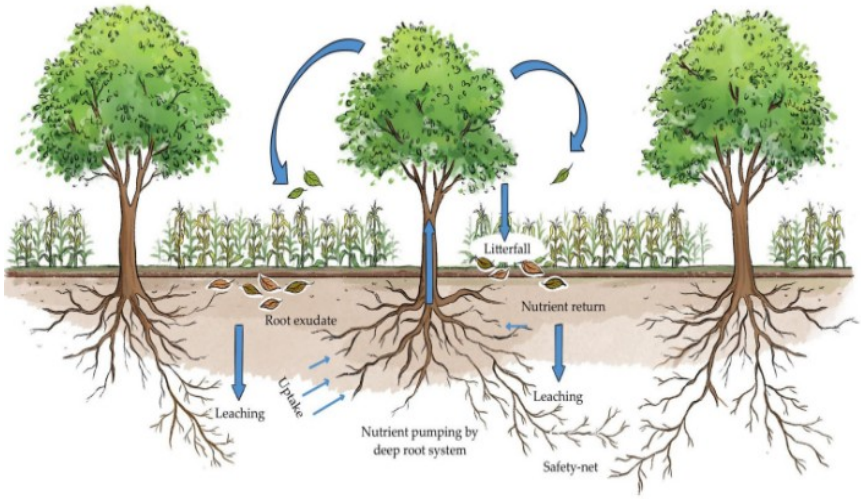

Figure 1.2: Benefits of Agroforestry (source: Environmental and Energy Study Institute) (a), Nutrient pumping and cycling via "safety net" formation (b).

These systems also contribute to carbon sequestration, with notable success in India and East Africa, improving soil stability, reducing erosion, and enhancing microclimate conditions [57, 58, 61]. Trees help maintain soil structure, improve aeration, and help with groundwater recharge [54, 60]. Agroforestry systems also show enhanced phosphorus, potassium, and soil organic carbon levels compared to monocropping [58, 61], with agrosilvopasture systems in Cameroon proving particularly effective [62]. Additionally, agroforestry improves soil acidity control and carbon stocks, and the carbon content of agroforestry plots is almost two times higher than that of monocultures, reducing dependence on chemical fertilisers and promoting sustainable land use.

1.2.3 Species Selection

Trees, due to their larger canopies and dense foliage, are more effective than shrubs at trapping sand dust and improving soil quality. Selecting species with complementary root depths, shade-tolerant plants, and nitrogen-fixing species can enhance soil nitrogen and water efficiency, minimising water loss through deep percolation *(Figure 1.4*).

1.2.3.1 Contribution of Sunflower in the mining restoration

Helianthus annuus (sunflower) has been widely recognised for its strong phytoremediation potential, particularly for heavy metals such as cadmium, lead, uranium, chromium, nickel, copper, and arsenic [63, 64]. Its hyperaccumulative nature allows it to function effectively in multi-metal contaminated sites [65]. Beyond remediation, sunflower is considered environmentally friendly due to their low input requirements, minimal nitrogen fertiliser, no irrigation, and limited pesticide use, while also supporting ecosystem services such as pollinator habitats [66]. Moreover, its high biomass makes it a valuable source for bioenergy production, further enhancing its role in sustainable land management and circular economy initiatives [67].

1.2.3.2 Benefits of Mustard in reforestation

Several studies have identified *Brassica juncea* (Indian mustard) as a highly effective phytoremediator due to its rapid growth, high biomass production, and robust heavy metal tolerance. Its hyperaccumulation ability arises from a synergistic combination of traits, including efficient metal uptake and translocation, vacuolar sequestration, metal chelation and complexation, and the upregulation of genes involved in metal homeostasis and detoxification [68]. These physiological and molecular mechanisms enable mustard to accumulate and detoxify elevated concentrations of heavy metals such as Cu, Cd, Ni, Pb, and Zn. Furthermore, its short life cycle and adaptability make it particularly suitable for repeated cropping cycles on contaminated soils [69].

1.2.3.3 Advantages of bamboo for mining agroforestry

Bamboo is an ideal species for soil erosion control, flood prevention, and eco-restoration due to its extensive root system, rapid growth, and adaptability to poor soils. Its ability to bind gravel and soil makes it highly effective in stabilizing slopes and rehabilitating degraded lands. Bamboo maintains a thick litter layer that supports soil moisture and creates a stable microclimate, crucial for land restoration [70]. Additionally, bamboo sequesters up to 12 metric tons of CO_2 per hectare, releases 35% more oxygen than other trees, and absorbs heavy metals from contaminated soil or water, enhancing its environmental benefits [71]. Its fast growth allows for harvesting every three to five years, enabling quick productivity restoration on degraded sites.

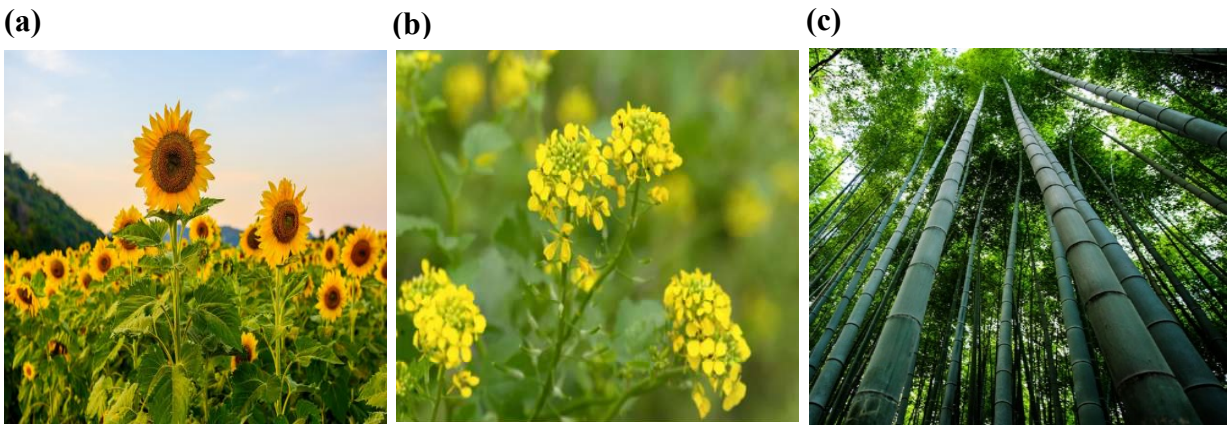

Figure 1.4: plants studied; (a) sunflower, (b) mustard, (c) Moso bamboo

1.3 Agri-PV: Microclimatic and Agricultural Benefits

Climate change and land use conflicts threaten agricultural productivity due to extreme weather and rising temperatures. Agri-PV, integrating photovoltaic (PV) systems with agriculture, enhances land use efficiency while mitigating climate impacts [23].

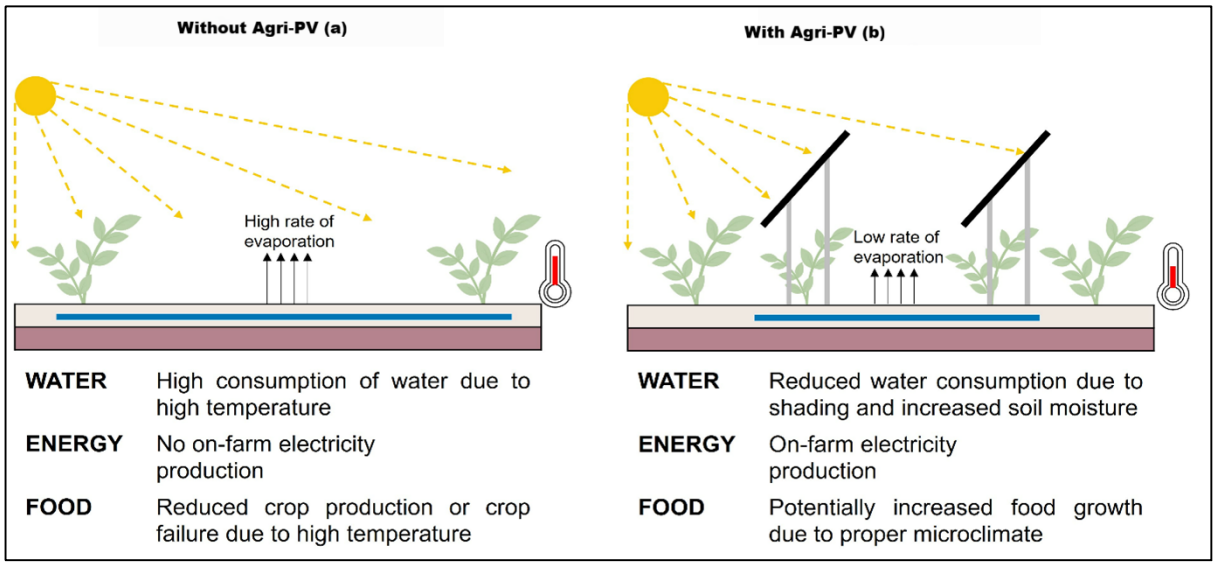

Figure 1.5: Behaviour of the crop with Agri-PV (b), and without Agri-PV (a). Source [72].

Agri-PV alters solar radiation levels based on panel orientation, tilt, and spacing, with crop-available radiation ranging from 60% to 85% of open-field conditions. It enhances quality, such as increased protein content [23], improves soil moisture and reduces irrigation needs by up to 40% [73, 74, 75], as shown in *Figure 1.5*. Beneath PV panels, air temperature can be lowered by up to 4°C, reducing drought and heat stress, which improves crop water productivity [76].

Agri-PV system efficiency depends on panel height, spacing, and tracking mechanisms. Panel spacing influences crop growth, with wider row distances enhancing light penetration [10]. Recommended heights are at least 1.8m for vegetable farming and 2.4m for optimal light

distribution, with systems ranging between 2.1m and 5.2m in various countries to ensure agricultural viability [10, 23, 77, 78].

Solar panel configurations, fixed, single-axis, and dual-axis tracking, enhance energy output. Dual-axis trackers improve efficiency by 29%, while bifacial panels achieve up to 80% efficiency by harnessing sunlight from multiple angles, improving radiation distribution and photosynthetically active radiation (PAR), benefiting crop growth [78, 79].

Agri-PV promotes simultaneous food and energy production, particularly in land-scarce and densely populated regions. It supports biodiversity through pollinator-friendly habitats, aligning with Sustainable Development Goals (SDGs) related to food security, water conservation, and climate mitigation [80, 81, 82].

In Germany, Agri-PV improved land productivity from 56% to 70% in 2017 and up to 90% during the 2018 drought [82]. Applying Agri-PV to less than 1% of global farmland could meet worldwide energy demands [83], and land productivity can increase by 60%–70%, with yield improvements of up to 30% for certain crops and 90% for grasslands [76, 82].

1.4 Hydrogen production

Hydrogen production using renewable technology includes water and biomass as feedstocks [17], and can be categorized into green hydrogen and biohydrogen [84]. Biohydrogen technology is further subcategorized into thermochemical and biological processes. The thermochemical process involves pyrolysis, combustion, gasification, and liquefaction. However, gasification and pyrolysis are the most commonly used and popular techniques in the current scenario [85]. Various biological processes used for hydrogen production include direct and indirect biophotolysis, photo fermentation, dark fermentation, and sequential dark and photo fermentation. The raw material for bio-hydrogen production can be obtained from a wide range of sources, e.g., energy crops, agricultural residues, forestry waste and residues, and industrial and municipal waste, all of which are sustainably supplied by nature [12]. Additionally, the renewable process for green hydrogen production includes water-splitting processes, such as electrolysis, thermolysis, and photoelectrolysis [17].

1.4.1 Gasification

Biomass gasification is one of the effective thermochemical conversion routes for the extraction of gaseous fuel from biomass feedstocks. This endothermic process requires high temperatures (between 700 and 1200 ◦C), a controlled oxidizing agent [86], and appropriate pressure (atmospheric to 33 bar) [17]. The syngas generated from biomass gasification mainly comprises hydrogen (H_2), carbon monoxide (CO), carbon dioxide (CO_2), water vapor (H_2O), methane (CH_4), and nitrogen (N_2) [17]. Some minor products or impurities, such as tar, char, oxides of nitrogen (NOx), and sulfur (SOx), can also be produced along with the main components of syngas during the gasification process [16]. Therefore, the consistency of the

product gas is mainly determined by the gasifying agent (air, steam, and/or O_2), type of biomass, process parameters (e.g., temperature and pressure), and design of the gasifier [87]. The biomass gasification process is divided into four stages: feedstock drying, pyrolysis, gasification (oxidation), and combustion (reduction). In the first stage, the biomass feedstock is dried at low to moderate temperatures (100-150 ◦C), depending on the moisture content of the feedstock. In the second stage, that is, the pyrolysis step, the biomass feedstock is heated at high temperatures (150-700 ◦C) and converted into volatile products and char. Additionally, a highly viscous black liquid designated as tar, which comprises heavy organic and inorganic components, is produced at this stage. Finally, these components undergo partial oxidation and reforming with the aid of a gasifying agent to produce syngas at considerably high temperatures (800-1100 ◦C) [16, 88]. *Figure 1.6* shows the process of biomass gasification during hydrogen production.

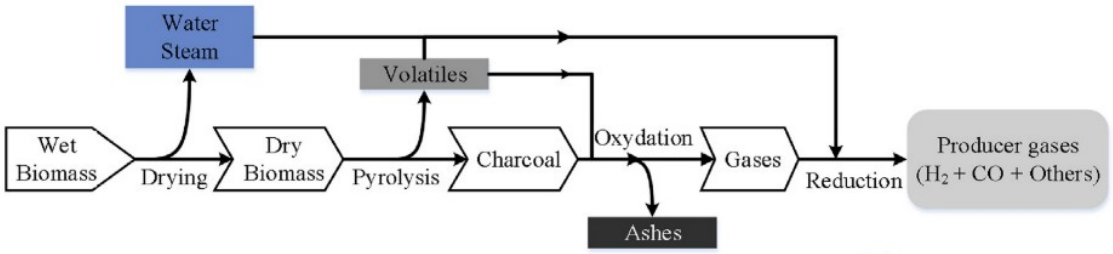

Figure 1.6 Schematic diagram of biomass gasification [85].

1.4.1.1 Parameters

The various parameters that affect the hydrogen yield are: gasifying agent, biomass type, temperature, particle size, type of catalyst, and steam to biomass ratio [17].

1.4.1.1.1 Gasifying agent:

Gasifying agents play a crucial role in determining the product gas composition and yield. Steam gasification utilizes steam to produce biohydrogen with a high concentration and is suitable for biomass with moisture contents of less than 35%. In supercritical water gasification, water at critical conditions (22.4 MPa, 374 ℃) becomes an oxidant and produces biohydrogen with high yield at low reactor temperatures compared to other techniques [89]. Meanwhile, this leads to a high calorific value of gas production and large energy consumption, and hence, it is more challenging [12, 85]. Air gasification produces low concentrations of biohydrogen and biomethane with a low lower heating value, i.e., 4 -7 MJ/Nm^3, mainly because of high nitrogen concentration in the product gas. In contrast, oxygen gasification produces high-concentration product gas with no nitrogen content in the product gas. Furthermore, oxygen gasification produces syngas with high heating values (up to 28 MJ/Nm^3) [89]. The content of hydrogen is 15%-20%, which is then increased up to 30%-40% if the air is replaced by steam [17].

1.4.1.1.2 Type of biomass

Biomass composition, which comprises varying amounts of cellulose, hemicellulose, and lignin, influences the products generated during conversion. Typically, higher cellulose content leads to higher biohydrogen yields, while increased lignin content results in more tar. Ash percentage is one of the most critical properties affecting the gasification process. A higher percentage of ash in biomass enhances coke production but does not affect the net production rate [89].

1.4.1.1.3 Effect of particle size:

The smaller particle size of biomass favors more gas production with a higher percentage of product and a lower percentage of tar [89]. Decreasing particle size from 2 cm^3 to 0.5 cm^3 had a significant effect on the char and gas yields, i.e., an approximately 31% decrease in the char yield and 29% increase in the gas yield. This is due to heat transfer limitations in larger particles, causing higher temperature gradients inside the particles [88].

1.4.1.1.4 Effect of the temperature:

The process temperature during gasification is not consistent because of the variations in the reaction temperature throughout the stages in the reaction zones. Therefore, the composition of combustible H_2 and CO increased with the process temperature, and the composition of CO_2 and CH_4 decreased as the gasification temperature increased because the lignin in the biomass feedstock and char components did not decompose well at lower temperatures. Therefore, a high temperature is required to convert the tar and char components to obtain an increased amount of H_2 gas [16].

1.4.1.1.5 Effect of the biomass feedstock moisture content

The typical water content for the gasification process is 10-15 %, but biomass with a water content of up to 35 % can also be used in the gasification process [89] by using the SCW gasification [17]. The amounts of H_2 and CO_2 produced increased with the biomass moisture content, whereas the amounts of CO and CH_4 produced decreased as the feedstock moisture content increased because the moisture converted to vapor at a high temperature and participated in water–gas shift and methanation reactions to form H_2 , CH_4, and CO [16].

1.4.1.1.6 Effect of the steam-to-biomass ratio (STBR):

The steam-to-biomass ratio plays a key role. The optimal value for biomass gasification is in the range of 0.3-1.0. The amounts of H_2 and CO increased with the STBM ratio, whereas the amount of CO_2 and CH_4 decreased; this is because the hot steam was converted to H_2 , CO, and methane at a high temperature through the water-gas shift and methanation reactions [16]. However, an excess STBR ratio leads to high energy requirements and tar formation [89].

1.4.1.2 Gas Reforming and Purification

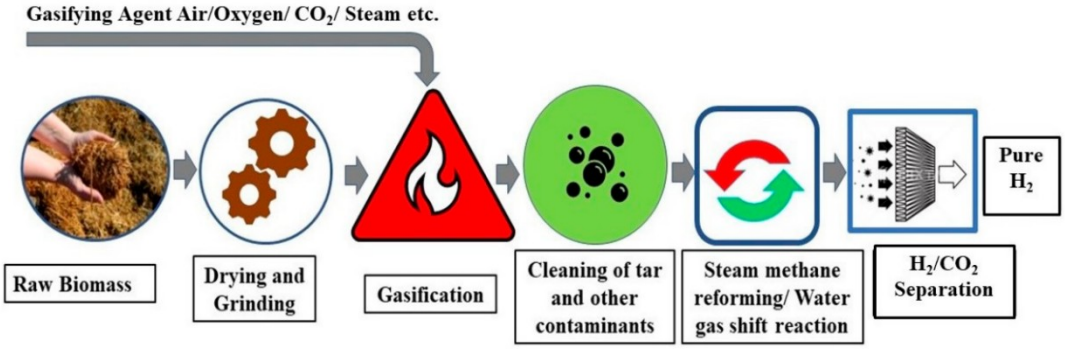

Figure 1.8: Schematic of the gasification process with integrated syngas reforming process [86]

To enhance the hydrogen (H_2) content in syngas, it can undergo additional purification via steam reforming and water gas shift (WGS) reactions. The different biomass-to-hydrogen conversion processes produce a gas mixture that cannot be directly used as renewable energy due to the presence of CO_2 and other trace gases, along with hydrogen. The purification process (*Figure 1.8*) involves purifying, compressing, and storing the impure hydrogen gas at a high density to match the energy values of other gases like gasoline and natural gas [86].

1.4.2 Electrolysis

Water is one of the most abundant and inexhaustible raw materials on Earth. About 71% of the surface of Earth is water-covered, and it is vital for all known forms of life. The various water-splitting processes are electrolysis, thermolysis, and photoelectrolysis [17].

Water electrolysis is one such electrochemical water splitting technique for green hydrogen production with the help of electricity, which is an emission-free technology. The basic reaction of water electrolysis is as follows: Eq**.** (1.1**)** [90].

$$H_2O + \text{Electricity}\ (237.2\ \text{kJ mol}^{-1}) + \text{Heat}\ (48.6\ \text{kJ mol}^{-1}) \longrightarrow H_2 + \frac{1}{2}O_2 \qquad (1.1)$$

Electrolysis is a well-established method of decomposing water molecules into hydrogen and oxygen using electric energy. A typical electrolysis unit or electrolyser consists of cells containing two submerged electrodes with an electrical potential applied, which separate the constituents of water by electrical force. The overall reaction of the electrolysis process includes Eq**.** (1.2**,** 1.3**,** and 1.4**)** [91].

$$\text{Anode: } H_2O \rightarrow \frac{1}{2}O_2 + 2H^+ + 2e^- \qquad (1.2)$$

$$\text{Cathode: } 2H^+ + 2e^- \rightarrow H_2 \qquad (1.3)$$

$$\text{Overall reaction: } H_2O \rightarrow H_2 + \frac{1}{2}O_2 \qquad (1.4)$$

By imposing a direct current into an aqueous solution containing electrolytes (such as sulfuric acid, sodium hydroxide, potassium hydroxide, etc.), hydrogen could be produced by

ionization of strong electrolytes dissolved in water after electrolysis. Hydrogen production from this method has the advantages of environmental benefits and flexible production. The efficiency is 75.85%, and the purity of hydrogen products can reach more than 99%. In addition, the combination of primary energy (wind energy, solar energy, etc.) with this method would give it a wider range of applications and lower pollution. Nevertheless, those energy sources are regional, intermittent, and sometimes unstable, thus leading to difficulty in the commercial application of hydrogen production by electrolysis. In addition, this method needs to consume a huge amount of electricity, (4.5- 5.5 Kw) to produce one cubic meter of hydrogen using this method, which contributes to 80% of the hydrogen energy produced [12].

Electrolysis is one of the most straightforward processes for producing hydrogen from water. It represents the conceptual setup for four electrolyser technologies: alkaline-based electrolysis (AE), proton exchange membrane (PEM), solid oxide electrolysis cells (SOEC), and anion exchange membrane (AEM) [92]. Today, the two main electrolysis technologies that exist commercially are the alkaline electrolysis and proton exchange membrane (PEM) systems. Alkaline electrolysis is a mature and commercial technology, used since the 1920s, for hydrogen production in the fertilizer and chlorine industries [17].

1.4.2.1 Energy requirement:

Water splitting is thermodynamically an uphill reaction and needs an energy input of ΔG of 237.1 kJ/mol; a potential of 1.23 V is required to drive the water electrolysis [90]. A much higher applied voltage, the so-called overpotential, is required to overcome several barriers. These include electrical resistance of the circuit, the activation energies of the electrochemical reactions, as well as hurdles related to gas bubbles. To make the process more affordable, the overpotentials for both half-reactions should be lowered. This can be achieved by using electrocatalysts that can reduce the energy input and activation energy [93].

1.4.2.2 Influence of the factors:

The influence of various combinations of the controlling factors, namely electrolysis time, electric voltage, and catalyst amount, affects the hydrogen generated by the water electrolysis process. The applied voltage has a significant effect on hydrogen production, especially at low and high catalyst loadings and prolonged electrolysis times. Moreover, the electrolysis time also has a significant effect on hydrogen production at the various catalyst loadings and at a high applied voltage. The applied voltage is known as the main driving force for splitting water molecules into oxygen and hydrogen. However, a balance between the applied voltage (energy consumption) and hydrogen production (hydrogen energy output) should be optimized to work under the best economic conditions [94].

1.4.2.3 Alkaline-based electrolysis

1.4.2.3.1 Working principle of alkaline water electrolysis

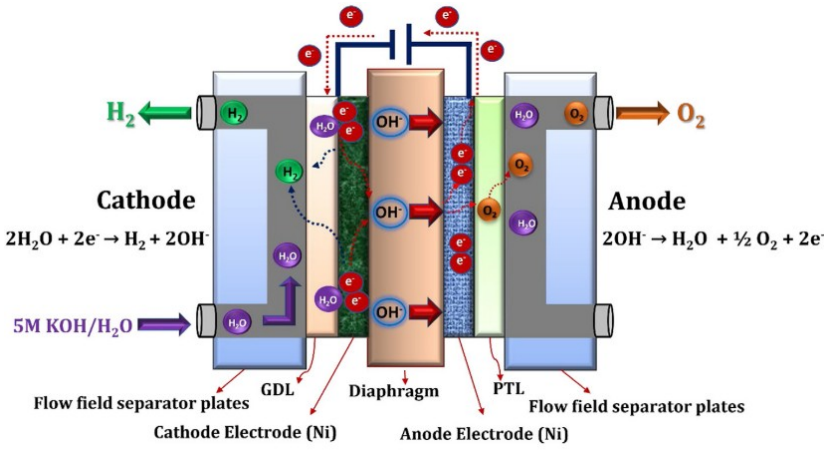

Figure 1.9: Schematic illustration of the alkaline water electrolysis working principle [90].

Alkaline electrolysis is a mature technology for H_2 production up to the MW scale and represents the most widely used electrolytic technology on a commercial level worldwide. The AWE cell consists of two electrodes (anode and cathode) immersed in a highly concentrated aqueous alkaline electrolyte consisting of 20 to 30 mass% KOH [95], and typically operates at 60-80 ºC [14]. In traditional AWE, the most commonly used anode and cathode materials are low-cost steel or nickel alloy-plated steel materials. The two electrodes are arranged in a zero-gap (or quasi-zero-gap) formation using a thin diaphragm, which enables separation of the product gases. The diaphragm is permeable to hydroxide ions and water [95].

Electrochemical water splitting consists of two half-reactions, namely, the hydrogen evolution reaction (HER) and the oxygen evolution reaction (OER). As illustrated in *Figure 1.9*, these reactions take place at the cathode and anode sites, respectively, and they are preferably separated by an ion-exchange membrane. Among other parameters and indicators (like temperature, pressure, type and concentration of electrolyte, electrode type, and cell configuration), both HER and OER are very sensitive to the pH of the electrolyte, and they proceed in different reaction pathways. In acidic media, water is oxidized to molecular oxygen, producing protons at the anode. The generated protons are transferred to the cathode and reduced to molecular hydrogen. Under alkaline conditions, as shown in *Figure 1.9* , hydroxide anions, generated by the water at the cathode site, act as electrochemical charge carriers. The oxidation of hydroxyl anions at the anode site results in O_2 and electrons, which are further used for H_2 generation at the cathode site. The electrochemical reactions take place at the interface between the electrode surface and the electrolyte, and the gas evolution rate is directly proportional to the flowing current through the electric circuit based on Faraday's law of electrolysis [90, 93].

1.4.2.3.2 Cell components of alkaline water electrolysis

The major alkaline water electrolysis cell components are diaphragms/separators, current collectors (gas diffusion layer), separator plates (bipolar plates), and end plates, respectively. In general, Asbestos/Zirfon/nickel-coated perforated stainless-steel diaphragms are used as separators in alkaline water electrolysis. The nickel mesh/foam is used as a gas diffusion layer, and stainless steel/nickel-coated stainless steel separator plates are used as bipolar and end plates, respectively [90].

For instance, the frequent start-stop cycles caused by intermittent renewable energy notably reduce the operational lifespan and hydrogen production efficiency of electrolysers, presenting a substantial barrier to the long-term sustainability and cost-effectiveness of green hydrogen production [96] .

In summary, mining is indispensable for technological and economic development but also produces significant environmental and social impacts. Although reclamation techniques such as physical, chemical, and biological (phytoremediation) methods have been implemented, they remain constrained by important limitations. To address these gaps and evaluate alternative sustainable approaches, the next section outlines the materials and methodology employed in this study.

Chapter 2: Materials and Methods

This study adopts an integrated methodological framework to assess the impacts of mining activities and the potential of sustainable restoration practices. The approach combines empirical data collection with the assessment of restoration strategies, such as agroforestry and agrivoltaics, together with hydrogen production simulation using Aspen Plus.

2.1 Study Framework

The study was conducted at Nchanga Mine in Chingola, a town in Zambia's Copperbelt Province. It is 1340 meters above sea level on the Central African Plateau, 12˚30'S latitude, 27˚50'E longitude. Nchanga Mine, the largest open pit mine in Africa, is operated by Konkola Copper Mines (KCM) Plc. It is a large reservoir of mining waste and present a significant concern of the environment due to potential heavy metals in surrounding water and soil, leading to health issues for nearby communities. The mine workings lie in an arc that is 11 km long around the west and north of the town (*Figure 2.1),* covering nearly 30km^2 as such, the extent of land degradation and soil contamination by heavy metals is of serious concern [97].

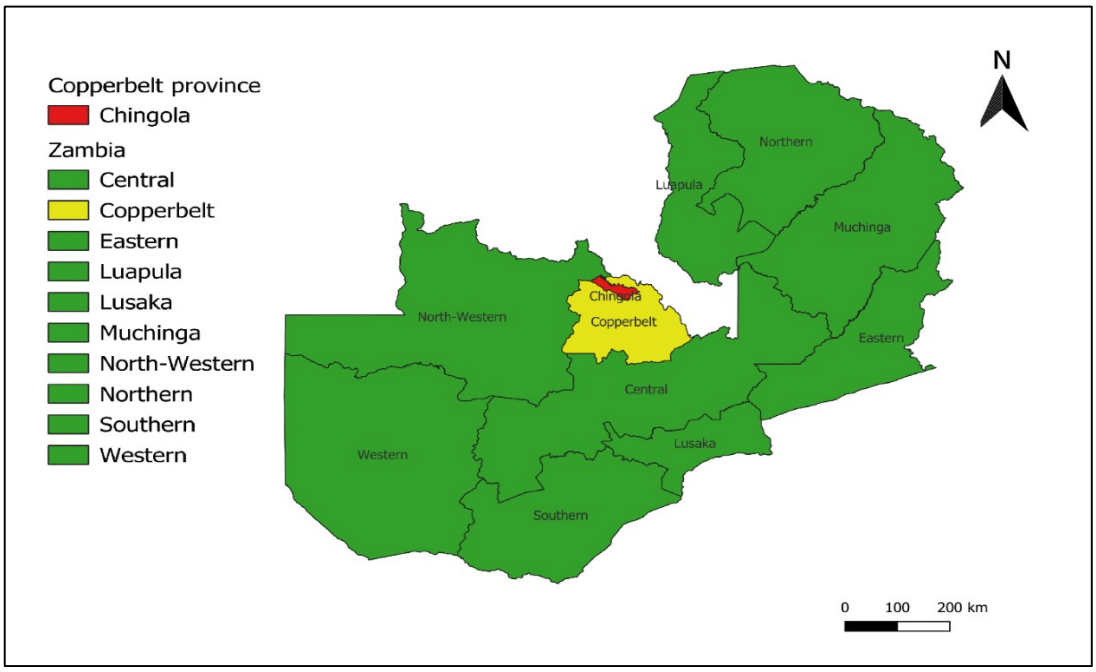

Figure 2.1: Map showing the location of the Nchanga open pit mine in Chingola

The area receives an average of 1,000 mm of rainfall annually. It has three distinct seasons: the rainy season (November-April), the cool dry season (May-August), and the hot dry season (August-November). Due to the elevation of the country, the area typically experiences a subtropical climate with mean monthly temperatures ranging from 15.8 to 15.9 ºC in June and July (the coldest months) to 26.3 ºC in October, which is the hottest month [97].

The underlying geology of the area is the mineralised Katanga system and the undifferentiated basement complex of mainly granites, granitic gneisses, and migmatites. The soils are of two distinctly different types. In the western part of the area, soils are chromic haplic Ferrasols (according to the FAO classification system), which are well-drained, deep to very deep yellowish red to strong brown, friable-clayey soils with a high silt/clay ratio and uniform texture throughout. In the eastern part, the chromic haplic Acrisols are the dominant form, which are well-drained, deep to very deep yellowish red to strong brown friable loamy to clayey soils having a clear clay increase with depth [98].

2.2 Conceptual Framework for Land Restoration

This study presents a theoretical model for rehabilitating a degraded mining site at Nchanga Mine in Chingola, Zambia, through the integration of agroforestry and agrivoltaics systems. The primary objectives are to assess improvements in soil quality, estimate biomass yield from selected plant species, and evaluate the energy output from photovoltaic installations. This integrated model serves as a foundation for further analysis of potential hydrogen production.

A randomly stratified 1-hectare area within the tailings dam was selected as the simulated site and evenly divided into two 0.5-hectare plots, with precise spatial delineation.

- Agroforestry plot: aimed at delivering ecosystem services, soil restoration, and biodiversity enhancement [99].
- Agri-PV plot: Designed to evaluate shading effects, irrigation efficiency, and energy co-generation [78].

Each 0.5-hectare subdivided into two quadrats to facilitate seasonal crop rotation, a practice that helps interrupt pest and pathogen life cycles and supports long-term soil health [100].

Table 2.1: soil physical and chemical properties of the mining site [3].

Composition of Various Waste Content (mg/kg)										
Mine waste	**Clay (%)**	**Organic C (%)**	**Total N**	**Bulk density (g/cm³)**	**P**	**K**	**Mg**	**Ca**	**Na**	**pH**
Tailings dam	5.85	1.32	500.48	1.49	5.05	35.9	853	3309.5	50	7.89
Composition of Heavy Metals (mg/kg)										
Mine waste	Cu	Co	Ba	Zn	V	Pb	Ni	Cr	As	Cd
Tailings dam	12,233	333.5	147.08	66.08	20.4	20.17	19.83	14.23	6.21	0.60

To enable comparative analysis, an adjacent uncontaminated site located outside the tailings dam will serve as the control area. The physical and chemical properties of both the contaminated and control sites are derived from existing literature [3, 101], respectively (*Table 2.1 and Table 2.2*). Key constraints at the contaminated site include moderately high bulk density (1.49 g/cm³) and elevated concentrations of heavy metals, particularly copper (Cu) and cobalt (Co). These data will support the evaluation of existing soil conditions and form the baseline for assessing the performance of phytoremediation treatments over time.

Table 2.2: Physical and chemical properties of the healthy soil [101].

Healthy soil	**Bulk density (g/cm)**	**P (mg/kg)**	**K (mg/kg)**	**Mg (mg/kg)**	**Ca (mg/kg)**	**N (mg/kg)**	**pH**
	1.3	120-150	130-170	100-130	1890-2580	780-1160	6.6-7.1
Cu (mg/kg)	Zn (mg/kg)	Co (mg/kg)	Pb (mg/kg)	Ni (mg/kg)	Cr (mg/kg)	As (mg/kg)	Cd
20	50	8	10	50	100	5-20	3-8

2.2.1 Crop and Tree Selection for Phytoremediation and Soil Improvement

The plant species selected for this model are based on their known ecological functions and documented performance on degraded land (*Table 2.3).*

Table 2.3: Plants chosen for the current study

Species	**Role**	**Key Functions**	**References**
***Phyllostachys edulis* (Moso Bamboo)**	Phytoremediator, biomass producer, soil regenerator	- Absorbs heavy metals (Cu, Zn, Cd, Pb) - High biomass yield for erosion control and carbon sequestration - Enhances nitrogen cycling and improves soil structure	[103], [104], [105]
***Brassica juncea* (Mustard)**	Versatile phytoremediator & soil conditioner	- Uptakes Mo, Cd, Zn, Cr, Ni, Cu, Pb, Au - Rapid growth enables quick land cover - Stimulates microbial activity, improves soil fertility	[69], [102], [106], [107], [108], [109]
***Helianthus annuus* (Sunflower)**	Hyperaccumulator & soil restorer	- Accumulates Cd, Pb, Zn, Ni, Cr, As, Fe - Tolerant of poor soils; ideal for mine tailings - Enhances microbial diversity, reduces erosion	[110], [111], [112]

Phytoremediation using hyperaccumulators is an emerging and cost-effective option for heavy metal pollution cleanup in soils [102]. Certain bamboo species, such as Moso bamboo, have been shown to have a high endurance in metal-contaminated soils, enabling a considerable uptake and accumulation of heavy metals. However, excessive concentrations of heavy metals may cause oxidative stress and damage bamboo plants. Therefore, several management strategies have been developed to improve the phytoremediation ability of bamboo species, including the selection of tolerant bamboo species, intercropping with hyperaccumulators [20], such as mustard (*Brassica juncea*) [102], and sunflower (*Helianthus annuus*) [63].

2.2.2 Spacing assumptions:

Optimal crop spacing in mustard has been shown to significantly enhance growth parameters, growth rates, and both seed and straw yield [113]. Similarly, increasing row spacing in sunflowers has been found to positively influence yield [114]. Sunflower and mustard must be sown both under and outside the panels, with 30 cm and 15 cm spacing between plants and between row distances of 50 cm and 45 cm, respectively. Bamboo plants will be established using 3-month-old seedlings, spaced 5×5 meters apart outside the panels [115].

2.2.3 Soil Remediation Estimation

To assess the extent of soil improvement through phytoremediation, the number of crops and trees established in each treatment plot will be recorded, and their performance will be evaluated using established metrics of phytoremediation efficiency.

2.2.3.1 Number of crops and trees in the study area

2.2.3.1.1 Number of crops under solar panels:

The number of crops under the solar panel is calculated using spacing formulas in Eq**.** (2.1**)**

$$nbr_{cr} = nbr_R \times nbr_{cr/R} \quad (2.1)$$

$$nbr_{sp} = \frac{l_{Au}}{sp} \Rightarrow nbr_{p/R} = nbr_{sp} + 1 \quad (2.2)$$

$$nbr_{sr} = \frac{L_{Au}}{2SR} \Rightarrow nbr_R = nbr_{sR} + 1 \quad (2.3)$$

Where:

nbr_{cr} is the number of crops, nbr_R is the number of rows, $nbr_{cr/R}$ is the number of plants/row, nbr_{sp} is the Number of spacing between plants, l_{Au} is the width of the area under PV, sp is the spacing between plants, nbr_{sR} is the number of spaces between rows, L_{Au} is the Length of the area under PV, and SR is the spacing between rows.

The Length (L_{Au}) and the width (l_{Au}) of the area under PV was calculated based on the number of panels in the row and the number of rows of panels, using these formulas in Eq**.** (2.4**).**

$$l_p \times nbr_{P/R} \times (2L_P + d_r) \times nbr_{Rp} = 5000m^2 \quad (2.4)$$

$$l_{Au} = l_P \times nbr_{P/R} \quad (2.5)$$

$$L_{Au} = ((L_p \times 2) + d_r) \times nbr_{Rp} \quad (2.6)$$

Where:

L_P is the length of the panel, $nbr_{P/R}$ is the number of panels in the row, l_p is the width of the panel, d_r is the spacing between rows of the panel, and nbr_{Rp} is the number of rows of panels.

2.2.3.1.2 Number of crops and trees in the open field:

Here, the distance between the panel array and the trees must be considered. In the northern hemisphere, solar panel systems are oriented to maximize exposure to the southern sky. According to NABCEP (The North American Board of Certified Energy Practitioners), shading may be caused by any obstructions in the vicinity of PV arrays that interfere with the solar window, especially obstructions to the east, south, and west of an array [116]. In this study, the trees will be positioned in the northern part of the photovoltaic field, and obstructions or trees to the north of a solar PV system in the northern hemisphere do not interfere with solar radiation capture, as the sun remains in the southern part of the sky. Therefore, no fixed minimum distance is required. However, though practical spacing for maintenance is better to take 3-5m. In addition, the average diameter breast height (DBH) of Mosso bamboo is 20.5 cm [103]. The available area for the trees (S_{avTr}) and crops (S_{avcr}) are calculated using Eqs. (2.7 and 2.8). The width of the open field (l_{Ao}) is the same as for the solar field (l_{Au}).

$$S_{avTr} = 5000m - (5 \times l_{Au}) \quad (2.7)$$

$$S_{avcr} = 5000m - [(0,205 \times l_{Au}) \times nbr_R] \quad (2.8)$$

Where:

$[(0\ 205 \times l_{Ao}) \times nbr_R]$, is the area occupied by the trees, and nbr_R the number of rows of the trees.

The length of the trees (L_{Tr}) and crops (L_{cr}) areas are in Eq. (2.9, and 2.10).

$$L_{cr} = \frac{S_{cr}}{l_{Ao}} \quad (2.9)$$

$$L_{Tr} = \frac{S_{Tr}}{l_{Ao}} \quad (2.10)$$

The number of crops and trees in the open field was calculated using Eq. (2.1**).**

2.2.3.2 Evaluation of metrics for plant phytoremediation efficiency

Over the past two decades, various efficiency indices have been employed in the field of phytoremediation of heavy metals (HM) to investigate plant–soil interactions, metal transport mechanisms, and accumulation patterns within plants. These indices serve as valuable tools

for researchers to assess the actual progress and effectiveness of remediation occurring in the targeted areas [117]. To estimate the phytoremediation potential, the HM concentration in plants(C_{plant}), shoots (C_{shoot}), and roots (C_{root}), and the plant biomass rate from the literature was used.

The data presented on the concentrations of heavy metals (Cu, Zn, Pb, Ni, As, Cd, Cr, and Co) in the soils and the aerial parts and roots of sunflower, mustard, and bamboo were derived from multiple studies specifically focused on these same plant species (Table 2.4 (Annex)). These studies spanned diverse environmental conditions and geographic locations, each with unique soil characteristics and pollution histories that directly influenced metal availability and plant uptake. One of the main reasons for not seeing the same concentrations of metals in plants across different sites is due to the complex interactions between soil properties and the physiological traits of the plants.

The pH of the soil influences the chemical form and solubility of metals. The bioavailability of heavy metals to plants depends on their mobility in the soil, which is largely affected by soil pH. A low pH favors cationic metal forms that are less likely to be adsorbed by soil particles, thus facilitating metal migration within plant tissues [118]. Soil alkalinity likely decreases the availability of heavy metals, hence reducing their uptake by plants. The pH significantly impacts the uptake of mineral elements; Cu and Ca exhibit higher bioaccumulation in alkaline soils, whereas Sr, Zn, and Mn are preferentially absorbed in acidic soils [119]. Organic matter (OM) is essential for the physical, chemical, and biological properties of soils. It forms complexes with heavy metals, retaining them in exchangeable forms, and generally limits their uptake by plants. OM-rich soils tend to hold more metallic elements, immobilising or releasing heavy metals as necessary. OM can also enhance lead (Pb) uptake by roots. Notably, low-molecular-weight OM fractions bind more cadmium (Cd) and boost its mobility compared to high-molecular-weight fractions [120]. However, in some instances, dissolved organic carbon can enhance metal mobility by creating soluble organometallic complexes. Essential nutrients (N, P, K, etc.) influence root growth and plant metabolism, indirectly affecting metal uptake [121]. Soils rich in clay or silt adsorb metals more effectively than sandy soils, leading to variations in metal availability to plants. A study of [122] stated that clay minerals and organic matter enhance heavy metal adsorption, while lead and cadmium, with their high affinity for soil particles, become strongly adsorbed and less available to plants. Electrical conductivity (EC) indicates soil salinity, which can influence plant physiology and root permeability. Schück & Greger. [123] reported that high salinity can decrease heavy metal uptake through several mechanisms, including the stimulation of root epidermis lignification by NaCl, which creates a physical barrier that limits metal absorption. Furthermore, sites may differ in the types and intensities of metal contamination (e.g., from industrial, agricultural, or natural sources), resulting in varying initial concentrations in the soil. However, due to these factors, even when the same plant

species is cultivated, the actual concentrations of metals in the aerial parts and roots will differ depending on the specific conditions of the site. In other words, metal uptake by plants is not uniform across sites; it is a dynamic process influenced by the local environment.

To ensure reliable comparisons and a more generalized understanding, this study calculated the mean values from reported ranges in 18 different studies. These averages represent typical concentrations for these plants under varied environmental scenarios, providing a robust baseline to compare with the local site data in this research.

By calculating the percentages of metal concentration in the shoots and roots relative to the soil **(**Table 2.5 (Annex)), this work highlights how both plant characteristics and local environmental conditions (including pH, organic matter, TOC, nutrient status, soil texture, and EC) collectively determine the observed accumulation of metals. Consequently, these percentages and the patterns of accumulation they reveal are directly applicable for understanding and evaluating metal uptake in the specific context of the current study.

2.2.3.2.1 Translocation factor

The translocation factor (TF) is the efficiency index of the plant species, which indicates the translocation of metals from the root part to the shoot or aerial part, and can be calculated as follows (Eq. 2.11) [117].

$$TF = \frac{C_{shoot}}{C_{root}} \quad (2.11)$$

where C_{shoot} indicates the metal concentration accumulated in the shoot part and C_{root} the metal concentration accumulated in the root part.

It is evaluated that a translocation factor greater than 1 for any plant shows its potential to phytoextract the metal from the root into the shoot. In contrast, a TF lower than 1 indicates its Phyto-stabilizing property.

2.2.3.2.2 Bioaccumulation factor

Bioaccumulation refers to the active transfer of chemicals or compounds (such as metals) from the environment to the tissues of living organisms via metabolic processes. The ratio of metal content in plants to total metal content in the soil is known as the Bioaccumulation Factor (BAF) [69]. The following *Eq. (2.12)* sourced from [69], and [124] are used to determine the bioaccumulation factor of heavy metals:

$$BAF = \frac{C_{plant}}{C_{soil}} \quad (2.12)$$

Where:

C_{plant} is the total heavy metal concentration in plants and C_{soil} metal concentration in the soil.

2.2.3.2.3 Total metal uptake (Mu_T)

The metal uptake is the product of the dry weight of the plant and the Concentration of the metal. It was calculated using *Eq. (*2.13*)* [125].

$$Mu_T = C_{plant} \times B_{plant} \times N_{plant} \quad (2.13)$$

Mu_T is the Total metal uptake (mg/ha), C_{plant} represents the heavy metal concentration in the plant (mg/kg), B_{plant} is the dry biomass weight produced in one harvest(g), and N_{plant} is the number of plants.

2.2.3.2.4 Remediation factor (RF)

The potential for phytoremediation, or the efficiency with which plants can extract metals from contaminated soils, depends on factors such as plant biomass, metal concentration in both the plant and the soil, and the soil mass within the rooting zone. It is assumed that metal pollution occurs only in the active rooting zone, at the top 20-cm soil layer [126], which gives a total soil mass (S_M). The following Eq. (2.14 and 2.15**)** calculate the phytoextraction rate or the metal extraction ratio of the plant [118, 128, 129, 130].

$$RF = \frac{C_{plant} \times B_{plant}}{C_{soil} \times S_M} \times 100 \quad (2.14)$$

$$RF_T = \frac{C_{plant} \times B_{plant}}{C_{soil} \times S_M} \times N_{plant} \times 100 \quad (2.15)$$

Where:

RF is the remediation factor by one crop (%), C_{plant} represents the heavy metal concentration in the plant (mg/Kg), B_{plant} is the dry biomass weight produced in one harvest(g), C_{soil} is the total metal content in soil(mg/Kg), S_M is the soil mass in the rooting zone), RF_T is the total remediation factor (%), and N_{plant} is the number of plants.

2.2.3.2.5 Removal Efficiency

The removal efficiency (RE) is the efficiency index of the plant to remove metal from a contaminated site. The metal removal efficiency was determined based on the Eq. (*2.16*) proposed by [118], [131].

$$RE = \frac{C_i - C_f}{C_i} \times 100 \quad (2.16)$$

Where:

C_i initial metal concentration and C_f final metal concentration in the soil after plantation.

2.2.3.2.6 Phytoremediation time

The phytoremediation time of heavy metals in soil is calculated using Eq. (*2.17)* from [126].

$$t_{p(year)} = \frac{C_{soil} \times S_M}{C_{plant} \times B_{plant} \times n} \quad (2.17)$$

n is the number of times the plant is cropped yearly.

2.2.4 Implementation of a Solar-Powered Pumping and Water Storage System

2.2.4.1 PV structure

Due to the arrangement of the PV modules, shading underneath the facility is not uniform and varies during the day depending on solar altitude. In studies with Agri-PV systems adapted for crop production, for example, through a reduced module density, crop-available radiation was predicted to reach values ranging between 60 and 85% of that in open-field conditions [23]. The installation heights of the PV modules found in studies were 4.5, 4.0, and 4-5 m [132]. In this study, solar panels with dimensions (1.7m × 1m) are installed above crops at a height of 4m, with row spacing of 2m (to allow crops to get more light), and an inclination of 10.91ºC southward [133] according to the attitude of the site. The total number of modules installed is obtained from *Eq. (2.18)*, refer to *Eq. (2.4)*, and the energy generated by the PV generator was estimated according to [134] in *Eq. (2.19)*.

$$N_{panels} = nbr_{P/R} \times nbr_{Rp} \quad (2.18)$$

N_{panels} is the number of panels, $nbr_{P/R}$ is the number of panels in the row, and nbr_{Rp} is the number of rows of panels.

$$E_{generated} = P_{pk} \times PSH \times PR \quad (2.19)$$

P_{pk} is the peak power of the PV field, obtained as the product of the PV module's power (375W) rating and the number of modules used in the construction of the PV field. PSH is the peak sun hours equal to the equivalent number of hours per day when solar irradiance averages 1.000 W/m2 (the solar radiation of the site is 5.7 kWh/m2-day, with an average peak sunshine of about 6-8 hours per day [135], and PR is the losses estimated as 20%.

2.2.4.2 Borehole and pump

A borehole will be drilled with a tank and a pump installed to ensure irrigation (a drip system setup will be adopted) when rain is low or during the dry season, and water needed for the electrolyser for green hydrogen production. To prevent further soil contamination and reduce the risk of damage to the electrolyser, a minimum distance of 50-100 meters between boreholes for water supply and soakaways for tailing dams is recommended [136].

2.2.4.3 Irrigation method

A drip irrigation system mulched with white plastic film (thickness, 0.01 mm; width, 900 mm) will be used to deliver the irrigation water, accompanied by a water meter installed at the inlet of the submain to measure the irrigated water amount [41]. Drip tubes with emitter intervals depending on the crop will be in the center of each bed to apply the irrigation water.

Precipitation accumulates along the dripline at the lower edge of the panels, potentially leading to increased runoff and erosion [137]. A suggested solution may involve implementing appropriate management practices, such as installing a system that captures water through pipes and directs it to a storage tank, to reduce water redistribution and minimize the risks of runoff and soil erosion.

2.3 Water and energy required

The water requirement for each crop in the system was determined based on literature values and adapted to the site-specific rainfall regime and growth period. For Moso bamboo, an irrigation rate of 1.644 mm/day (equivalent to 0.0805 L/day per pot radius) has to be applied continuously to meet its needs throughout the year, aligning with reported annual irrigation rates of approximately 600 mm/year [138, 139]. When it comes to sunflowers, the water requirements during the growing season are approximately 500-670 mm, which corresponds to an estimated daily need of 7.1 mm/day [140]. Sunflowers are recognized as dryland crops and typically rely on stored soil moisture and rainfall to meet their water demands. Similarly, the seasonal water requirement for mustard ranges from 31-40 cm (310-400 mm) [141]. In this study, these water demands were considered to plan the daily and seasonal irrigation schedules accordingly.

The volume of water needed for each crop based on their surface area occupied within a 1ha in this study is calculated using *Eq. (2.20)*.

$$V = W_d \times A \tag{2.20}$$

Where:

V is the volume of water (m^3/day), W_d is the daily water needs (mm/day) and A is the area occupied by the crop (m^2).

The overall daily irrigation volume (V_t) for the system is obtained by summing the individual daily water (V) requirements of the three crops.

A 1.6m^3/day of water is assumed for the hydrogen production, which is added to the overall daily irrigation volume (V_t), giving the total daily water demand ($\mathrm{DWDtotal}$). The required optimal flow rate can then be computed by dividing the total required volume of water per day needed by the available hours, using the following *Eq. (2.21)* [134].

$$Q = \frac{\mathrm{DWDtotal}}{\mathrm{tsh}} \tag{2.21}$$

Where:

Q is the optimum flow rate (m^3/h), DWDtotal is the total daily water demand (m^3), and tsh is the computed solar hours.

The size of the water pump and the hydraulic system is calculated based on the following *Eq. (2.22)* [142].

$$P=\frac{\rho g H Q}{\eta} \quad (2.22)$$

Where:

P is the pumping power in W; ρ is the density of water in kg/m^3; g is the acceleration due to gravity (9.81 m/s^2); H is the total pumping head and hydraulic losses in m (35); Q is the water flow rate in m^3/s; η is the efficiency of the pump and the motor (0.7).

The hydraulic energy (E_h) required per day (kWh) is calculated based on the *Eq. (2.23)* [142].

$$E_h = \rho g H DWDtotal \quad (2.23)$$

The energy required for the green hydrogen production (E_r) will be the remaining energy obtained from Eq. (*2.24*)

$$E_r=E_{generated}-E_h \quad (2.24)$$

$E_{generated}$ is the energy generated by the PV system and the E_h is the hydraulic energy (energy required for the pump).

2.4 Biomass production:

Since sunflower, mustard, and bamboo plants accumulate heavy metals from contaminated soil, they should not be consumed either as food or fodder. However, their entire harvestable biomass can be considered as potential feedstock for biohydrogen production without needing to account for theoretical and recoverable residue potentials. In this study, the harvestable biomass of each plant (g) was obtained from different literature sources, and the mean value (*Table 2.4*) was used. The total biomass (B_t) produced by those plants was calculated using the average biomass per plant ($B_{av/p}$) from the literature and the number of plants per hectare in *Eq. (2.25)*.

$$B_t=B_{av/p}\times N_{plant} \quad (2.25)$$

2.5 Hydrogen Production via Simulation with Aspen Plus software

2.5.1 Gasification modelling

In the present study, the simulation program ASPEN Plus V14 is used to develop a steady-state model with char and tar modelling for a downdraft biomass gasification. The model describes the pyrolysis and air-steam gasification of three biomass feedstocks, including

sunflower, mustard, and Moso bamboo. Each biomass is simulated separately but using the same model.

Aspen Plus is a Chemical Process Simulator by Aspen Tech, used to model, simulate, and optimise complex processes such as biomass gasification. Biomass, due to its complex and variable structure, is not represented as a pure compound in databases. In Aspen Plus, it is defined as a nonconventional component using proximate and ultimate analyses for material balance calculations. *Figure 2.2* presents the flowsheet developed to simulate the sequence of thermochemical processes that biomass undergoes for hydrogen production. *Table 2.6* presents the list of units employed in the flowsheet with a short description of each block.

Table 2.6: List of units used in the Aspen Plus flowsheet. Block

Block	Type	Description
DRYER	RStoic	Simulates the drying process.
DRYER-FLSH	Flash 2	Separates the solid dry biomass from the hot gas and water vapour.
SEP1	SSOLID	Separates the hot gas from the water extracted from the biomass.
DECOMP	RYield	Converts the nonconventional component into tar, char, and conventional components.
SEP2	Separator	Separates char, tar, and a mixture of conventional components.
PYRO	RGibbs	Simulates the reactions between conventional components through Gibbs free energy minimisation.
MIX 1	Mixer	Mixes char, tar, and gas, producing the pyrolysis products stream.
MIX2	Mixer	Mixes the pyrolysis products with air.
OXI	RPlug	Computes the kinetics of the oxidation zone.
MIX - STEAM	Mixer	Mixes oxidation products with additional steam.
RED	RPlug	Computes the kinetics of the redaction zone.
SSPLIT	SSPLIT	Separate the gases from the solid
PSA	Separator	Separate hydrogen from other components in the syngas for high purity

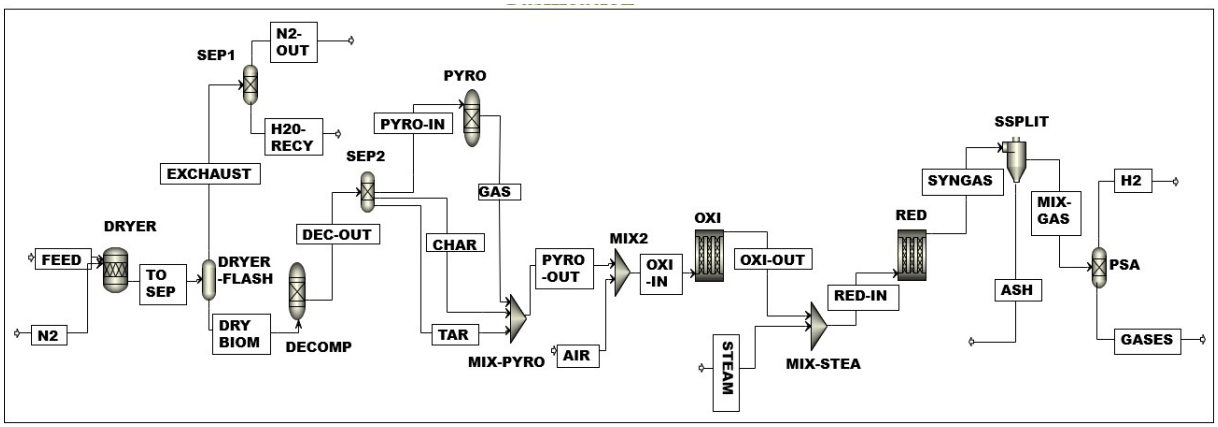

Figure 2.2: Aspen Plus flowsheet constructed for the present work

2.5.1.1 Process simulation

Aspen Plus allows the user to select several sets of property calculation methods. In this work, the IDEAL property method has been chosen as the process involves low pressure and relatively small quantities of condensable components (tars). Since biomass and ash were defined as nonconventional components, the density and enthalpy calculation methods must be specified, which were DCOALIGT and HCOALGEN, respectively. The stream class was defined as MIXCINC for the presence of both conventional and nonconventional solid streams. The compounds included in the simulation are listed in *Table 2.7.* Given the complexity of the process, a set of assumptions was adopted: the method described is steady-state, pyrolysis is considered instantaneous, while oxidation and reduction are governed by chemical kinetics, and each block is modelled as isothermal. Char is modelled as carbon (graphite), and tars are represented by a surrogate mixture of benzene and naphthalene, in a ratio of 3/7.

The first step of this model is the drying process of biomass. In the gasification process, the drying was carried out in the reactor RStoic. The function of RStoic was to eliminate the excess moisture present in the biomass feedstock. It converts an amount of biomass from the feed to produce water. Excel has been utilized for running the drying operation. After that, the water was used to make the reaction happen. At this time, some of the water in the biomass that was put in went away because it had been made hot. A separator block (DRYER FLASH) was then used to carry out the separation, which involved splitting the streamlines after the process of fractionation had been completed. The dry biomass was sent into the next block for the decomposition process, and the evaporated moisture was drained out through the exhaust. Since biomass is defined as a nonconventional component, before modelling a chemical process, it needs to be 'decomposed' into its elemental constituents. This was done in an RYield block (DECOMP). The dry feedstock is transferred by the DRYBIO stream to the RYIELD reactor (pyrolysis zone), where decomposition occurs, and the volatile matter it contains is devolatilised. In this reactor, biomass was converted, and constituent components

were produced. It was assumed that the volatile content of the biomass material could be used for the gasification process. Excel is used to determine the fractional conversion of moisture from the feed and to calculate the yield distribution of biomass into products based on the ultimate analysis.

Table 2.7: Components used in the Aspen Plus model

Component ID	Type component	Name	formula
H_2	Conventional	Hydrogen	H_2
H_2O	Conventional	Water	H_2O
CO	Conventional	Carbon monoxide	CO
CO_2	Conventional	Carbon dioxide	CO_2
N_2	Conventional	Nitrogen	N_2
O_2	Conventional	Oxygen	O_2
CH_4	Conventional	Methane	CH_4
C	Conventional	Carbon graphite	C
S	Conventional	Sulfur	S
Cl	Conventional	Chlorine	Cl
Benzene	Conventional	Benzene	C_6H_6
Naphthal	Conventional	Naphthal	$C_{10}H_8$
H_2S	Conventional	Hydrogen-sulfide	H_2S
SO_2	Conventional	Sulfur-dioxide	SO_2
SO_3	Conventional	Sulfur-trioxide	SO_3
BIOMASS	Non-conventional		
Ash	Non-conventional		
Char	Non-conventional		

To account for the formation of specified yields of tar and char, the empirical formula *Eq. (2.26)* reported by [143] was used. The condensable and non-condensable components were then separated into three sub-streams: CHAR, TAR, and a mixture of elemental species (C, H_2, O_2, N_2, S...) and ash. The latter stream was input into an RGibbs reactor unit to calculate the equilibrium composition of the expected pyrolysis gas mixture, based on the minimization of the Gibbs free energy of the system. The product streams from the pyrolysis stage, GAS, TAR, and CHAR, were mixed and then mixed with air before entering the oxidation reactor (OXI). In this work, oxidation is assumed to be governed by chemical kinetics. An RPlug reactor was chosen for this section of the model, and the reaction scheme and kinetic parameters are those proposed by Gerun et al [144] and include oxidation of the tar species, benzene, and naphthalene, presented in *Table 2.8*.

Table 2.8: Reaction and reference values for kinetic constants in the oxidation reactor.

Reaction	**Ks**	**Ea (J/ kmol)**	**a**	**b**
$\mathbf{CO + \frac{1}{2} O_2 \rightarrow CO_2}$	$1.3\times10^{11}\times$ [H_2O] ^0.5	1.256×10^{8}	1	0.5
$\mathbf{CH_4 + 1.5\ O_2 \rightarrow CO + 2\ H_2O}$	4.4×10^{11}	1.2552×10^{8}	0.5	1.25
$\mathbf{C_6H_6 + 4.5\ O_2 \rightarrow 6\ CO + 3\ H_2O}$	2.4×10^{11}	1.2552×10^{8}	-0.1	1.85
$\mathbf{C_{10}H_8 + 7\ O_2 \rightarrow 10\ CO + 4\ H_2O}$	$9.2\times10^{6}\times T$	8×10^{7}	0.5	1
$\mathbf{CO + H_2O \rightleftharpoons CO_2 + H_2}$	1389	1.256×10^{7}	1	1
$\mathbf{CH_4 + H_2O \rightarrow CO + 3\ H_2}$	1.65×10^{11}	3.29×10^{8}	1.7	-0.8

The reactor was modelled as isothermal. The size of the reactor was determined using the ratio of air/volume from the work of Catalanotti et al [145]. Oxidation products exit the OXI block and can be mixed with steam for steam-enhanced gasification before entering the reduction zone, modelled with a second RPlug reactor (named RED). The hot flue gas and the ash produced during the gasification process were then separated by passing the out stream of the reactor via a cyclone separator. Subsequently, the heated gas has been directed to the PSA separator, where the hydrogen (H_2) is meticulously extracted from the residual gas.

The heterogeneous reactions in the reduction zone and their kinetic parameters were referred to Catalanotti et al. [145] in *Table 2.9.*

Table 2.9: Reaction and Kinetic parameters used in the reduction reactor

Reaction	Frequency factor (s-1)	CRF	k (s-1)	E (kJ/kmol)
C+CO2 → 2 CO	36.16	14.8	535	77,390
C+H2O → CO + H2	15,170	14.8	224,705	121,620
C+2H2 → CH4	0.004	14.8	0.062	19,210

$$f(T) = a_0 + a_1.\frac{T_{pyr}}{T_{ref}} + a_2.(\frac{T_{pyr}}{T_{ref}})^2 \quad (2.26)$$

where:

a_0 , a_1 , and a_2 are polynomial coefficients, listed in *Table 2.10*, T_{ref} is the reference temperature, an empirical parameter set at 500 °C by [146] and T_{pyr} is the pyrolysis temperature in 0°C, which can be controlled and adjusted in order to obtain different species compositions in the pyrolysis zone.

Table 2.10: Polynomial coefficients [143].

Coefficients	Char wt %	Tar wt %	Gas wt %	CO vol %	CO_2 vol %	H_2 vol %	CH_4 vol %
a_0	-15.03	-196.07	311.10	240.53	-206.86	234.97	-168.64
a_1	50.58	300.86	-351.45	-225.12	267.66	-257.01	214.47
a_2	-18.09	103.34	121.43	67.50	-77.50	72.50	-62.51

2.5.2 Alkaline water electrolysis modelling

Aspen Plus was used to develop the model of an alkaline water electrolysis system, which includes an alkaline electrolysis cell stack and the balance of plant, referred to [147]. *Figure 2.3* shows the simulation diagram of the AWE that was studied. The core of the system is the cell stack (STACK). Hydrogen is released from the cathode, and hydroxide anions pass through the porous diaphragm, forming water and oxygen at the anode surface. The process of water decomposition into hydrogen and oxygen is catalysed by an electrochemical reaction (see *Eq. (2.29)* [148]. This reaction is made possible by supplying the cells with electricity and heat. The following assumptions were made.

- All processes operate at steady state;
- All the gases in the system behave like ideal gases;
- 10% of the total heat produced by the stack is lost due to convection and radiation;

- Liquid deionised H_2O is fed to the system at 25 °C;
- The hydrogen and oxygen output are at 25 °C;
- The AWE stack is operated at balanced anode and cathode pressure.

$$\text{Cathode}: 2H_2O + 2e^- \rightarrow H_2 + 2OH^- \quad (2.27)$$

$$\text{Anode}: 2OH^- \rightarrow H_2O + \frac{1}{2}O_2 + 2e^- \quad (2.28)$$

$$\text{Overall}: H_2O \rightarrow H_2 + \frac{1}{2}O_2 \quad (2.29)$$

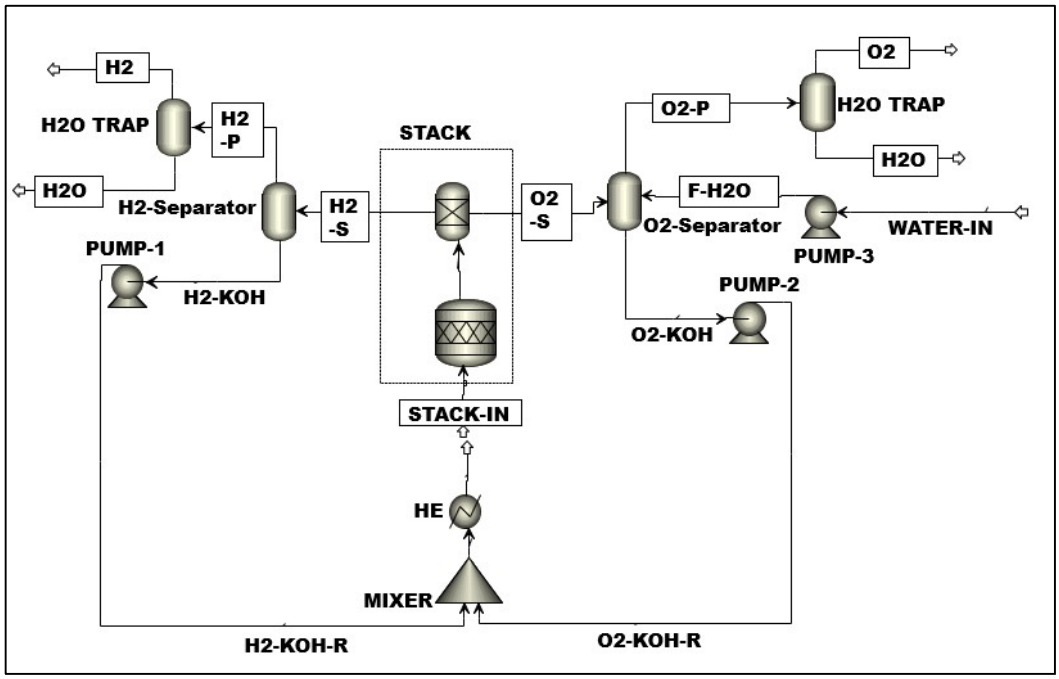

Figure 2.3: AWE flowsheet.

The hydrogen ($H_2 - S$) and oxygen (O_2 - S) produced in the cell stack are led with the electrolyte (KOH, 35% wt) to the liquid-gas separation vessels ($H_2 - SEPARATOR$ and $O_2\ SEPARATOR$ respectively). The electrolyte is separated from the gas in these vessels and returned to the stack by recirculation pumps (PUMP-1 for the cathode and PUMP-2 for the anode). Both KOH recycles (H_2-KOH-R and O_2-KOH-R) were mixed and passed through a heat exchanger (HE) to cool down the electrolyte before entering the stack (STACK-IN).

The purpose of the heat exchangers is to remove waste heat and maintain cell temperature. The hydrogen and oxygen pass through water traps. These are called H_2 and O_2. The purpose of the traps is to eliminate as much condensate water as possible. Finally, there is the feeding of deionised water (WATER-IN) from a water tank into the oxygen separator (O_2-SEPARATOR) by (PUMP-3) to provide water to the electrolysis process (F-H_2O). The gases produced by the stack, hydrogen and oxygen, leave the stack immersed in a KOH electrolyte, which the process later separates and recirculates back to the stack.

2.5.2.1 Electrochemical model

The electrochemical model can predict how an alkaline water electrolysis stack behaves under different conditions, like temperature (T) and pressure (P) [147]. The suggested math works out the polarization curve, Faradaic efficiency, and gas purity as a function of the current. This is based on the laws of physics related to electrolysis and statistics [149, 150]. The polarization curve analyses the different overpotentials that occur during water electrolysis to determine the cell potential (V_{cell}) according to the current density. For the reaction to happen, a minimum voltage is required, which is called the reversible voltage (V_{rev}). This is 1.23 V at standard conditions (1 bar and 25 °C) [145, 149, 150]. However, the cell voltage (V_{cell}) is always higher than the theoretical value due to the appearance of a series of overpotentials caused by kinetic and resistive effects [145, 147]. The real cell voltage is therefore defined as the sum of the reversible voltage (V_{rev}) and the overpotentials (η), as shown in *Eq. (2.30)* [91, 145].

$$V_{cell} = V_{rev} + \sum \eta_0 \tag{2.30}$$

The term $\sum \eta_0$ is the sum of activation, ohmic, and concentration overpotentials.

The polarization curve can be determined using a semi-empirical model that includes additional parameters and new empirical relationships for modelling temperature (T), pressure (P), and current density (i) in Eq. (*2.31*) [147, 151].

$$V_{cell} = V_{rev} + [(r_1 + d_1) + (r_2 \times T) + (d_2 \times p)]i + s \times \log\left[\left(t_1 + \frac{t_2}{T} + \frac{t_3}{T^2}\right)i + 1\right] \tag{2.31}$$

T, P, and i are the operating temperature, pressure, and current density of the electrolyser, respectively. Following the model proposed by Sánchez, the parameters t and r are depicted as a function of the temperature, with an additional parameter d incorporated to quantify the influence of pressure. The present study used the above semi-empirical model to describe the electrochemical characteristics of an alkaline electrolyser.

Faraday's efficiency can be modelled in a similar way to the polarization curve. To do this, an empirical expression for a given temperature is used, with four parameters for this purpose, as in the *Eq. (2.32)* [144, 148].

$$\eta_F = \left(\frac{i^2}{f_{11} + f_{12} + T + i^2}\right) \times (f_{21} + f_{22} + T) \tag{2.32}$$

At last, a model for the diffusion of hydrogen to oxygen (HTO) has been proposed in *Eq. (2.33),* based on [147].

$$HTO = \left[C_1 + (C_2 \times T) + (C_3 \times T^2) + (C_4 + (C_5 \times T) + (C_6 \times T^2)) \times \exp\left(\frac{C_7 + (C_8 \times T) + (C_9 \times T^2)}{i}\right)\right] + \left[E_1 + (E_2 \times p) + (E_3 \times p^2) + (E_4 + (E_5 \times p) + (E_6 \times p^2)) \times \exp\left(\frac{E_7 + (E_8 \times p) + (E_9 \times p^2)}{i}\right)\right] \tag{2.33}$$

Where:

T and P are the operating temperature and pressure of the electrolyser, C and E represent the influence of temperature and pressure, respectively.

All coefficients and parameters used for the model in this study have been sourced from [147] shown in *Table 2.11*.

Table 2.11 coefficients used in the electrochemical model of an alkaline water electrolysis cell

Model	Coefficients	Value	Unit	Model	Coefficient	value	Unit
Polarization curve	r1	4.45153×10^{-5}	W m^2	**Gas purity**	C_4	-0.08483	–
	r2	6.88874×10^{-9}	W m^2 $°C^{-1}$		C_5	0.00179	$°C^{-1}$
	d1	-3.12996×10^{-6}	W m^2		C_6	-1.1339×10^{-5}	$°C^{-2}$
	d2	4.47137×10^{-7}	W m^2 bar^{-1}		C_7	1481.45	A m^{-2}
	s	0.33824	V		C_8	-23.60345	A m^{-2} $°C^{-1}$
	t1	-0.01539	m^2 A^{-1}		C_9	-0.25774	A m^{-2} $°C^{-2}$
	t2	2.00181	m^2 °C A^{-1}		E_1	3.71417	–
	t3	15.24178	m^2 $°C^2$ A^{-1}		E_2	-0.93063	bar^{-1}
Faraday efficiency	f11	478645.74	A^2 m^{-4}		E_3	0.05817	bar^{-2}
	f12	-2953.15	A^2 m^{-4} $°C^{-1}$		E_4	-3.72068	–
	f21	1.0396			E_5	0.93219	bar^{-1}
	f22	-0.00104	$°C^{-1}$		E_6	-0.05826	bar^{-2}
Gas purity	C_1	0.09901	–		E_7	-18.38215	A m^{-2}
	C_2	-0.00207	$°C^{-1}$		E_8	5.87316	A m^{-2} bar^{-1}
	C_3	1.31064×10^{-5}	$°C^{-2}$		E_9	-0.46425	A m^{-2} bar^{-2}

The operating parameters in the AWE model are shown in *Table 2.12.*

Table 2.12: Operating parameters for the AWE

Parameter	**Value**	**Unit**
Stack operating temperature, $\mathbf{T_{Stack}}$	80	°C
Stack operating pressure, $\mathbf{P_{Stack}}$	5	bar
Electrolyte concentration	35	wt% KOH
Active electrode area, $\mathbf{A_{ccell}}$	0.4	m^2
Cell number, **N**	298	cells
Input power stack, $\mathbf{W_{Stack}}$	549.82	kW

2.5.2.2 Mass balances

According to Faraday's law, the hydrogen production rate in an electrolyser cell is directly proportional to the electron transfer rate at the electrodes, which is equal to the electrical current in the external circuit. The total hydrogen production rate for an electrolyser, consisting of multiple cells connected in series, is given as follows Eq. *(2.34)* [149], [152].

$$\dot{n}_{H_2.prod} = \eta_F \times \frac{I}{z \times F} \times N \tag{2.34}$$

Where:

N is the number of cells, z is the number of electrons (two for water electrolysis), η_F is the Faraday efficiency, I is the supplied current, and F is the Faraday constant.

Stoichiometric calculations (see Eq. *2.29*) were used to determine the rates of water consumption and oxygen production, expressed in *Eq. (2.35).* The mass balance is very important, and it considers the amount of hydrogen that is diffused across the diaphragms. However, the diffusion of oxygen to hydrogen (OTH) has been regarded as negligible, given that the rate is approximately 0.1-0.5% [147].

$$\dot{n}_{H_2.prod} = \dot{n}_{H_2O} = 2\dot{n}_{O_2} \tag{2.35}$$

2.5.2.3 System efficiency

To evaluate the overall performance of the system, it is necessary to calculate the energy efficiency. Energy efficiency is defined as the ratio of the energy contained in the useful products of a process to the energy contained in all input streams. Accordingly, the energy

efficiency for hydrogen production from an electrolysis system is formulated as follows, *Eq. (2.36)* [147].

$$\eta_{sys} = \frac{\dot{n}_{H_2} \times LHV_{H_2}}{W_{net}} \times 100 \quad (2.36)$$

Where:

LHV_{H_2} is the hydrogen lower heating value, $\dot{n}_{H_2}$ is the outlet flow rate of hydrogen in the electrolysis plant; W_{net} is the electric power input to the AWE system, which is calculated as follows Eq. (2.37) for the entire alkaline electrolysis system displayed in Figure 2.3.

$$W_{net} = W_{stack} + W_{PUMP-1} + W_{PUMP-2} + W_{PUMP-3} + W_{HE} \quad (2.37)$$

where W_{PUMP-1}, W_{PUMP-2},W_{PUMP-3},W_{HE} denote the power input to the pumps of the system and the heat exchanger consumption, respectively. W_{stack} is the electric power input for the stack operation and can be determined according to Eq. (2.38), where N is the number of cells of the stack.

$$W_{stack} = V_{cell} \times N \times i \times A_{cell} \quad (2.38)$$

Where:

A_{cell} is the activated area of the cell.

In conclusion, With the methodology established and all necessary procedures completed, the following section presents and discusses the key findings obtained from the experimental and analytical approaches outlined above.

Chapter 3: Results and Discussion

This section presents the main findings derived from the theoretical model of the conceptual framework and simulation methods described previously. The results are analysed and discussed in relation to the objectives of the study, existing literature, and theoretical expectations to draw meaningful interpretations and insights.

3.1 Results

3.1.1 Conceptual Framework for Land Restoration

3.1.1.1 Plant distribution

Table 3.1 summarizes the distribution of sunflowers, mustard, and bamboo under photovoltaic (PV) panels and in open fields. Sunflower had a total density of 33,082 plants/ha covering 4,896.37 m². Moreover, Mustard had the highest density at 72,836 plants/ha, spanning 4,896.37 m². By contrast, Bamboo, only present in open fields, had a density of 204 plants occupying 204.92 m². Overall, the total planted area across treatments was 9,997.67 m².

Table 3.1: Distribution of plants in the study area

Plants	Number of plants under PV	Number of plants in the open fields	Total plants/ha	Area (m^2)
Sunflower	16958	16124	33082	4896.37
Mustard	37252	35584	72836	4896.37
Bamboo	0	204	204	204.92
Total area				9997.67

3.1.1.2 Plant metal concentration

The accumulation of heavy metals in plant roots and aerial parts is summarized in *Figure 3.1*. For sunflower, copper (Cu) showed the highest accumulation, with roots reaching 2026.94 mg/kg and aerial parts 309.01 mg/kg. Zinc (Zn) also accumulated notably in roots (32.28 mg/kg) and aerial parts (40.88 mg/kg). Other metals, including lead (Pb), nickel (Ni), arsenic (As), cadmium (Cd), chromium (Cr), and cobalt (Co), exhibited lower concentrations.

In mustard, copper was also the most accumulated metal, with root concentrations of 9934.19 mg/kg and aerial parts 5405.66 mg/kg. Zinc (1663.77 mg/kg) and lead (654.45 mg/kg) also showed significant accumulation.

Bamboo demonstrated exceptional metal accumulation capacity, especially for copper (roots: 58790.45 mg/kg, aerial parts: 17287.53 mg/kg), with similarly high values for zinc and lead, highlighting bamboo's potential for heavy metal remediation.

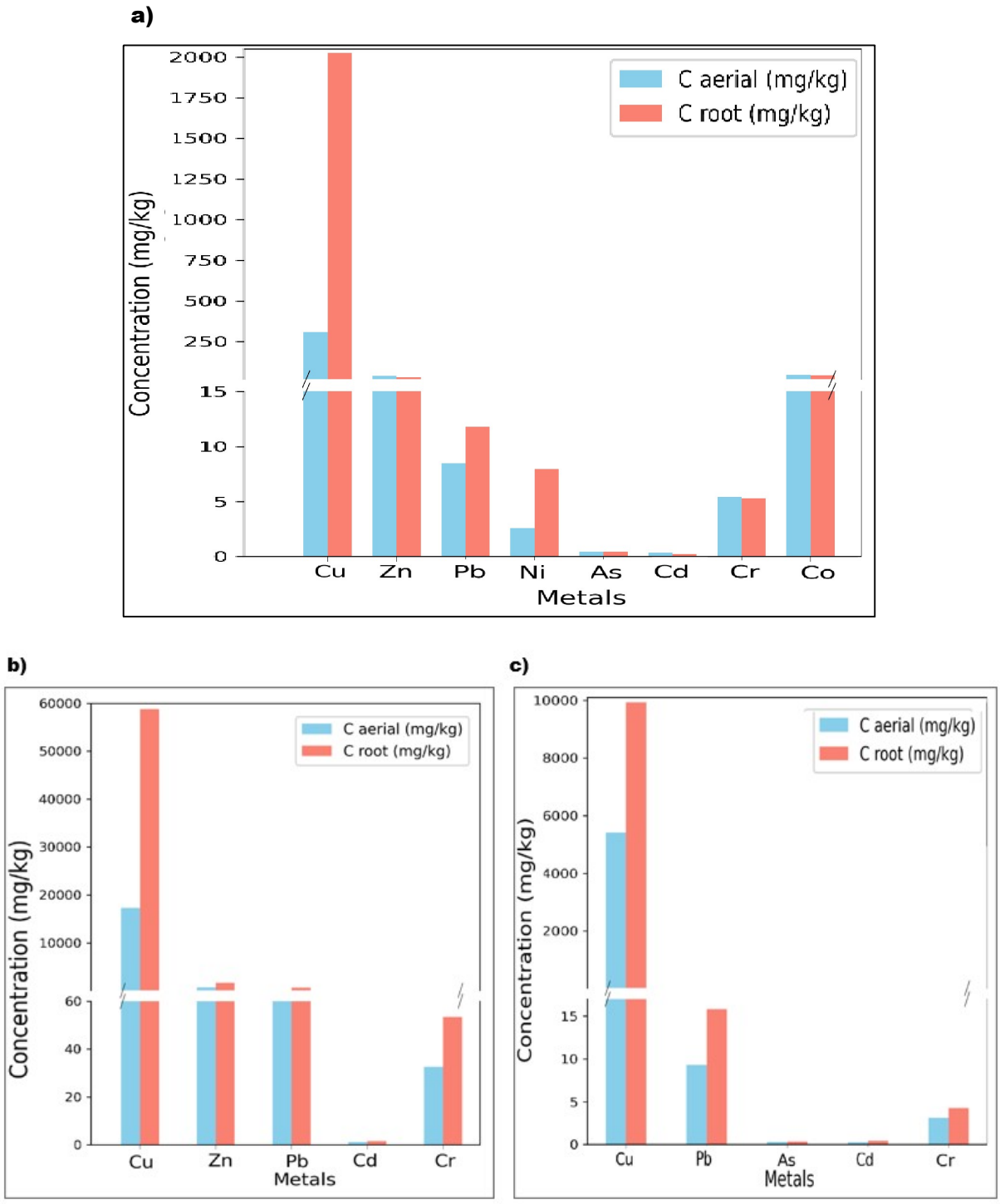

Figure 3.1: Concentrations of heavy metals in the roots and aerial parts of sunflower (a), mustard (b), and bamboo (c) plants

3.1.1.3 Translocation factor

The translocation factor (TF), which reflects the ability of plants to transport metals from roots to aerial parts, varied across species and metals (*Figure 3.2*). In sunflower, cadmium had the highest TF (1.6), followed by zinc (1.27), cobalt (1.08), arsenic (1.02), and chromium (1.02). These values above 1 indicate efficient translocation to shoots. In contrast, copper (0.15), lead (0.72), and nickel (0.32) had TFs below 1, indicating retention in the roots.

Mustard exhibited moderate TF values for arsenic (0.91) and chromium (0.73), while lead, cadmium, and copper had TFs consistently below 1, suggesting less efficient translocation.

For bamboo, TF values were generally lower, with the highest observed for cadmium (0.73) and chromium (0.61), while copper and lead had even lower TFs. Overall, bamboo retained most metals in its roots, limiting translocation to above-ground parts.

The comparative TF analysis highlights that sunflower is the most effective at transporting certain metals (Cd, Zn, Cr, Co, As) to aerial parts (TF > 1), making it suitable for phytoextraction. In contrast, mustard and bamboo showed lower TFs, making them more suited for phytostabilisation.

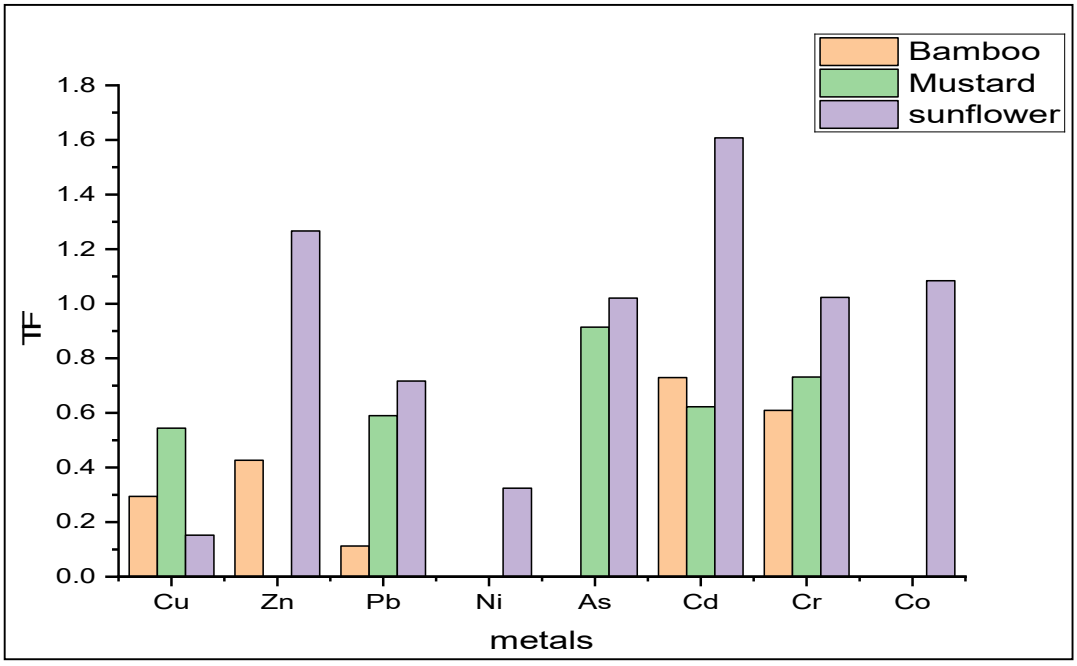

Figure 3.2: Comparative Translocation Factor (TF) of Heavy Metals in Sunflower, Mustard, and Bamboo for Evaluating Phytoremediation Potential

3.1.1.4 Bioaccumulation factor

In sunflower, BAF values exceeded 1 for zinc (1.11) and lead (1.00), indicating effective uptake, while other metals (e.g., Cu at 0.19, As at 0.14) had BAFs below 1. Mustard exhibited BAF values above 1 for copper (1.25), lead (1.24), and cadmium (1.14), while arsenic (0.09) and chromium (0.51) had BAFs below 1. Bamboo displayed exceptionally high BAFs for zinc

(35.91), lead (36.09), copper (6.21), chromium (6.04), and cadmium (4.59), underscoring the remarkable capacity of bamboo to absorb heavy metals from contaminated soils.

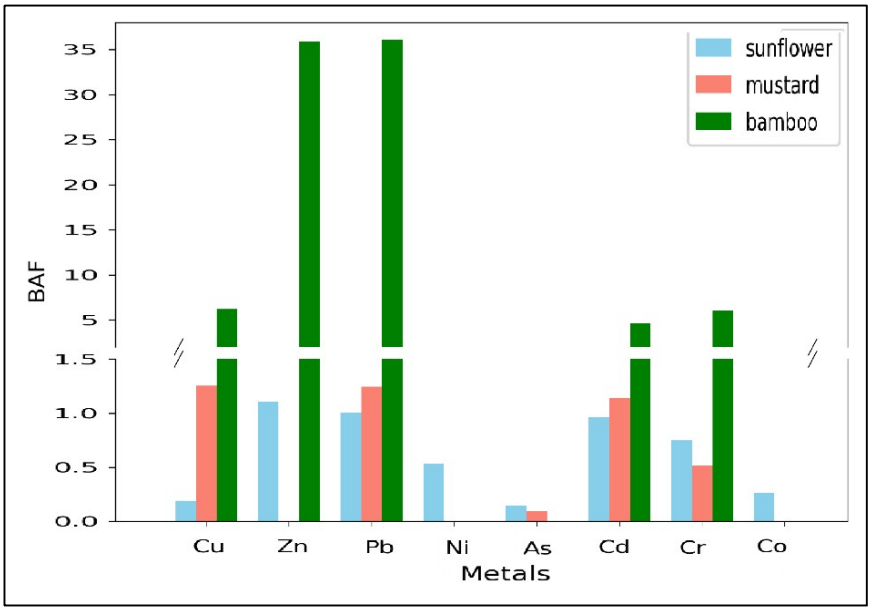

Figure 3.3: BAF of Heavy Metals in Sunflower, Mustard, and Bamboo for Evaluating Phytoremediation Potential

3.1.1.5 Total metal uptake (Mu_T)

The remediation factor (RF%) and total metal uptake (Mu_T) varied significantly among the plants (*Table 3.2*). The variation of the RF is shown in *Figure 3.4*.

Table 3.2: Total metal uptake of the plants

	Sunflower	**Mustard**	**Bamboo**
metals	Mu_T(mg)	Mu_T(mg)	Mu_T(mg)
Cu	1380958.615	1220085.24	4950850.514
Cd	341.0206772	54.48294379	179.166202
Cr	6302.757125	581.6372915	5590.924321
Pb	11972.77579	1999.805741	47382.26141
As	532.066851	47.68838378	
Zn	43252.2295		154433.0585
Ni	6215.538307		
Co	52534.4478		

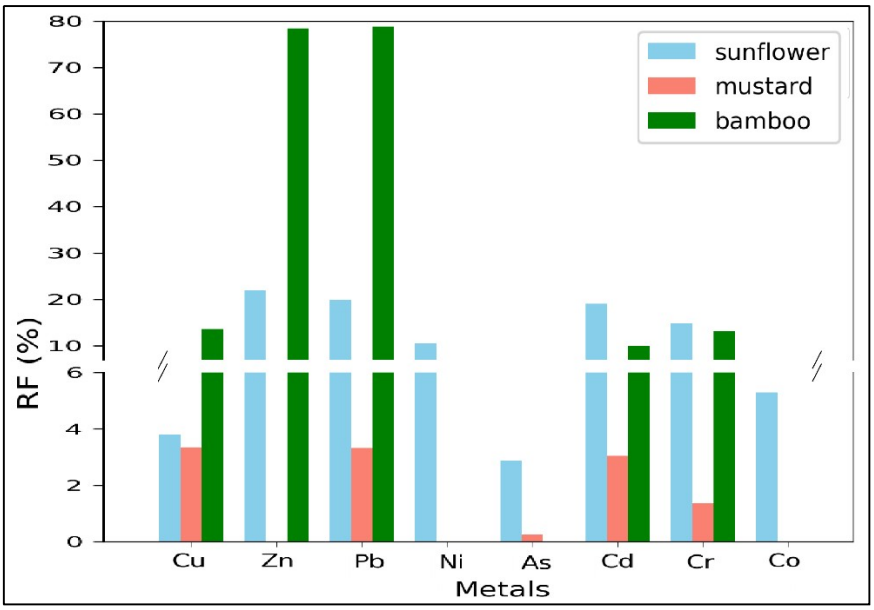

Figure 3.4: Remediation factor of the different plants studied

In sunflowers, the highest RFs were recorded for zinc (21.96%), cadmium (19.07%), and lead (19.92%). Copper and arsenic had lower RFs (3.78% and 2.88%, respectively). The total uptake for copper (1,380,958.615 mg) and zinc (43,252.23 mg) was notably high. For mustard, the RF for zinc was also highest (21.96%), with moderate RFs for cadmium (3.05%), lead (3.33%), and copper (3.35%). Arsenic had a very low RF (0.26%). The total uptake of copper (1,220,085.24 mg) was significant. Bamboo demonstrated the highest overall RF values, with lead (78.83%) and zinc (78.42%) showing exceptional removal, followed by copper (13.58%) and chromium (13.18%). Total uptake was greatest for copper (4,950,850.51 mg) and zinc (154,433.06 mg).

3.1.1.6 Removal efficiency (RE)

The removal efficiency (RE%) over one growing season showed substantial decreases in soil metal concentrations (*Table 3.3*):

- Copper decreased from 12,233.33 mg/kg to 9,699.14 mg/kg (20.72% RE).
- Nickel and chromium had final concentrations of 17.74 mg/kg and 10.04 mg/kg, with REs of 10.52% and 29.42%, respectively.
- Cadmium showed a moderate RE of 32.14%.
- Arsenic (3.13%) and cobalt (5.29%) had minimal removal.
- Notably, zinc and lead had negative final concentrations (-0.26 mg/kg and -0.42 mg/kg, respectively), indicating that these metals were completely remediated before the end of the season (RE > 100%).

Table 3.3: Initial and final metal contamination levels in soil, along with removal efficiency

Metals	C soil	Cf	RE (%) for one season
Cu	12233.33	9699.137	20.71548
Zn	66.08	-0.25734	100.3894
Pb	20.17	-0.41887	102.0767
Ni	19.83	17.74425	10.51816
As	6.21	6.015451	3.13283
Cd	0.6	0.407158	32.14037
Cr	14.23	10.04365	29.41917
Co	333.5	315.871	5.28606

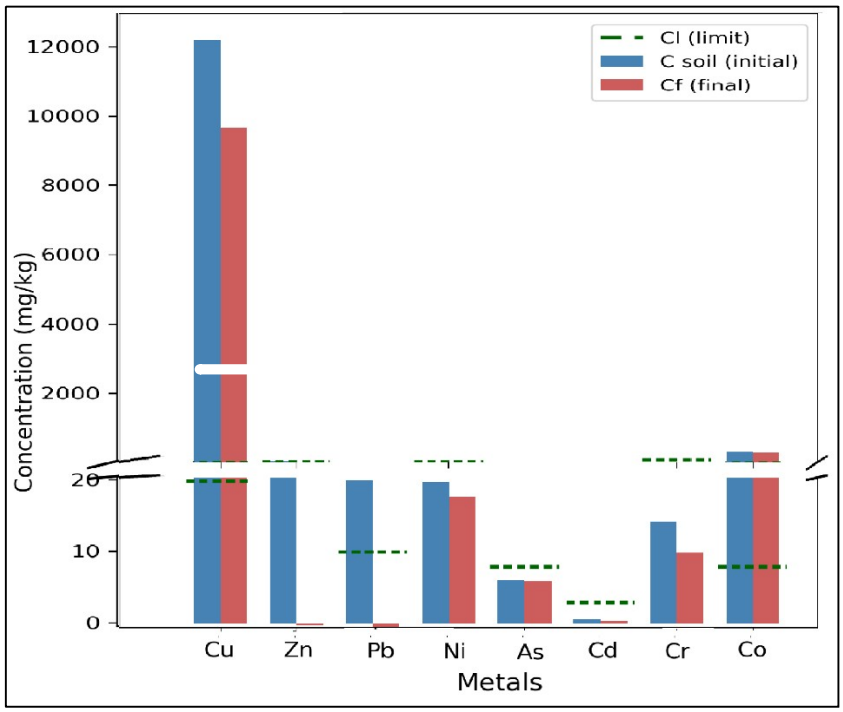

Figure 3.5: Initial and final metal concentration in soil

The initial and final concentration of metal in soil after one season are presented in *Figure 3.5.* where the zinc and lead exhibited negative changes in concentration, whereas Cobalt and arsenic showed no notable difference between their initial and final levels. The horizontal dashed line for each metal represents the regulatory or accepted limit of that metal in soil, allowing comparison with measured concentrations (C soil and Cf).

3.1.1.7 Phytoremediation time

The estimated remediation times for each metal are summarised in *Table 3.4.*

Theoretical removal time was calculated both with and without considering acceptable soil limits (see T*able 2.2*). Only copper and cobalt required additional time to reach safe concentrations, as all other metals were already within acceptable limits.

Table 3.4: Time for the complete remediation of the soil

Metals	Time without considering the acceptable limit	Time that considers the acceptable limit
Cu	2.413654	1.909708
Zn	0.49806	-
Pb	0.489828	-
Ni	4.753683	-
As	15.96001	-
Cd	1.555676	-
Cr	1.699572	-
Co	9.458841	8.731942

3.1.2 Implementation of a Solar-Powered Pumping and Water Storage System

3.1.2.1 Structure

The system comprises a total of 1,470 photovoltaic panels, which collectively generate 2,513.7 kWh of energy.

3.1.2.2 Water and energy required

The overall daily irrigation volume (V_T)was calculated as 49.59 m³/day. The corresponding total daily water demand (D_{TW}) for both irrigation and green hydrogen production was 51.19 m³/day. The required flow rate (Q) for this operation was determined to be 8.98 m³/h.

The pumping power (P) required to meet this demand was estimated at 1.224 kW. The daily hydraulic energy required (E_h) for the pumping system was 4.883 kWh/day. In contrast, the remaining energy for green hydrogen production (E_r) was found to be 2,508.817 kWh/day. The summary is given in *Table 3.5*.

Table 3.5: Water and energy requirements for both irrigation and green hydrogen production

V_T (m³/day)	D_{TW} (m³/day)	Q (m³/h)	P (kW)	E_h (kWh/day)	E_r (kWh/d)
49.594	51.194	8.981	1.224	4.883	2508.81694

3.1.3 Biomass produced

The integration of Agri-PV systems with agroforestry practices in the mining area led to notable biomass yields across three plant species. The harvested dry biomass masses were present in (*Table 3.6*).

The total dry biomass yield obtained was 735.79 kg. These results demonstrate the effective establishment of the integrated agroforestry-Agri-PV system in the mining-impacted landscape, providing a significant biomass output despite the challenging environmental conditions.

Table 3.6: Total dry biomass yield from plants

	Sunflower	**Mustard**	**Bamboo**	**Total**
Dry biomass (kg)	591.18	79.54	65.08	735.79

3.1.4 Hydrogen production through Aspen Plus software

3.1.4.1 Gasification

The simulation yielded hydrogen production rates of 0.0353 kg/h, 0.0371 kg/h, and 0.3397 kg/h for bamboo, mustard, and sunflower biomass, respectively. Based on site-specific solar irradiation data, the system operates for 5.7 hours per day, and biomass availability from seasonal harvests allows for a 4-month production period annually. This results in estimated hydrogen yields of 24.35 kg/year, 25.62 kg/year, and 234.31 kg/year, with a total of 284.27kg/year.

3.1.4.1.1 Model validation of the gasification

3.1.4.1.1.1 Mosso Bamboo:

The gasification model for Moso bamboo was validated against experimental results reported by [153], who studied air–steam gasification in a downdraft reactor using bamboo feedstock with varying steam-to-biomass ratios (SBRs) from 0.1 to 0.4 and ER, 0.4. Due to differences in bamboo species, the composition used in this work (Moso bamboo) does not exactly match the feedstock in the referenced study. Nevertheless, the comparison remains valuable because Moso bamboo is scarcely represented in gasification literature, and this study addresses that gap. The proximate analysis and the ultimate analysis used for the model [154], and

experiment [153] are presented in *Table 3.8* , respectively. The LHV in the table for the model is determined from the HHV using Eq. (*3.1and 3.2*) from [155].

$$HHV_{biomass} = 0.3419C + 1.1783H + 0.1005S - 0.1034O - 0.015N - 0.0211\,Ash \quad (3.1)$$

$$LHV_{biomass} = HHV - hfg \times \frac{(9H + MC)}{100} \quad (3.2)$$

A comparison was performed at SBR = 0.35 and ER=0.4 with the modelled syngas composition compared to experimental results. The data are summarized in *Figure 3.6*. The model significantly overpredicts hydrogen (H_2), giving a mole fraction of 0.4337 compared to the experimental value of 0.37, while it underpredicts CO_2 (model: 0.0808 vs. experimental: 0.23.5), CO (0.0307 vs. 0.095), and CH_4 (2.1×10^{-11} vs. 0.015).

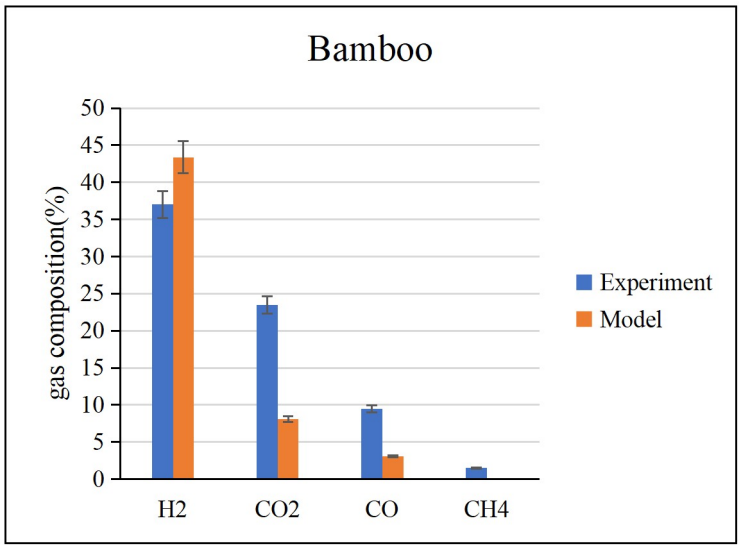

Figure 3.6: model validation against experiment

The model includes a comprehensive set of gasification reactions, including devolatilization, char gasification, and tar cracking, as well as volatile-phase reactions such as partial oxidation, steam reforming, methanation, and water–gas shift, all implemented with their respective kinetic parameters. Despite this, discrepancies remain, likely due to uncertainties in kinetic parameters, variability in tar composition, or differences in the physical structure and reactivity of Moso bamboo compared to the experimental feedstock. The overprediction of H_2 may result from an overestimation of tar and char reforming rates, which favor hydrogen production, while the underprediction of CO, CO_2, and CH_4 could indicate that further calibration of volatile-phase reactions is needed.

Despite these quantitative differences, the model captures the qualitative gasification trends, correctly predicting H_2 as the dominant product. These results suggest that while the key kinetic pathways are represented, model accuracy could be improved through feedstock-specific kinetic calibration, particularly for tar chemistry and devolatilization behaviour. This would allow for a more precise representation of the gasification characteristics of Moso bamboo.

Table 3.8: Characterisation of Bamboo for experiment and model

Proximate analysis (wt.%)			**Ultimate analysis (wt.%)**		
	Bamboo	**Moso Bamboo**		**Bamboo**	**Mosso bamboo**
Lower heating value (MJ/kg)	16.52	18.5	C	43.09	49
Moisture	6.82	7	H	5.94	6
Volatile matter	75.00	81	N	1.11	0.3
Fixed carbon[a]	16.08	11.8	O[a]	49.86	44.5
Ash	2.10	0.2			

3.1.4.1.1.2 Mustard and Sunflower:

The model was applied to mustard biomass and validated using experimental data from [153], whose feedstock shares similar characteristics and LHV. For mustard, the model overpredicts H_2 and underpredicts CO, CO_2, and CH_4 (see *Figure 3.7a*), consistent with the trend observed in the Moso bamboo case. To further evaluate the model, simulations were also performed using sunflower biomass, validated against experimental data from a study that included char cracking [156]. In that case, the predicted H_2 closely matched the experimental value, but CO, CO_2, and CH_4 remained underpredicted (*Figure 3.7b*). Since the model incorporates a comprehensive kinetic framework, including devolatilization, tar and char reactions, and volatile-phase chemistry, these discrepancies are likely related to feedstock-specific differences in tar behaviour and volatile composition. Overall, the model reliably captures major trends in syngas composition across different biomasses.

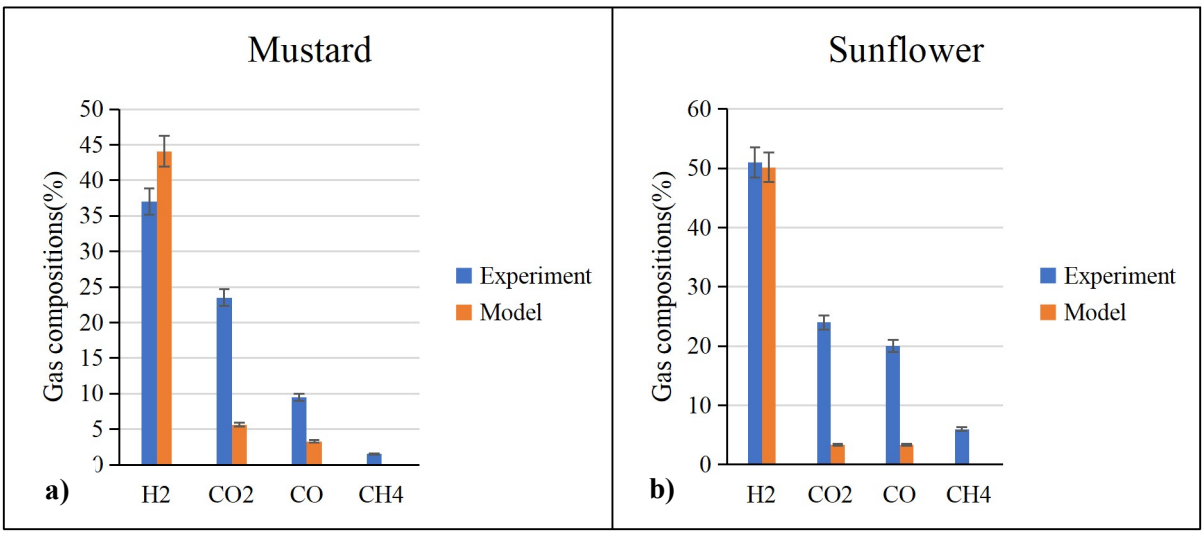

Figure 3.7: Model validation of mustard(a). and sunflower(b) with experimental data

The operating parameters used for all the models are shown in *Table 3.7*

Table 3.7: Block unit pressure and temperature

Block and stream	Temperature (°C)			Pressure (bar)
	Bamboo	Mustard	Sunflower	
feed	25	25	25	1.013
Air-steam	150	150	150	1.013
RStoic	150	150	150	1.013
RYield	500	500	500	1.013
RGibbs	700	700	700	1.013
RPlug Oxi	938	938	750	1.013
RPlug Red	564	564	750	1.013

3.1.4.1.2 Sensitivity analysis

3.1.4.1.2.1 Bamboo:

3.1.4.1.2.1.1 Temperature Sensitivity Analysis for Moso Bamboo

Figure 3.8 presents the sensitivity analysis of Moso bamboo gasification to temperature variation (700-1000 °C). The model reveals that as the temperature increases, the mole fractions of H_2 and CO_2 increase, while those of CO and CH_4 decrease, with CH_4 reaching extremely low levels. These trends are consistent with the thermodynamic and kinetic behaviour of key gasification reactions.

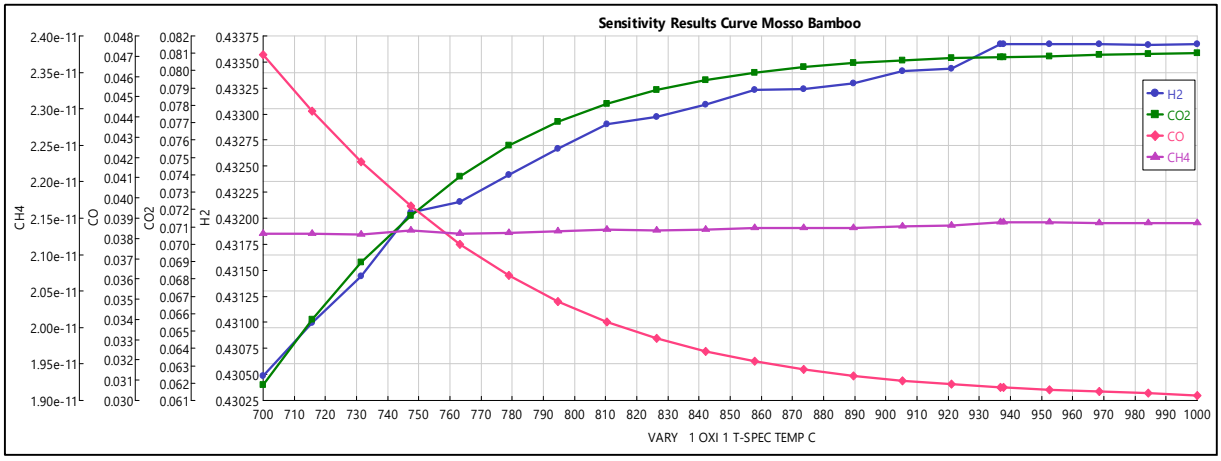

Figure 3.8: Variation of temperature from 700 to 1000 with a fixed SBR=0.35 and ER=0.4

The increase in H_2 is attributed to enhanced rates of steam reforming and water-gas shift (WGS) reactions at elevated temperatures, both of which are endothermic. CO_2 rises due to the forward shift of the WGS reaction, converting CO and H_2O into H_2 and CO_2. The decline in CO results from its consumption via both WGS and reforming pathways. CH_4 diminishes sharply due to thermal cracking and reforming of methane, which are strongly favoured at high temperatures.

These model-based findings align with recent experimental findings from [153] and [157] who report similar trends, where H_2 and CO_2 increased steadily with temperature, while CO and CH_4 decreased due to intensified reforming and tar cracking. Unlike the model, [158] reported an increase in CO and a decrease in CO_2 with temperature. This is attributed to the dominance of the Boudouard reaction at lower temperatures and less WGS activity due to limited steam reforming, and it uses a dual-bed setup (pyrolysis + gasification), changing gas residence time and potentially reducing CO_2 formation via WGS. Like Alipour Moghadam et al. [158], Ngamchompoo & Triratanasirichai. [159] reported the same trends.

3.1.4.2 Alkaline Water Electrolysis

The result of the alkaline electrolysis model is presented in this section. As shown in *Figure 2.3*, which illustrates the flow diagram under base case operating conditions (*Table 2.12*), the detailed composition of the result is provided in *Table 3.9, and Table 3.10*

Table 3.9: Stream result of H_2 and O_2 produced and out

	Temperature (∘C)	**Pressure (bar)**	**Composition (kg/hr)**		
			H_2O	**H_2**	**O_2**
H_2	25	1	3.386	11.488	0
H_2-P	81.857	4.7	6.544	11.488	0
O_2	25	1	1.695	0	90.821
O_2-P	81.86	4.7	3.309	0	90.821

Table 3.10: Result obtained at temperature 80 °C, and pressure 5bar

HTO (%)	Mass balance (mol/s)			LHV (kJ/kmol)	HHV (kJ/kmol)	$\dot{n}_{H_2.out}$ (kmol/hr)	W_{net} (kW)	η_{sys} (%)
	$\dot{n}_{H_2.prod}$	$\dot{n}_{O_2}$	$\dot{n}_{H_2O}$					
1.02	1.422	0.71	1.42	233847.3	278917.4	5.699	646.985	57.22

3.1.4.2.1 Model validation

The electrochemical response of the model was validated by comparing simulated polarization curves (V_{cell}^{model}) against those experimentally obtained for the electrolysis cell (V_{cell}^{test}). The model characterized a cell stack composed of 298 cells of $4000 cm^2$ surface area and current density $0.25\,A.cm^{-2}$ at a temperature of 80°C and a pressure of 5 bars. The experiment used for the validation has been characterized at different operating conditions into a fully automated test bench developed by Centro Nacional del Hidrogeno (CNH2) [147], which has been designed to be able to operate in a wide range of temperatures (40-80 °C) and pressures (1-10 bar). The root-mean-square (RMS_{error}) was calculated according to Eq. (3.3) [151] to ensure the accuracy and validity of the proposed model.

$$RMS_{error} = \sqrt{\frac{\sum (V_{cell}^{model} - V_{cell}^{test})^2}{N-1}} \quad (3.3)$$

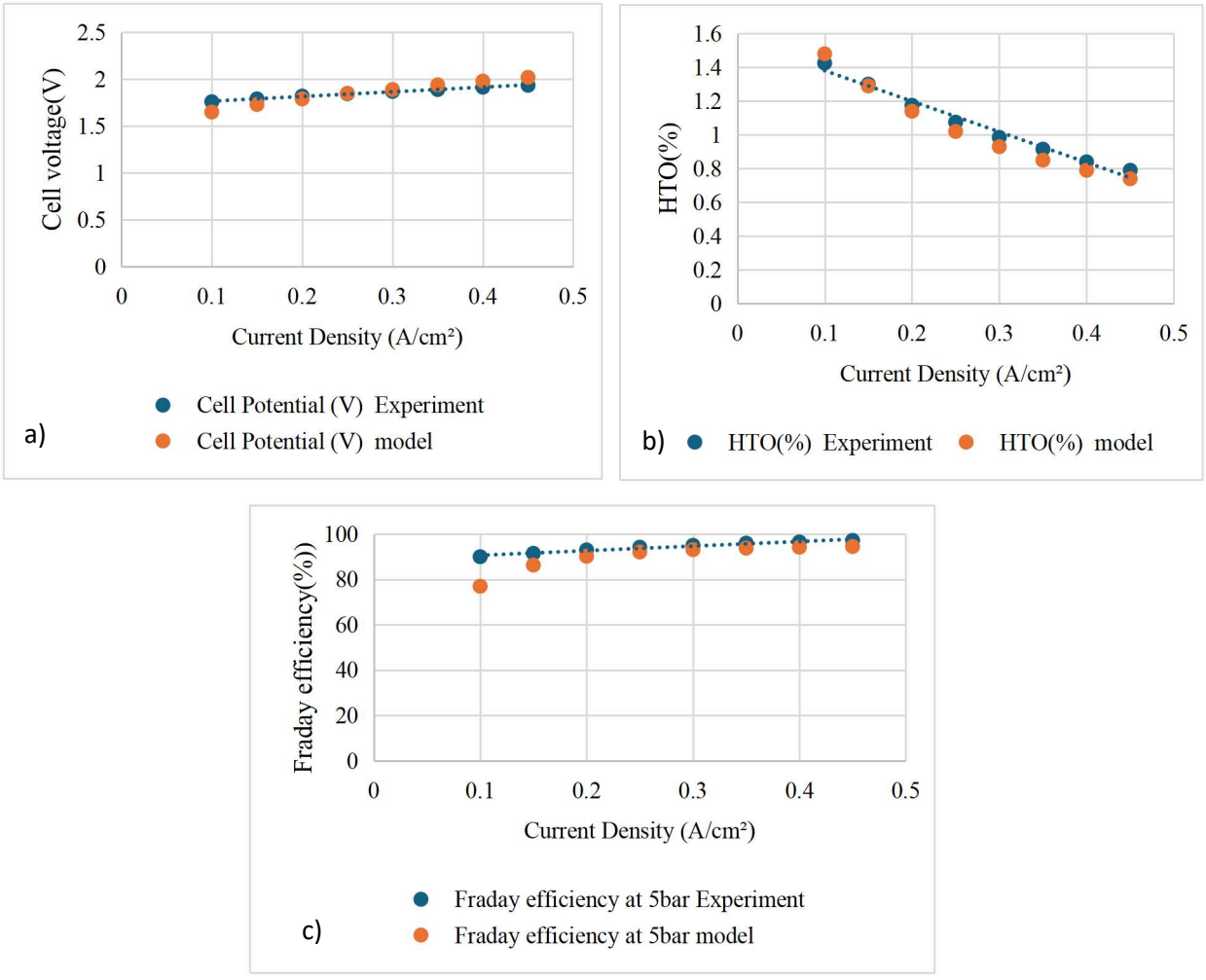

Figure 3.9: Scatter chart of the experimental and model results: a) Cell potential; b) Gas purity; c) Faraday efficiency

Figure 3.9 shows a scatter chart of the model and experimental results used in this paper. The results show a good correlation between experimental and modelled data. The RMS error is

approximately 66.5 mV (*Figure 3.9a*) per cell and 5.7% (*Figure 3.9c*) for the Faraday efficiency and 0.0028% (*Figure 3.9b*) for HTO. This shows the value of the model in anticipating the reaction of the electrolyser in different testing situations.

3.1.4.2.2 Sensitivity analysis of AWE

3.1.4.2.2.1 Influence of the temperature and current density

Cell voltage is a key performance indicator for an AWE system. Several operating parameters influence it, including temperature, pressure, and current densities. The cell voltage of the alkaline electrolyser was analysed over a temperature range of 40-80°C, under constant pressure, and across a current density range of 1000 to 4500 A/m². The polarization curves of the alkaline electrolysis stack are shown in *Figure 3.10*a at various temperatures and current densities. According to the model, as the temperature increases from 40°C to 80°C, the cell voltage progressively decreases. In contrast, the cell voltage increases with rising current density. Overall, the results confirm that increasing temperature leads to improved electrochemical performance. Therefore, the stack power required in the electrolysis decreases when the temperature is higher (*Figure 3.10*b).

As illustrated in *Figure 3.10*c, the hydrogen content in oxygen (HTO) is displayed as a function of temperature and current density. The hydrogen content in oxygen rises as the temperature rises. This behaviour is attributed to the fact that higher temperatures reduce resistance. However, they also lead to greater parasitic current losses and lower Faraday efficiencies [147]. The results show that higher temperatures have a big effect on impurity levels. This is because increased diffusion and gas migration result in greater hydrogen crossover. Additionally, as shown in *Figure 3.10*c, gas purity decreases considerably at low current densities. This occurs because the aforementioned diffusion and migration processes are largely independent of the electrolyser load, meaning that when the gas production rate is low, the relative proportion of impurities becomes higher [156].

In this study, we observed that the hydrogen content in oxygen (HTO) increased at high temperatures and that gas purity decreased significantly at low current densities. These results are consistent with those reported by [147], who also found that increasing temperature led to higher hydrogen crossover due to enhanced diffusion rates. Similarly, Ren et al. [150] observed a decline in gas purity at low current densities under comparable operating conditions. The observed consistency across studies reinforces the critical role of temperature and current density in maintaining both efficiency and gas purity. In this work, an efficiency of 57.257% was achieved at 80 °C and 5 bar, which is in close agreement with the results reported by [147], who predicted similar efficiency values under comparable operating conditions. This alignment validates the reliability of this model and supports the notion that elevated temperatures enhance electrochemical performance by reducing ohmic resistance and activation losses. However, as noted by [149], operating at high temperatures can also

increase hydrogen crossover due to enhanced diffusion and parasitic current losses, thus compromising gas purity. This trade-off between efficiency and purity highlights the importance of carefully optimizing operational parameters. In this study, high temperature (80 °C), low pressure (5 bar), and low current density (2500A/m^2) were selected to optimize efficiency. The results demonstrate that although higher temperatures significantly enhance efficiency, they also promote diffusion-driven impurity transport, especially under low current density conditions where gas production rates are insufficient to dilute contaminants effectively. This finding is consistent with observations by [147], further confirming that gas purity is more sensitive to current density than efficiency. Therefore, optimizing electrolyser operation requires a careful balance, leveraging higher temperatures to boost performance while maintaining current densities sufficient to mitigate impurity concentration.

Ultimately, this work contributes to the growing understanding that temperature, pressure, and current density must be co-optimized rather than adjusted independently. The results from the current model underscore the importance of system-level design strategies that integrate membrane durability, gas separation requirements, and energy efficiency goals. As noted by [160], achieving this balance is particularly critical in industrial applications, where both high-purity hydrogen and long-term system stability are essential for safe and cost-effective operation.

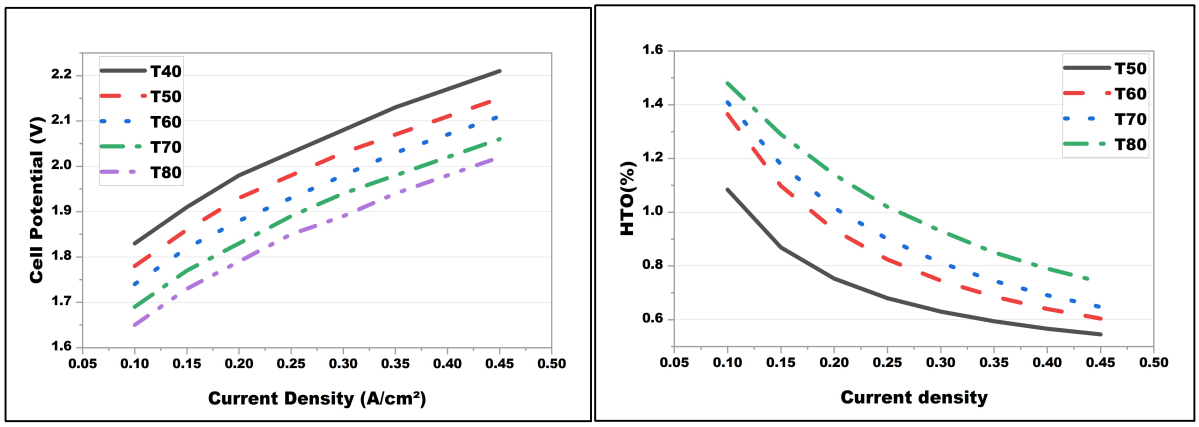

Figure 3.10: sensitivity analysis of AWE based on cell potential(a), power stack(b), and HTO(c).

3.2 Discussion

This study examined the phytoremediation potential of an integrated agroforestry and agrivoltaics system applied to a copper tailings dump in Zambia, using a combination of sunflower (*Helianthus annuus*), mustard (*Brassica juncea*), and Moso bamboo (*Phyllostachys edulis*). These species are known hyperaccumulators, which is particularly very relevant because, while phytoremediation is generally a slow process, some studies indicate that remediation using hyperaccumulator plants typically takes between 2 to 60 years, whereas non-hyperaccumulator species may require 25 to 2800 years [161]. Remarkably, results from

this study indicate that nearly all monitored heavy metals, except copper (Cu) and cobalt (Co), were reduced to acceptable environmental levels within a single growing season. Furthermore, Cu and Co are projected to reach acceptable thresholds within 2 years (4 seasons) and 9 years (18 seasons), respectively. These timelines are significantly shorter than those reported in many comparable studies, which often estimate remediation periods spanning several decades [162, 163], particularly for persistent metals. This enhanced efficiency can be attributed to the strategic combination of plant species and the complementary benefits of agroforestry and agrivoltaics, which together created a synergistic environment for accelerated metal uptake and soil recovery.

3.2.1 Factors Contributing to Accelerated Remediation

3.2.1.1 Species Selection and Functional Complementarity

The results of this study confirm the well-documented role of sunflower (*Helianthus annuus*) as an effective phytoremediator, particularly for zinc, cadmium, and lead, for which it demonstrated the highest removal efficiencies. Despite lower RF values for copper and arsenic, the total uptake for copper was substantial, reflecting the contribution of the high biomass of sunflower and deep root system to its phytoextraction performance. As a fast-growing species with a short life cycle, sunflower allows for multiple harvests per year, enhancing their annual accumulation potential and making them especially suitable for rapid remediation strategies. This observation is consistent with insights discussed by [110] who noted, based on previous literature, that metal accumulation in sunflowers tends to peak around four weeks after planting, and that early harvesting followed by replanting could improve overall phytoremediation efficiency. These characteristics, combined with their broad environmental tolerance and ease of management, support the suitability of sunflowers in integrated remediation systems targeting a range of heavy metals.

The performance of Indian mustard (*Brassica juncea*) in this study reinforces its reputation as a valuable species for phytoremediation, particularly in multi-species systems on degraded or post-mining soils. While its removal efficiency (RE) values for most metals were moderate, its substantial total copper uptake reflects the advantage of combining moderate metal accumulation capacity with high biomass productivity. As a member of the Brassicaceae family, mustard is known for its rapid growth, tolerance to poor soil fertility, and adaptability to harsh environmental conditions, making it well-suited for sites such as copper tailings dumps. These findings align with the works of [164], who emphasize that the biomass yield and stress tolerance of Indian mustard significantly enhance its performance in contaminated environments where vegetation establishment is often limited. Its ability to uptake lead and cadmium complements other species in mixed planting systems, supporting more complete remediation across a broader range of contaminants. In the current study, the contribution of

mustard was not only in metal removal but also in improving plant cover and soil resilience, key goals in sustainable Phyto-management of industrially impacted landscapes.

In this study, Moso bamboo (*Phyllostachys pubescens*) confirms its potential for use in phytoremediation, particularly for lead and zinc, which showed notably high removal efficiencies. While copper and chromium had lower RE values, the substantial total uptake of copper highlights the capacity of species to accumulate metals over time, a feature closely tied to its large biomass production. These outcomes align with existing literature that emphasizes the suitability of Moso bamboo for remediating copper-contaminated soils, especially in post-mining or degraded landscapes. As discussed by [138], its extensive root system, stress tolerance, and ability to enhance soil health make it well-suited for long-term phytoextraction and phytostabilisation strategies. The selective uptake observed in this study further suggests that Moso bamboo may be particularly effective when it is used in combination with other species to target a wider range of contaminants. The effectiveness of Moso bamboo in phytoremediation can be further enhanced when integrated into an intercropping system, as demonstrated in this study through its combination with *Helianthus annuus* and *Brassica juncea.* Intercropping enabled the complementary use of root architectures, with the deep roots of bamboo and the shallow roots of sunflower and mustard, allowing for more comprehensive exploitation of the soil profile. This configuration likely contributed to the observed improvements in metal uptake and soil condition. Comparable findings have been reported in other studies [165], where Moso bamboo intercropped with Sedum not only improved heavy metal (HM) extraction but also enhanced plant growth due to shade benefits, improved light use efficiency, and nutrient sharing across the root zones. In that study, the intercropped system led to reduced levels of soil organic matter (SOM), available potassium (AK), and available phosphorus (AP) in the rhizosphere, indicating more effective nutrient absorption [165]. These observations are consistent with [166], who reported that intercropping systems combining deep-rooted and shallow-rooted species resulted in more efficient nutrient utilization, improved soil structure, and reduced nutrient leaching. These synergistic interactions observed in this agroforestry-based intercropping approach may help explain the accelerated remediation performance seen in this study.

3.2.1.2 Agroforestry System Enhancements

This study demonstrates that agroforestry-based phytoremediation, combining deep-rooted perennials like Moso bamboo with fast-growing hyperaccumulators such as sunflower and mustard, can significantly enhance the restoration of post-mining landscapes. This functional diversity enables both rapid heavy metal removal and long-term ecosystem recovery, providing an advantage over conventional monoculture approaches commonly used in phytoremediation.

One of the most prominent benefits of agroforestry observed in this study was accelerated soil rehabilitation, which aligns with multiple findings in the literature. Trees such as bamboo act as nutrient pumps, recycling leached minerals back to the surface through litterfall and root turnover, thus enhancing nutrient cycling and preventing long-term soil nutrient loss [167], [168]. The bamboo litter, rich in N, P, K, Ca, and Mg, functions as a slow-release fertilizer that improves soil organic matter (SOM), structure, and fertility [115]. This organic matter improves water-holding capacity, reduces evapotranspiration, and supports stable soil aggregation, factors that were reflected in the improved pH, moisture, and cation exchange capacity (CEC) seen in agroforestry plots compared to monocultures.

These findings echo broader research that agroforestry enhances soil stability through increased ground cover, mulching effects, and physical root structures that reduce runoff, prevent erosion, and buffer against harsh microclimates [56]. Bamboo, in particular, contributes to these processes not only through its dense root system, which enhances aeration and porosity, but also through its litter, which acts as a mulch layer that reduces soil temperature and evaporation losses [165, 169].

In addition to soil improvement, agroforestry supports ecological resilience and biodiversity conservation. The structural diversity created by combining woody and herbaceous species provides habitats and movement corridors for a variety of animal species, aiding both local biodiversity recovery and broader landscape connectivity [167]. This contributes to conservation outcomes while simultaneously delivering productive land use. The inclusion of nitrogen-fixing or high-organic-matter species further supports ecosystem functions by boosting biological nitrogen fixation, stimulating microbial activity, and improving enzyme dynamics in the rhizosphere [168].

Microbial community shifts associated with bamboo agroforestry also enhance soil functionality. Although microbial diversity in the bamboo rhizosphere may decline compared to natural forests, diversity in the surrounding bulk soil tends to increase, creating a more heterogeneous and functionally diverse microbial environment. These microbial communities play a central role in nutrient mineralization and metal transformation processes, further contributing to the observed remediation efficiency [169].

The success of this system in shortening remediation time reflects the combined benefits of high biomass production, root depth complementarity, efficient nutrient cycling, and improved microclimate conditions. These findings align with research indicating that agroforestry systems, especially those incorporating bamboo, outperform monocultures in degraded soils by offering sustained productivity, enhanced ecological services, and long-term land rehabilitation [165, 169, 170].

3.2.1.3 Agri-PV System Contributions

The Agri-PV system plays a key role in restoring post-mining landscapes by improving microclimatic conditions, conserving soil moisture, and supporting vegetation recovery. Shading from solar panels reduced surface temperatures and evapotranspiration, creating cooler, more stable environments that benefited both crops and animals. These shaded areas provided shelter for small wildlife and insects, helping reestablish habitat complexity in degraded areas, consistent with findings by [137].

By powering irrigation pumps with solar energy, the system ensured a reliable water supply without external energy inputs. This not only supported plant growth but also decreased reliance on fossil fuels. Notably, excess electricity was used for green hydrogen production, adding a clean energy output to the ecological benefits. Overall, the Agri-PV setup promotes rapid ecosystem recovery, supports local biodiversity, and demonstrates how renewable energy can be integrated into land rehabilitation strategies for environmental and climate advantages.

3.2.2 Phytoremediation biomass for hydrogen production

The production of hydrogen from biomass harvested in the phytoremediation system demonstrates a tangible valorisation pathway that links ecological restoration with renewable energy generation. In this study, Indian mustard, sunflower, and bamboo not only accelerated contaminant removal but also generated substantial biomass that was converted into hydrogen. This addresses a central challenge in phytoremediation, the disposal of contaminated biomass. Instead of creating secondary pollution risks, the harvested material became a resource for clean energy production. These results are supported by [171], who showed that biomass from hyperaccumulator plants can be converted into hydrogen while simultaneously stabilizing heavy metals in residual biochar, highlighting the feasibility of coupling remediation with energy recovery.

The link between phytoremediation outcomes and hydrogen production lies in the biomass-metal interaction. Improved soil fertility and vegetation cover through agroforestry and phytoremediation enhanced biomass accumulation, increasing the available feedstock for hydrogen generation. Meanwhile, the conversion process immobilized the extracted metals, ensuring safe handling and closing the remediation cycle. This demonstrates that post-mining landscapes can evolve into multifunctional systems where ecological recovery and clean energy generation are not competing objectives but complementary, mutually reinforcing processes.

Conclusion and perspectives

This study integrated agroforestry and agrivoltaics systems to rehabilitate post-mining land while simultaneously producing green and bio-hydrogen, respectively generated from solar energy and biomass produced in the areas. The main objective was to maximise biomass production by rehabilitating the mining area for high-yield hydrogen production.

To achieve this goal, the first specific objective was to structure a system of agroforestry and Agri-PV for soil improvement. Strategically, the site was divided into two equal plots where the cultures of sunflower and mustard were intercropped with the bamboo for an agroforestry system. In addition, sunflowers and mustard were planted under the solar photovoltaics for an Agri-PV system. The combination of these two systems demonstrates effective removal of heavy metals from the soil. Indeed, the bamboo showed strong phytostabilisation capacity for Cu, Zn, Pb, and Cr, while sunflower effectively translocated metals such as Cd, Zn, and As, supporting phytoextraction. Indian mustard provided a balance of metal uptake and biomass yield. After one season, nearly all target heavy metals, except Cu and Co, were reduced to safe limits, with Pb and Zn showing complete remediation.

The second specific objective was to estimate the available biomass potential after remediation for bio-hydrogen production. The number of plants and crops under the study area was calculated to estimate the total dry biomass based on the plant biomass rate from the literature.

The third specific objective was planned to evaluate the water required and the energy generated from the solar panel for green hydrogen production. On this aspect, the number of panels was calculated with respect to the spacing to allow plants to get sufficient irradiation. The energy generated from the solar panels was used to power a pump, which stored water in a tank to ensure the irrigation system and the supply for an electrolyser. The surplus energy was used to power the electrolyser for green hydrogen production.

The fourth and last specific objective consisted of optimising the potential green and bio-hydrogen production from mixed technologies using Aspen Plus. The optimisation of green and bio-hydrogen production with this software considered some key process variables such as temperature, pressure, steam-to-biomass ratio, equivalent ratio and air supply. Additionally, the integration of reforming and water-gas shift reactions, as well as the char and tar cracking, was explored to maximise hydrogen yield and process efficiency. These findings highlight that tuning operating conditions and process configuration are critical levers for enhancing sustainable hydrogen production from mixed technologies.

The dual pathway demonstrated the potential of post-mining landscapes to evolve into multifunctional hubs that simultaneously foster ecological restoration and carbon-neutral energy generation. Through the integration of phytoremediation with biomass gasification and advanced tar/char cracking, the approach resolved a critical limitation of phytoremediation:

the safe management of contaminated biomass. By converting harvested material into clean energy, the pathway not only mitigated disposal risks but also established a closed-loop system that couples environmental recovery with renewable energy production.

Despite the contributions of the study, several limitations and gaps remain that require further investigation. First, region-specific primary data are absent on soil conditions and plant uptake efficiency, which limits the accuracy and applicability of the results to local contexts. Second, limited research exists on cobalt uptake in the plant species studied, which may explain the comparatively long remediation period required for this metal. Third, there is currently a lack of studies on the utilisation of Moso bamboo, sunflower, and mustard as feedstock in gasification processes, leaving their potential underexplored in the literature. Fourth, the calibration of kinetic models remains insufficient, and the understanding of feedstock property variations is limited, contributing to uncertainties in simulation outcomes. The study lacks integration of economic feasibility analysis and does not address strategies for channelling residual solar energy into the national grid.

Perspectives and Practice

Based on all of the findings of this study, several actionable steps can guide the sustainable implementation of integrated agroforestry, phytoremediation, and Agri-PV systems for post-mining land rehabilitation and renewable energy production. These perspectives aim to support policymakers, practitioners, and researchers in scaling up multifunctional land management while ensuring ecological restoration and clean energy generation.

- Conduct field experiment to confirm its effectiveness and demostrate its practical relevance
- Collect localised primary data on soil conditions and plant uptake efficiency to improve result accuracy and relevance
- Study the feasibility of using Moso bamboo, sunflower, and mustard as feedstock in gasification processes to assess their energy recovery potential.
- Channel remaining electricity, after meeting irrigation and hydrogen production needs, into the grid supply or local community uses to maximise sustainability and economic benefits.
- Conduct cost-benefit analyses to guide scalable deployment and attract long-term investment.

In sum, this work provides a scalable blueprint for multifunctional land rehabilitation, where degraded landscapes not only recover ecological function but also contribute directly to renewable energy systems. With targeted policy support, such models can be aligned with national sustainability and energy transition strategies, positioning post-mining regions as key contributors to climate-neutral development goals.

Bibliography references

[1] A. Kovač, M. Paranos, and D. Marciuš, "Hydrogen in energy transition: A review," *Int. J. Hydrogen Energy*, vol. 46, no. 16, pp. 10016–10035, 2021, doi: 10.1016/j.ijhydene.2020.11.256.

[2] M. Islam, A. Pranto, R. Shabab, and R. I. Rone, "Revitalizing the Land : Ecosystem Restoration in Post- Mining Areas," *North Am. Acad. Res.*, vol. 7, no. 11, pp. 11–19, 2024, doi: https://doi.org/10.5281/zenodo.14261457 Conflicts.

[3] A. S. Worlanyo and L. Jiangfeng, "Evaluating the environmental and economic impact of mining for post-mined land restoration and land-use: A review," *J. Environ. Manage.*, vol. 279, pp. 1–16, 2021, doi: 10.1016/j.jenvman.2020.111623.

[4] Y. Xu, S. An, Y. Chen, C. Yuan, and P. Tao, "Effect of Biomass Improvement Method on Reclaimed Soil of Mining Wasteland," *Adv. Civ. Eng.*, vol. 2022, pp. 1–10, Jan. 2022, doi: 10.1155/2022/8375918.

[5] F. G. Damptey, E. A. Djoudi, and K. Birkhofer, "Effects of post-mining forest restoration and alternative land uses on ground-dwelling arthropods in Ghana," *Community Ecol.*, vol. 24, no. 2, pp. 215–228, 2023, doi: 10.1007/s42974-023-00144-8.

[6] F. G. Damptey, K. Birkhofer, P. K. Nsiah, and E. G. de la Riva, "Soil Properties and Biomass Attributes in a Former Gravel Mine Area after Two Decades of Forest Restoration," *Land*, vol. 9, no. 6, pp. 1–18, Jun. 2020, doi: 10.3390/land9060209.

[7] B. Lee, D. Joung, W. Kim, J. Ko, and H. Rhee, "The Social and Ecological Dimension of Ecosystem Service Enhancement in Post-Mining Forest Rehabilitation: Integrating Stakeholder Perspectives," *Forests*, vol. 16, no. 7, p. 28, Dec. 2024, doi: 10.3390/f16010007.

[8] D. Ranđelović and V. C. Pandey, "Bioenergy Crop-Based Ecological Restoration of Degraded Land," in *Bio-Inspired Land Remediation*, 2023, pp. 1–29. doi: 10.1007/978-3-031-04931-6_1.

[9] S. Singh, D. K. Jaiswal, R. Krishna, A. Mukherjee, and J. P. Verma, "Restoration of degraded lands through bioenergy plantations," *Restor. Ecol.*, vol. 28, no. 2, pp. 263–266, Mar. 2020, doi: 10.1111/rec.13095.

[10] A. Sarr, Y. M. Soro, A. K. Tossa, and L. Diop, "Agrivoltaic, a Synergistic Co-Location of Agricultural and Energy Production in Perpetual Mutation: A Comprehensive Review," *Processes*, vol. 11, no. 3, pp. 1–27, 2023, doi: 10.3390/pr11030948.

[11] O. Sarkar, J. A. Modestra, U. Rova, P. Christakopoulos, and L. Matsakas, "Waste-Derived Renewable Hydrogen and Methane: Towards a Potential Energy Transition Solution," *Fermentation*, vol. 9, no. 4, Apr. 2023, doi: 10.3390/fermentation9040368.

[12] X. Xu, Q. Zhou, and D. Yu, "The future of hydrogen energy: Bio-hydrogen production technology," *Int. J. Hydrogen Energy*, vol. 47, no. 79, pp. 33677–33698, 2022, doi: 10.1016/j.ijhydene.2022.07.261.

[13] T. Rohilla and M. Kumar, "Challenges with Sustainable Green Hydrogen Production: Role of Materials, Design, Multi-scale Modeling, and Up-Scaling," in *Energy, Environment, and Sustainability Series Editor: Challenges and Opportunities in Green Hydrogen Production*, A. K. Agarwal, Ed., 2024, ch. 19, pp. 455–490. doi: 10.1007/978-981-97-1339-4_19.

[14] A. Nicita, G. Maggio, A. P. F. Andaloro, and G. Squadrito, "Green hydrogen as feedstock: Financial analysis of a photovoltaic-powered electrolysis plant," *Int. J. Hydrogen Energy*, vol. 45, no. 20, pp. 11395–11408, 2020, doi: 10.1016/j.ijhydene.2020.02.062.

[15] C. S. Fermanelli, E. D. Galarza, L. B. Pierella, M. S. Renzini, and C. Saux, “How to Valorize Peanut Shells by a Simple Thermal-Catalytic Method,” *Top. Catal.*, vol. 62, pp. 918–930, 2019, doi: 10.1007/s11244-019-01176-z.

[16] H. M. U. Ayub, M. A. Qyyum, K. Qadeer, M. Binns, A. Tawfik, and M. Lee, “Robustness enhancement of biomass steam gasification thermodynamic models for biohydrogen production: Introducing new correction factors,” *J. Clean. Prod.*, vol. 321, 2021, doi: 10.1016/j.jclepro.2021.128954.

[17] R. Kaur, P. Gera, M. K. Jha, and T. Bhaskar, “Thermochemical Route for Biohydrogen Production,” in *Biohydrogen*, Elsevier, 2019, ch. 8, pp. 187–218. doi: 10.1016/B978-0-444-64203-5.00008-3.

[18] J. Wang and M. Aghajani Delavar, “Modelling phytoremediation: Concepts, methods, challenges and perspectives,” *Soil Environ. Heal.*, vol. 2, no. 1, p. 100062, 2024, doi: 10.1016/j.seh.2024.100062.

[19] Y. Y. Lee, K. S. Cho, and J. Yun, “Phytoremediaton Strategies for Co-Contaminated Soils: Overcoming Challenges, Enhancing Efficiency, and Exploring Future Advancements and Innovations,” *Processes*, vol. 13, no. 1, pp. 1–28, 2025, doi: 10.3390/pr13010132.

[20] F. Bian, Z. Zhong, X. Zhang, C. Yang, and X. Gai, “Bamboo – An untapped plant resource for the phytoremediation of heavy metal contaminated soils,” *Chemosphere*, vol. 246, May 2020, doi: 10.1016/j.chemosphere.2019.125750.

[21] V. N. Edgar, F. L. Fabián, P. C. Julián Mario, and V. R. Ileana, “Coupling plant biomass derived from phytoremediation of potential toxic-metal-polluted soils to bioenergy production and high-value by-products-a review,” *Appl. Sci.*, vol. 11, no. 7, 2021, doi: 10.3390/app11072982.

[22] B. A. Johnson, Y. Arino, D. B. Magcale-Macandog, X. Liu, and M. Yamanoshita, “Potential of agrivoltaics in ASEAN considering a scenario where agroforestry expansion is also pursued,” *Resour. Conserv. Recycl.*, vol. 209, pp. 1–11, 2024, doi: 10.1016/j.resconrec.2024.107808.

[23] A. Weselek, A. Ehmann, S. Zikeli, I. Lewandowski, S. Schindele, and P. Högy, “Agrophotovoltaic systems: applications, challenges, and opportunities. A review,” *Agron. Sustain. Dev.*, vol. 39, no. 35, pp. 1–20, 2019, doi: 10.1007/s13593-019-0581-3.

[24] Z. J. S. Wager, L. Kuhn, H. Vertadier, J. K. Schingler, and C. Robinson, “Defining the notion of mining, extraction and collection: A step toward a sustainable use of lunar resources,” *Acta Astronaut.*, vol. 201, pp. 592–596, Dec. 2022, doi: 10.1016/j.actaastro.2022.09.037.

[25] S. Jia, W. Meng, and S. Li, “Risks of mineral resources in the supply of renewable energy batteries,” Mar. 2025. doi: 10.1038/s41598-025-94848-8.

[26] M. Podobińska-Staniec, A. Wiktor-Sułkowska, A. Kustra, and S. Lorenc-Szot, “Copper as a Critical Resource in the Energy Transition,” *Energies*, vol. 18, no. 4, p. 969, Feb. 2025, doi: 10.3390/en18040969.

[27] J. Xiao *et al.*, “From Mining to Manufacturing: Scientific Challenges and Opportunities behind Battery Production,” *Chem. Rev.*, vol. 125, no. 13, pp. 6397–6431, Jul. 2025, doi: 10.1021/acs.chemrev.4c00980.

[28] H. Zhang, “Resilience of critical transition minerals supply chain in the context of strategic rivalry: implications for the national policy and regulatory frameworks,” *J. Energy Nat. Resour. Law*, pp. 1–27, May 2025, doi: 10.1080/02646811.2025.2495920.

[29] S. Carr-Wilson, S. K. Pattanayak, and E. Weinthal, “Critical mineral mining in the energy transition: A systematic review of environmental, social, and governance risks and opportunities,” *Energy Res. Soc. Sci.*, vol. 116, Oct. 2024, doi: 10.1016/j.erss.2024.103672.

[30] D. C. Smith, “Geopolitical realities of the energy transition supply chain: energy security risks and opportunities,” *J. Energy Nat. Resour. Law*, vol. 41, no. 3, pp. 233–239, Jul. 2023, doi: 10.1080/02646811.2023.2230732.

[31] M. Negrete, M. Fuentes, A. Kraslawski, F. Irarrazaval, and S. Herrera-León, “Socio-environmental implications of the decarbonization of copper and lithium mining and mineral processing,” *Resour. Policy*, vol. 95, Aug. 2024, doi: 10.1016/j.resourpol.2024.105135.

[32] E. S. Festin, M. Tigabu, M. N. Chileshe, S. Syampungani, and P. C. Odén, “Progresses in restoration of post-mining landscape in Africa,” *J. For. Res.*, vol. 30, no. 2, pp. 381–396, Apr. 2019, doi: 10.1007/s11676-018-0621-x.

[33] L. Benidire, S. I. A. Pereira, A. Naylo, P. M. L. Castro, and A. Boularbah, “Do metal contamination and plant species affect microbial abundance and bacterial diversity in the rhizosphere of metallophytes growing in mining areas in a semiarid climate?,” *J. Soils Sediments*, pp. 1003–1017, Feb. 2019, doi: 10.1007/s11368-019-02475-4.

[34] Pratiwi *et al.*, “Managing and Reforesting Degraded Post-Mining Landscape in Indonesia: A Review,” *Land*, vol. 10, p. 30, Jun. 2021, doi: 10.3390/land10060658.

[35] L. Benidire, L. Benidire, and A. Boularbah, “Impacts of mining activities on soil properties: Case studies from Morocco mine sites,” *Soil Sci. Annu.*, vol. 71, no. 4, pp. 395–407, 2020, doi: 10.37501/soilsa/133011.

[36] N. Islam, S. Rabha, K. S. V. Subramanyam, and B. K. Saikia, “Geochemistry and mineralogy of coal mine overburden (waste): A study towards their environmental implications,” *Chemosphere*, vol. 274, 2021, doi: 10.1016/j.chemosphere.2021.129736.

[37] X. Hou *et al.*, “Selection of suitable species as a key factor for vegetation restoration of degraded areas in an open-pit manganese-ore mine in Southern China using multivariate-analysis methods,” *L. Degrad. Dev.*, vol. 30, no. 8, pp. 942–950, May 2019, doi: 10.1002/ldr.3281.

[38] Y. Zhang and S. Sun, “Study on the Reclamation and Ecological Reconstruction of Abandoned Land in Mining Area,” in *IOP Conference Series: Earth and Environmental Science*, 2020, pp. 3–7. doi: 10.1088/1755-1315/514/2/022073.

[39] M. Xia, S. Dong, Y. Chen, and H. Liu, “Study on evolution of groundwater-lake system in typical prairie open-pit coal mine area,” *Environ. Geochem. Health*, vol. 43, pp. 4075–4087, 2021, doi: 10.1007/s10653-021-00890-6.

[40] G. Luo *et al.*, “Detection of soil physical properties of reclaimed land in open-pit mining area: feasibility of application of ground penetrating radar,” *Environ. Monit. Assess.*, vol. 193, no. 392, 2021, doi: 10.1007/s10661-021-09153-4.

[41] J. Li and J. Wang, “Optimal sampling design for reclaimed land management in mining area: An improved simulated annealing approach,” *J. Clean. Prod.*, vol. 231, pp. 1059–1069, 2019, doi: 10.1016/j.jclepro.2019.05.230.

[42] C. Li, B. Zhao, and Y. Wang, “Nestedness of waterbird assemblages in the subsidence wetlands recently created by underground coal mining,” *Curr. Zool.*, vol. 65, no. 2, pp. 155–163, Apr. 2019, doi: 10.1093/cz/zoy034.

[43] C. Han *et al.*, “Restoration of damaged ecosystems in desert steppe open-pit coal mines: Effects on soil nematode communities and functions,” *L. Degrad. Dev.*, vol. 32, no. 15, pp. 4402–4416, Sep. 2021, doi: 10.1002/ldr.4045.

[44] X. Hou, S. Liu, S. Zhao, S. Dong, Y. Sun, and R. Beazley, “The alpine meadow around the mining areas on the Qinghai-Tibetan Plateau will degenerate as a result of the change of dominant species under the disturbance of open-pit mining,” *Environ. Pollut.*, vol. 254, 2019, doi: 10.1016/j.envpol.2019.113111.

[45] B. R. M. Walmer, D. R. L. Michael, de O. B. J. Udson, S. V.-B. A. Larissa, de A. O. F. Gustavo, and Schwartz, "Ecological methods and indicators for recovering and monitoring ecosystems after mining: A global literature review," *Ecol. Eng.*, vol. 145, 2020, doi: 10.1016/j.ecoleng.2019.105707.

[46] Y. Feng, J. Wang, Z. Bai, and L. Reading, "Effects of surface coal mining and land reclamation on soil properties: A review," *Earth-Science Rev.*, vol. 191, pp. 12–25, Apr. 2019, doi: 10.1016/j.earscirev.2019.02.015.

[47] M. Chen, S. Zhang, L. Liu, L. Wu, and X. Ding, "Combined organic amendments and mineral fertilizer application increase rice yield by improving soil structure, P availability and root growth in saline-alkaline soil," *Soil Tillage Res.*, vol. 212, 2021, doi: 10.1016/j.still.2021.105060.

[48] X. Wu, C. Xing, Q. Ju, S. Su, X. Zhang, and T. Zhu, "Research progress in mining ecological restoration technology," *J. Ind. Saf.*, vol. 1, no. 1, 2024, doi: 10.1016/j.jinse.2024.100004.

[49] A. Adegbite, "Practical Approach to Reclamation of Post- Mining Sites," Universität Cottbus-Senftenberg zur Erlangung des akademischen Grades eines Doktors der Naturwissenschaften (Dr. rer. nat), 2022. doi: 10.26127/BTUOpen-5871.

[50] A. Basu *et al.*, "Plant growth promoting rhizobacteria (Pgpr) as green bioinoculants: Recent developments, constraints, and prospects," *Sustain.*, vol. 13, no. 3, pp. 1–20, 2021, doi: 10.3390/su13031140.

[51] D. Xu, X. Li, J. Chen, and J. Li, "Research Progress of Soil and Vegetation Restoration Technology in Open-Pit Coal Mine: A Review," *Agric.*, vol. 13, no. 2, 2023, doi: 10.3390/agriculture13020226.

[52] S. K. Gautam, Y. Mallesh, P. Tiwari, and G. Gupta, "Agroforestry : Concept , Principles and Latest Advancements," *ResearchGate*, pp. 77–89, 2024, [Online]. Available: https://www.researchgate.net/publication/384466675_Agroforestry_Concept_Principles_and_Latest_Advancements

[53] M. A. Arshad *et al.*, "Navigating Synergies: A Comprehensive Review of Agroforestry System and Agronomy Crops," *Haya Saudi J. Life Sci.*, vol. 9, no. 04, pp. 97–113, 2024, doi: 10.36348/sjls.2024.v09i04.003.

[54] P. K. R. Nair, B. M. Kumar, and V. D. Nair, "Agroforestry and Land Management in the Future," in *An Introduction to Agroforestry Four Decades of Scientific Developments*, Springer, Cham, 2021, ch. 24, pp. 609–614. doi: https://doi.org/10.1007/978-3-030-75358-0_24.

[55] S. Sow *et al.*, "Sustainable fodder production in South Asia through silvopastoral systems," *Curr. Sci.*, vol. 126, no. 10, p. 1217, May 2024, doi: 10.18520/cs/v126/i10/1217-1224.

[56] S.-N. Maya, B. B. Ghaley, and N. L. J. Rintoul, "Agroforestry benefits and challenges for adoption in Europe and beyond," *Sustain.*, vol. 12, no. 17, pp. 1–20, 2020, doi: 10.3390/su12177001.

[57] H. B. M. ROGHAN *et al.*, "THE CURRENT ROLE AND IMPORTANCE OF AGROFORESTRY-A REVIEW ARTICLE," vol. 22, no. 5, pp. 3907–3918, 2024, [Online]. Available: http://www.aloki.xn--huissn15891623-wf3h

[58] S. Fahad *et al.*, "Agroforestry Systems for Soil Health Improvement and Maintenance," *Sustain.*, vol. 14, no. 22, pp. 1–25, 2022, doi: 10.3390/su142214877.

[59] V. Singh, J. Vishal, R. Kumar, and M. Chaudhary, "Socio-economic and Environmental Assets Sustainability by Agroforestry Systems: A Review," *Int. J. Agric. Environ. Biotechnol.*, vol. 14, no. 4, pp. 521–533, 2021, doi: 10.30954/0974-1712.04.2021.6.

[60] D. Octavia *et al.*, “Smart agroforestry for sustaining soil fertility and community livelihood,” *Forest Sci. Technol.*, vol. 19, no. 4, pp. 315–328, 2023, doi: 10.1080/21580103.2023.2269970.

[61] Pantera, M. R. Mosquera-Losada, F. Herzog, and M. den Herder, “Agroforestry and the environment,” *Agrofor. Syst.*, vol. 95, no. 5, pp. 767–774, 2021, doi: 10.1007/s10457-021-00640-8.

[62] A. R. Tsufac, N. P. Awazi, and B. P. K. Yerima, “Assessing the determinants of soil fertility in cocoa-based (Theobroma cacao) agroforestry systems in the Littoral region of Cameroon,” *Int. J. Plant Soil Sci.*, vol. 32, no. 17, pp. 52–60, Dec. 2020, doi: 10.9734/ijpss/2020/v32i1730386.

[63] L. G. Dente, F. M. S. Dagalea, and M. L. C. Alvarez, “Phytoremediation of Arsenic (As), Lead (Pb), and Mercury (Hg) Contaminated Soil Using Sunflower (Helianthus annuus L.),” *Asian Plant Res. J.*, vol. 12, no. 4, pp. 57–65, Jul. 2024, doi: 10.9734/aprj/2024/v12i4262.

[64] D. T. C. Nguyen *et al.*, “The sunflower plant family for bioenergy, environmental remediation, nanotechnology, medicine, food and agriculture: a review,” *Environ. Chem. Lett.*, vol. 19, no. 5, pp. 3701–3726, 2021, doi: 10.1007/s10311-021-01266-z.

[65] K. A. Alaboudi, B. Ahmed, and G. Brodie, “Phytoremediation of Pb and Cd contaminated soils by using sunflower (Helianthus annuus) plant,” *Ann. Agric. Sci.*, vol. 63, no. 1, pp. 123–127, 2018, doi: 10.1016/j.aoas.2018.05.007.

[66] P. Debaeke *et al.*, “Sunflower crop: environmental-friendly and agroecological,” *OCL*, vol. 24, no. 3, p. D304, May 2017, doi: 10.1051/ocl/2017020.

[67] O. A. V. Brazil *et al.*, “Integral use of lignocellulosic residues from different sunflower accessions: Analysis of the production potential for biofuels,” *J. Clean. Prod.*, vol. 221, pp. 430–438, 2019, doi: 10.1016/j.jclepro.2019.02.274.

[68] P. K. Singh, I. Kumar, U. Kumar, and R. K. Sharma, “Soil-mustard revitalization via rice husk ash, a promising soil amendment material for sustainable management of heavy metal contamination in tropical ecosystem,” *J. Environ. Manage.*, vol. 355, 2024, doi: 10.1016/j.jenvman.2024.120538.

[69] A. Nepal, G. F. Antonious, F. N. Bebe, T. C. Webster, B. R. Gyawali, and B. Neupane, “Heavy Metal Accumulation in Three Varieties of Mustard Grown under Five Soil Management Practices,” *Environ. - MDPI*, vol. 11, no. 4, 2024, doi: 10.3390/environments11040077.

[70] G. Mishra, K. Giri, S. Panday, R. Kumar, and N. S. Bisht, “Bamboo : potential resource for eco-restoration of degraded lands,” *J. Biol. Earth Sci.*, vol. 4, no. 2, pp. 130–136, 2014, [Online]. Available: https://citeseerx.ist.psu.edu/document?repid=rep1&type=pdf&doi=1133bef77d42f8e9db25dd22f7a940f6f254b544

[71] F. S. . Penarroyo, “Bamboo Offers Flexible Solutions to Mine Rehabilitation,” *AmCham J.*, p. 5, 2021, [Online]. Available: https://www.academia.edu/70111785/Bamboo_Offers_Flexible_Solutions_to_Mine_Rehabilitation

[72] K. Mehta, M. J. Shah, and W. Zörner, “Agri-PV (Agrivoltaics) in Developing Countries: Advancing Sustainable Farming to Address the Water–Energy–Food Nexus,” *Energies*, vol. 17, no. 17, pp. 1–23, 2024, doi: 10.3390/en17174440.

[73] E. Mouhib *et al.*, “Enhancing land use: Integrating bifacial PV and olive trees in agrivoltaic systems,” *Appl. Energy*, vol. 359, Apr. 2024, doi: 10.1016/j.apenergy.2024.122660.

[74] M. Uchanski, T. Hickey, J. Bousselot, and K. L. Barth, “Characterization of Agrivoltaic Crop Environment Conditions Using Opaque and Thin-Film Semi-Transparent Modules,” *Energies*, vol. 16, no. 7, Mar. 2023, doi: 10.3390/en16073012.

[75] E. Warmann, G. D. Jenerette, and G. A. Barron-Gafford, “Agrivoltaic system design tools for managing trade-offs between energy production, crop productivity and water consumption,” *Environ. Res. Lett.*, vol. 19, no. 3, Mar. 2024, doi: 10.1088/1748-9326/ad2ab8.

[76] K. Wydra, V. Vollmer, C. Busch, and S. Prichta, “Agrivoltaic: Solar Radiation for Clean Energy and Sustainable Agriculture with Positive Impact on Nature,” in *Solar Radiation - Enabling Technologies, Recent Innovations, and Advancements for Energy Transition*, 2023, ch. 7. doi: 10.5772/intechopen.111728.

[77] C. Toledo and A. Scognamiglio, “Agrivoltaic Systems Design and Assessment: A Critical Review, and a Descriptive Model towards a Sustainable Landscape Vision (Three-Dimensional Agrivoltaic Patterns),” *Sustainability*, vol. 13, no. 12, Jun. 2021, doi: 10.3390/su13126871.

[78] D. Soto-Gómez, “Integration of Crops, Livestock, and Solar Panels: A Review of Agrivoltaic Systems,” *Agronomy*, vol. 14, no. 8, pp. 1–30, 2024, doi: 10.3390/agronomy14081824.

[79] L. J. Walston *et al.*, “Opportunities for agrivoltaic systems to achieve synergistic food-energy-environmental needs and address sustainability goals,” *Front. Sustain. Food Syst.*, vol. 6, Sep. 2022, doi: 10.3389/fsufs.2022.932018.

[80] S. Sreenath, K. Sudhakar, and A. F. Yusop, “Sustainability at airports: Technologies and best practices from ASEAN countries,” *J. Environ. Manage.*, vol. 299, 2021, doi: 10.1016/j.jenvman.2021.113639.

[81] R. Maity, K. Sudhakar, A. Abdul Razak, A. Karthick, and D. Barbulescu, “Agrivoltaic: A Strategic Assessment Using SWOT and TOWS Matrix,” *Energies*, vol. 16, no. 8, pp. 1–18, 2023, doi: 10.3390/en16083313.

[82] M. Trommsdorff *et al.*, “Combining food and energy production: Design of an agrivoltaic system applied in arable and vegetable farming in Germany,” *Renew. Sustain. Energy Rev.*, vol. 140, Apr. 2021, doi: 10.1016/j.rser.2020.110694.

[83] M. A. Zainol Abidin, M. N. Mahyuddin, and M. A. A. Mohd Zainuri, “Solar Photovoltaic Architecture and Agronomic Management in Agrivoltaic System: A Review,” *Sustainability*, vol. 13, no. 14, Jul. 2021, doi: 10.3390/su13147846.

[84] A. Kumar Sharma, P. Kumar Ghodke, N. Goyal, S. Nethaji, and W. H. Chen, “Machine learning technology in biohydrogen production from agriculture waste: Recent advances and future perspectives,” *Bioresour. Technol.*, vol. 364, 2022, doi: 10.1016/j.biortech.2022.128076.

[85] B. Pandey, Y. K. Prajapati, and P. N. Sheth, “Recent progress in thermochemical techniques to produce hydrogen gas from biomass: A state of the art review,” *Int. J. Hydrogen Energy*, vol. 44, no. 47, pp. 25384–25415, 2019, doi: 10.1016/j.ijhydene.2019.08.031.

[86] R. K. Sharma, M. A. Nazari, J. Haydary, T. P. Singh, and S. Mandal, “A Review on Advanced Processes of Biohydrogen Generation from Lignocellulosic Biomass with Special Emphasis on Thermochemical Conversion,” *Energies*, vol. 16, no. 17, Sep. 2023, doi: 10.3390/en16176349.

[87] A. Habibollahzade, P. Ahmadi, and M. A. Rosen, “Biomass gasification using various gasification agents: Optimum feedstock selection, detailed numerical analyses and tri-objective grey wolf optimization,” *J. Clean. Prod.*, vol. 284, p. 124718, 2021, doi: 10.1016/j.jclepro.2020.124718.

[88] P. Prasertcharoensuk, S. J. Bull, and A. N. Phan, “Gasification of waste biomass for hydrogen production: Effects of pyrolysis parameters,” *Renew. Energy*, vol. 143, pp. 112–120, 2019, doi: 10.1016/j.renene.2019.05.009.

[89] A. Naquash *et al.*, “Biohydrogen and biomethane production from biomass gasification: Compositional analysis, recent advancements, challenges, and prospects,” *Process Saf. Environ. Prot.*, vol. 194, pp. 1526–1537, 2025, doi: 10.1016/j.psep.2024.12.029.

[90] S. Shiva Kumar and H. Lim, “An overview of water electrolysis technologies for green hydrogen production,” *Energy Reports*, vol. 8, pp. 13793–13813, 2022, doi: 10.1016/j.egyr.2022.10.127.

[91] L. Järvinen *et al.*, “Experimental study of alkaline water electrolyzer performance and frequency behavior under high frequency dynamic operation,” *Int. J. Hydrogen Energy*, vol. 67, no. December 2023, pp. 50–61, 2024, doi: 10.1016/j.ijhydene.2024.04.093.

[92] M. A. Khan *et al.*, “Seawater electrolysis for hydrogen production: A solution looking for a problem?,” *Energy Environ. Sci.*, vol. 14, no. 9, pp. 4831–4839, 2021, doi: 10.1039/d1ee00870f.

[93] H. Tüysüz, “Alkaline Water Electrolysis for Green Hydrogen Production,” *Acc. Chem. Res.*, vol. 57, no. 4, pp. 558–567, 2024, doi: 10.1021/acs.accounts.3c00709.

[94] H. Rezk, A. G. Olabi, M. A. Abdelkareem, A. Alahmer, and E. T. Sayed, “Maximizing Green Hydrogen Production from Water Electrocatalysis: Modeling and Optimization,” *J. Mar. Sci. Eng.*, vol. 11, no. 3, Mar. 2023, doi: 10.3390/jmse11030617.

[95] H. A. Miller *et al.*, “Green hydrogen from anion exchange membrane water electrolysis: A review of recent developments in critical materials and operating conditions,” *Sustain. Energy Fuels*, vol. 4, no. 5, pp. 2114–2133, 2020, doi: 10.1039/c9se01240k.

[96] J. Wang, J. Wen, J. Wang, B. Yang, and L. Jiang, “Water electrolyzer operation scheduling for green hydrogen production: A review,” *Renew. Sustain. Energy Rev.*, vol. 203, 2024, doi: 10.1016/j.rser.2024.114779.

[97] M. N. Chileshe, S. Syampungani, E. S. Festin, M. Tigabu, A. Daneshvar, and P. C. Odén, “Physico-chemical characteristics and heavy metal concentrations of copper mine wastes in Zambia: implications for pollution risk and restoration,” *J. For. Res.*, vol. 31, no. 4, pp. 1283–1293, Aug. 2020, doi: 10.1007/s11676-019-00921-0.

[98] L. Kachenga, H. N. Chabwela, and K. Mwauluka, “Phytoremediation Potential of Indigenous Plants Growing at Nchanga Mine in Chingola, Zambia,” *Open J. Ecol.*, vol. 10, no. 02, pp. 45–61, 2020, doi: 10.4236/oje.2020.102004.

[99] H. Sharma, D. Kumar, and K. Pant, “Agroforestry: Concept, importance and research trends,” in *Research Trends in Silviculture and Agroforestry*, vol. 1, researchGate, 2023, ch. 4, pp. 65–77. [Online]. Available: https://www.researchgate.net/publication/372658217%0AAgroforestry-

[100] K. K. Shah *et al.*, “Diversified Crop Rotation: An Approach for Sustainable Agriculture Production,” *Adv. Agric.*, vol. 2021, pp. 1–9, Jul. 2021, doi: 10.1155/2021/8924087.

[101] M. Rani, M. Lathwal, A. N. Singh, and N. Chongtham, “Bamboo Act as a Phytoremediation Candidate for Heavy Metal Contaminated Soil: A Synthesis,” in *Bamboo Science and Technology*, 2023, ch. 6, pp. 125–161. [Online]. Available: https://link.springer.com/book/10.1007/978-981-99-0015-2

[102] H. Chaudhry, N. Nisar, S. Mehmood, M. Iqbal, A. Nazir, and M. Yasir, “Indian Mustard Brassica juncea efficiency for the accumulation, tolerance and translocation of zinc from metal contaminated soil,” *Biocatal. Agric. Biotechnol.*, vol. 23, 2020, doi: 10.1016/j.bcab.2019.101489.

[103] X. Chen, X. Chen, S. Huang, and D. Fang, “Impacts of Moso bamboo (Phyllostachys

pubescens) invasion on species diversity and aboveground biomass of secondary coniferous and broad-leaved mixed forest," *Front. Plant Sci.*, vol. 13, pp. 1–12, Sep. 2022, doi: 10.3389/fpls.2022.1001785.

[104] Z. Huang, Q. Li, F. Bian, Z. Zhong, and X. Zhang, "Effects of Bamboo-Sourced Organic Fertilizer on the Soil Microbial Necromass Carbon and Its Contribution to Soil Organic Carbon in Moso Bamboo (Phyllostachys edulis) Forest," *Forests*, vol. 16, no. 3, Mar. 2025, doi: 10.3390/f16030553.

[105] Y. Wu *et al.*, "Moso bamboo (Phyllostachys edulis) expansion enhances soil pH and alters soil nutrients and microbial communities," *Sci. Total Environ.*, vol. 912, 2024, doi: 10.1016/j.scitotenv.2023.169346.

[106] N. Gayatri, A. R. Sailesh, and N. Srinivas, "Phytoremediation potential of Brassica juncea for removal of selected heavy metals in urban soil amended with cow dung," *J. Mater. Environ. Sci.*, vol. 10, no. 5, pp. 463–469, 2019, [Online]. Available: http://www.jmaterenvironsci.com

[107] M. I. S. Gonzaga, J. C. de Jesus Santos, L. F. Ganassali Junior, P. T. N. Fontes, J. da S. Araújo, and T. A. S. Gonzaga, "Copper uptake, physiological response, and phytoremediation potential of Brassica juncea under biochar application," *Int. J. Phytoremediation*, vol. 24, no. 5, pp. 474–482, 2022, doi: 10.1080/15226514.2021.1954875.

[108] B. O. Otunola, M. P. Aghoghovwia, M. Thwala, and O. O. Ololade, "Heavy Metal Phytoremediation Potential of Vetiver Grass and Indian Mustard Update on Enhancements and Research Opportunities," *Water. Air. Soil Pollut.*, vol. 233, no. 5, 2022, doi: 10.1007/s11270-022-05620-x.

[109] H. K. Gurajala, X. Cao, L. Tang, T. M. Ramesh, M. Lu, and X. Yang, "Comparative assessment of Indian mustard (Brassica juncea L.) genotypes for phytoremediation of Cd and Pb contaminated soils," *Environ. Pollut.*, vol. 254, p. 113085, 2019, doi: 10.1016/j.envpol.2019.113085.

[110] M. K. M. Kaonda and K. Chileshe, "Assessment of Sunflower (<i>Helianthus annuus</i> L.) for Phytoremediation of Heavy Metal Polluted Mine Tailings—A Case Study of Nampundwe Mine Tailings Dam, Zambia," *J. Environ. Prot. (Irvine,. Calif).*, vol. 14, no. 07, pp. 481–492, 2023, doi: 10.4236/jep.2023.147028.

[111] M. AYBAR, B. SAĞLAM, H. DAĞHAN, A. TÜFEKÇIOĞLU, N. KÖLELI, and F. N. YILMAZ, "Phytoextraction of Heavy Metal (Cu, Zn, Pb) from Mining Area by Sunflower (Helianthus annuus)," *Kastamonu Univ., J. For. Fac.*, vol. 23, no. 1, pp. 75–85, Mar. 2023, doi: 10.17475/kastorman.1269527.

[112] S. Petrović, J. Mrmošanin, B. Arsić, A. Pavlović, and S. Tošić, "Uptake of some heavy metal(oid)s by sunflower," *Chem. Naissensis*, vol. 5, no. 2, pp. 73–84, 2022, doi: 10.46793/ChemN5.2.73P.

[113] P. C. Lalruatfeli, A. A. Choudhary, and N. R. Mairan, "Growth and yield attributes and yield of mustard (Brassica juncea L .) as influenced by different nutrient sources," *Biol. Forum – An Int. J.*, vol. 10, no. 12, pp. 104–106, 2021.

[114] A. Baghdadi, R. A. Halim, A. Nasiri, I. Ahmad, and F. Aslani, "Influence of plant spacing and sowing time on yield of sunflower (Helianthus annuus L.)," *J. Food, Agric. Environ.*, vol. 12, no. 2, pp. 688–691, 2014, [Online]. Available: https://www.researchgate.net/publication/263279191%0AInfluence

[115] D. S. Akoto, S. T. Partey, M. Denich, M. Kwaku, C. Borgemeister, and C. B. Schmitt, "Towards bamboo agroforestry development in Ghana: evaluation of crop performance, soil properties and economic benefit," *Agrofor. Syst.*, vol. 94, no. 5, pp. 1759–1780, 2020,

doi: 10.1007/s10457-020-00493-7.

[116] W. Brooks and J. Dunlop, *NABCEP PV Installation Professional Resource Guide*. 2013. [Online]. Available: www.nabcep.org

[117] A. Kumar, Tripti, D. Raj, S. K. Maiti, M. Maleva, and G. Borisova, "Soil Pollution and Plant Efficiency Indices for Phytoremediation of Heavy Metal(loid)s: Two-Decade Study (2002–2021)," *Metals (Basel).*, vol. 12, no. 8, p. 1330, Aug. 2022, doi: 10.3390/met12081330.

[118] D. Adamczyk-Szabela and W. M. Wolf, "The Impact of Soil pH on Heavy Metals Uptake and Photosynthesis Efficiency in Melissa officinalis, Taraxacum officinalis, Ocimum basilicum," *Molecules*, vol. 27, no. 15, 2022, doi: 10.3390/molecules27154671.

[119] S. Bravo *et al.*, "Influence of the soil pH in the uptake and bioaccumulation of heavy metals (Fe, Zn, Cu, Pb and Mn) and other elements (Ca, K, Al, Sr and Ba) in vine leaves, Castilla-La Mancha (Spain)," *J. Geochemical Explor.*, vol. 174, pp. 79–83, 2017, doi: 10.1016/j.gexplo.2015.12.012.

[120] A. Parvin *et al.*, "Chemical Speciation and Potential Mobility of Heavy Metals in Organic Matter Amended Soil," *Appl. Environ. Soil Sci.*, pp. 1–13, Jul. 2022, doi: 10.1155/2022/2028860.

[121] T. B. da Silva, J. G. da Cunha, and F. C. R. Vilar, "ROOTS OF LIFE: THE ESSENTIAL ROLE OF NUTRIENTS IN PLANT GROWTH," in *Do Solo à Colheita: Princípios e Práticas da Produção Vegetal*, vol. 1, Editora Científica Digital, 2025, ch. 7, pp. 83–92. doi: 10.37885/241218577.

[122] P. B. Angon *et al.*, "Sources, effects and present perspectives of heavy metals contamination: Soil, plants and human food chain," *Heliyon*, vol. 10, no. 7, p. e28357, 2024, doi: 10.1016/j.heliyon.2024.e28357.

[123] M. Schück and M. Greger, "Salinity and temperature influence removal levels of heavy metals and chloride from water by wetland plants," *Environ. Sci. Pollut. Res.*, vol. 30, no. 20, pp. 58030–58040, 2023, doi: 10.1007/s11356-023-26490-8.

[124] J. C. Mendoza-Hernández *et al.*, "Phytoremediation of mine tailings by Brassica juncea inoculated with plant growth-promoting bacteria," *Microbiol. Res.*, vol. 228, no. March, p. 126308, 2019, doi: 10.1016/j.micres.2019.126308.

[125] S. K. Samal *et al.*, "Comparing the Efficiency of Sunflower, Marigold and Spinach Plants for Their Phytoextraction Ability of Zinc and Copper in Contaminated Soil," *Agric. Res.*, vol. 13, no. 3, pp. 542–552, Sep. 2024, doi: 10.1007/s40003-024-00713-x.

[126] R. A. Wuana and F. E. Okieimen, "Heavy Metals in Contaminated Soils: A Review of Sources, Chemistry, Risks and Best Available Strategies for Remediation," *ISRN Ecol.*, vol. 2011, pp. 1–20, Oct. 2011, doi: 10.5402/2011/402647.

[127] "Bulk Density Definition, Formula & Calculation - Lesson | Study.com." Accessed: Aug. 22, 2025. [Online]. Available: https://study.com/learn/lesson/bulk-density-equation-compaction.html

[128] P. Zhuang, Z. H. Ye, C. Y. Lan, Z. W. Xie, and W. S. Shu, "Chemically Assisted Phytoextraction of Heavy Metal Contaminated Soils using Three Plant Species," *Plant Soil*, vol. 276, no. 1–2, pp. 153–162, Oct. 2005, doi: 10.1007/s11104-005-3901-0.

[129] M. A. Ashraf, M. J. Maah, and I. Yusoff, "Assessment of phytoextraction efficiency of naturally grown plant species at the former tin mining catchment," *Fresenius Environ. Bull.*, vol. 21, no. 3, pp. 523–533, 2012, [Online]. Available: https://www.researchgate.net/publication/221711167_Assessment_of_phytoextraction_efficiency_of_naturally_grown_plant_species_at_the_former_tin_mining_catchment#full-text

[130] A. Yazdanbakhsh, S. N. Alavi, S. A. Valadabadi, F. Karimi, and Z. Karimi, "Heavy Metals

Uptake of Salty Soils by Ornamental Sunflower, Using Cow Manure and Biosolids: A Case Study in Alborz city, Iran," *Air, Soil Water Res.*, vol. 13, Jan. 2020, doi: 10.1177/1178622119898460.

[131] C. Firincă *et al.*, "Microbial Removal of Heavy Metals from Contaminated Environments Using Metal-Resistant Indigenous Strains," *J. Xenobiotics*, vol. 14, no. 1, pp. 51–78, Dec. 2023, doi: 10.3390/jox14010004.

[132] S. Lee *et al.*, "Agrivoltaic system designing for sustainability and smart farming: Agronomic aspects and design criteria with safety assessment," *Appl. Energy*, vol. 341, no. December 2022, p. 121130, 2023, doi: 10.1016/j.apenergy.2023.121130.

[133] "Solar Panel Angles for Chingola, Copperbelt, ZM — Solarific." Accessed: Aug. 22, 2025. [Online]. Available: https://solarific.co/zm/copperbelt/chingola

[134] M. Makenzi, J. Muguthu, and E. Murimi, "Novel Design and Sizing Approach for Optimal Installation of Solar Water Pumping Setups," *Appl. Sol. Energy*, vol. 57, no. 5, pp. 391–402, Oct. 2021, doi: 10.3103/S0003701X21050091.

[135] M. Mwanza and K. Ulgen, "GIS-Based Assessment of Solar Energy Harvesting Sites and Electricity Generation Potential in Zambia," in *African Handbook of Climate Change Adaptation*, Cham: Springer International Publishing, 2021, ch. 47, pp. 899–946. doi: 10.1007/978-3-030-45106-6_60.

[136] M. Khan *et al.*, "The Effect of Distance between Soakaway and Borehole on the Quality of Underground Water in Nowshera," *Heliyon*, pp. 1–33, 2024, [Online]. Available: https://papers.ssrn.com/sol3/papers.cfm?abstract_id=4946388

[137] A. A. Zahrawi and A. M. Aly, "A Review of Agrivoltaic Systems: Addressing Challenges and Enhancing Sustainability," *Sustain.*, vol. 16, no. 18, pp. 1–36, 2024, doi: 10.3390/su16188271.

[138] E. Ranieri *et al.*, "Copper Phytoextraction Using Phyllostachys pubescens," *Sustainability*, vol. 15, no. 6, Mar. 2023, doi: 10.3390/su15065238.

[139] E. Ranieri, P. Gikas, F. Ranieri, G. D'Onghia, and A. C. Ranieri, "Phytoextraction by Moso Bamboo under high level chromium stress in mediterranean conditions," *J. Environ. Manage.*, vol. 317, 2022, doi: 10.1016/j.jenvman.2022.115479.

[140] "Irrigation of Sunflower | Wikifarmer." Accessed: Aug. 22, 2025. [Online]. Available: https://wikifarmer.com/library/en/article/irrigation-of-sunflower

[141] "Irrigation requirements and methods for white mustard | Wikifarmer." Accessed: Aug. 22, 2025. [Online]. Available: https://wikifarmer.com/library/en/article/irrigation-requirements-and-methods-for-white-mustard

[142] A. Al-Badi, H. Yousef, T. Al Mahmoudi, M. Al-Shammaki, A. Al-Abri, and A. Al-Hinai, "Sizing and modelling of photovoltaic water pumping system," *Int. J. Sustain. Energy*, vol. 37, no. 5, pp. 415–427, May 2018, doi: 10.1080/14786451.2016.1276906.

[143] E. Catalanotti, R. T. J. Porter, M. M. Chalchooghi, and H. Mahgerefteh, "Biomass gasification in a downdraft gasifier with in-situ CO2 capture: A pyrolysis, oxidation and reduction staged model," *Chem. Eng. Trans.*, vol. 80, pp. 85–90, 2020, doi: 10.3303/CET2080015.

[144] L. Gerun *et al.*, "Numerical investigation of the partial oxidation in a two-stage downdraft gasifier," *Fuel*, vol. 87, no. 7, pp. 1383–1393, Jun. 2008, doi: 10.1016/j.fuel.2007.07.009.

[145] E. Catalanotti, R. T. J. Porter, and H. Mahgerefteh, "An Aspen Plus Kinetic Model for the Gasification of Biomass in a Downdraft Gasifier," *Chem. Eng. Trans.*, vol. 92, no. August, pp. 679–684, 2022, doi: 10.3303/CET2292114.

[146] A. Gomez-Barea, S. Nilsson, F. V. Barrero, and M. Campoy, "Devolatilization of wood

and wastes in fluidized bed," *Fuel Process. Technol.*, vol. 91, no. 11, pp. 1624–1633, 2010, doi: 10.1016/j.fuproc.2010.06.011.

[147] M. Sánchez, E. Amores, D. Abad, L. Rodríguez, and C. Clemente-Jul, "Aspen Plus model of an alkaline electrolysis system for hydrogen production," *Int. J. Hydrogen Energy*, vol. 45, no. 7, pp. 3916–3929, Feb. 2020, doi: 10.1016/j.ijhydene.2019.12.027.

[148] J. Rodríguez and E. Amores, "Cfd modeling and experimental validation of an alkaline water electrolysis cell for hydrogen production," *Processes*, vol. 8, no. 12, pp. 1–17, 2020, doi: 10.3390/pr8121634.

[149] J. Gu *et al.*, "Experimental studies on dynamic performance of 250-kW alkaline electrolytic system," *J. Power Sources*, vol. 592, no. October 2023, p. 233920, 2024, doi: 10.1016/j.jpowsour.2023.233920.

[150] Z. Ren, J. Wang, Z. Yu, C. Zhang, S. Gao, and P. Wang, "Experimental studies and modeling of a 250-kW alkaline water electrolyzer for hydrogen production," *J. Power Sources*, vol. 544, no. June, p. 231886, 2022, doi: 10.1016/j.jpowsour.2022.231886.

[151] M. Sánchez, E. Amores, L. Rodríguez, and C. Clemente-Jul, "Semi-empirical model and experimental validation for the performance evaluation of a 15 kW alkaline water electrolyzer," *Int. J. Hydrogen Energy*, vol. 43, no. 45, pp. 20332–20345, 2018, doi: 10.1016/j.ijhydene.2018.09.029.

[152] D. Jang, H. S. Cho, and S. Kang, "Numerical modeling and analysis of the effect of pressure on the performance of an alkaline water electrolysis system," *Appl. Energy*, vol. 287, no. October 2020, p. 116554, 2021, doi: 10.1016/j.apenergy.2021.116554.

[153] U. Kakati *et al.*, "Sustainable utilization of bamboo through air-steam gasification in downdraft gasifier: Experimental and simulation approach," *Energy*, vol. 252, p. 124055, 2022, doi: 10.1016/j.energy.2022.124055.

[154] Y. Guo and Q. Wang, "Fabrication and Characterization of Activated Carbon from Phyllostachys edulis Using Single-Step KOH Activation with Different Temperatures," *Processes*, vol. 10, no. 9, p. 1712, Aug. 2022, doi: 10.3390/pr10091712.

[155] K. Rabea, S. Michailos, K. J. Hughes, D. Ingham, and M. Pourkashanian, "Comprehensive process simulation of a biomass-based hydrogen production system through gasification within the BECCS concept in a commercial two-stage fixed bed gasifier," *Energy Convers. Manag.*, vol. 298, Dec. 2023, doi: 10.1016/j.enconman.2023.117812.

[156] J. F. González, S. Román, D. Bragado, and M. Calderón, "Investigation on the reactions influencing biomass air and air/steam gasification for hydrogen production," *Fuel Process. Technol.*, vol. 89, no. 8, pp. 764–772, 2008, doi: 10.1016/j.fuproc.2008.01.011.

[157] P. P. Dutta, V. Pandey, A. R. Das, S. Sen, and D. C. Baruah, "Down draft gasification modelling and experimentation of some indigenous biomass for thermal applications," *Energy Procedia*, vol. 54, no. 03712, pp. 21–34, 2014, doi: 10.1016/j.egypro.2014.07.246.

[158] R. Alipour Moghadam, S. Yusup, W. Azlina, S. Nehzati, and A. Tavasoli, "Investigation on syngas production via biomass conversion through the integration of pyrolysis and air-steam gasification processes," *Energy Convers. Manag.*, vol. 87, pp. 670–675, 2014, doi: 10.1016/j.enconman.2014.07.065.

[159] W. Ngamchompoo and K. Triratanasirichai, "Experimental investigation of high temperature air and steam biomass gasification in a fixed-bed downdraft gasifier," *Energy Sources, Part A Recover. Util. Environ. Eff.*, vol. 39, no. 8, pp. 733–740, 2017, doi: 10.1080/15567036.2013.783657.

[160] S. Luo *et al.*, "Optimizing Alkaline Water Electrolysis: A Dual-Model Approach for Enhanced Hydrogen Production Efficiency," *Energies*, vol. 17, no. 21, pp. 1–15, Nov. 2024, doi: 10.3390/en17215512.

[161] A. Mocek-Płóciniak, J. Mencel, W. Zakrzewski, and S. Roszkowski, “Phytoremediation as an Effective Remedy for Removing Trace Elements from Ecosystems,” *Plants*, vol. 12, no. 8, pp. 1–29, 2023, doi: 10.3390/plants12081653.

[162] C. W. A. Do Nascimento, C. M. Biondi, F. B. V. da Silva, and L. H. V. Lima, “Using plants to remediate or manage metal-polluted soils: An overview on the current state of phytotechnologies,” *Acta Sci. - Agron.*, vol. 43, 2021, doi: 10.4025/ACTASCIAGRON.V43I1.58283.

[163] C. Bassegio *et al.*, “Growth and accumulation of Pb by roots and shoots of Brassica juncea L.,” *Int. J. Phytoremediation*, vol. 22, no. 2, pp. 134–139, 2020, doi: 10.1080/15226514.2019.1647406.

[164] Z. U. Ahmad, *Phytoremediation of heavy metal contaminated soil using Indian mustard and marigold plant*, no. June. 2015. [Online]. Available: http://lib.buet.ac.bd:8080/xmlui/handle/123456789/3420

[165] F. Bian *et al.*, “Intercropping improves heavy metal phytoremediation efficiency through changing properties of rhizosphere soil in bamboo plantation,” *J. Hazard. Mater.*, vol. 416, 2021, doi: 10.1016/j.jhazmat.2021.125898.

[166] Y. Ding *et al.*, “Nitrate leaching losses mitigated with intercropping of deep-rooted and shallow-rooted plants,” *J. Soils Sediments*, vol. 21, no. 1, pp. 364–375, Jan. 2021, doi: 10.1007/s11368-020-02733-w.

[167] M. Sagastuy and T. Krause, “Agroforestry as a biodiversity conservation tool in the atlantic forest? Motivations and limitations for small-scale farmers to implement agroforestry systems in North-Eastern Brazil,” *Sustain.*, vol. 11, no. 24, pp. 1–24, 2019, doi: 10.3390/su11246932.

[168] J. C. Dagar, S. R. Gupta, and D. Teketay, *Agroforestry for Degraded Landscapes*, vol. 2. Singapore: Springer Singapore, 2020. doi: 10.1007/978-981-15-6807-7.

[169] F. Bian, Z. Zhong, X. Zhang, Q. Li, and Z. Huang, “Bamboo-based agroforestry changes phytoremediation efficiency by affecting soil properties in rhizosphere and non-rhizosphere in heavy metal-polluted soil (Cd/Zn/Cu),” *J. Soils Sediments*, vol. 23, no. 1, pp. 368–378, 2023, doi: 10.1007/s11368-022-03303-y.

[170] T. Plieninger, J. Muñoz-Rojas, L. E. Buck, and S. J. Scherr, “Agroforestry for sustainable landscape management,” *Sustain. Sci.*, vol. 15, no. 5, pp. 1255–1266, 2020, doi: 10.1007/s11625-020-00836-4.

[171] W. Su, P. Liu, C. Cai, H. Ma, B. Jiang, and Y. Xing, “Hydrogen production and heavy metal immobilization using hyperaccumulators in supercritical water gasification,” *J. Hazard. Mater.*, vol. 402, no. April 2020, p. 123541, 2021, doi: 10.1016/j.jhazmat.2020.123541.

[172] E. A. Dovletyarova *et al.*, “Copper Phytotoxicity Thresholds for Sunflower: A Field Experiment at a Site with Unique Monometallic Soil Contamination,” *Russ. J. Plant Physiol.*, vol. 71, no. 6, Dec. 2024, doi: 10.1134/S1021443724608735.

[173] Z. Razali, M. F. Abd Wahab, R. Md Kawi, M. Omar, and C. C. Tay, “Sunflower Helianthus annuus for Phytoremediation of Zinc in Hydroponic System,” *Sci. Res. J.*, vol. 17, no. 2, p. 99, Aug. 2020, doi: 10.24191/srj.v17i2.9733.

[174] P. O. Ogungbile *et al.*, “Phytoremediation with Sunflower (Helionthus annus) and Its Capacity for Cadmium Removal in Contaminated Soils,” *Trop. Aquat. Soil Pollut.*, vol. 4, no. 1, pp. 1–9, Feb. 2024, doi: 10.53623/tasp.v4i1.343.

[175] J. Chua *et al.*, “Phytoremediation potential and copper uptake kinetics of Philippine bamboo species in copper contaminated substrate,” *Heliyon*, vol. 5, no. 9, 2019, doi: 10.1016/j.heliyon.2019.e02440.

Annex

Table 2.4: Concentration ranges of metals in roots, aerial parts, and initial soil contamination from plant studies across various reviews

Plants	Metal	Soil (mg/kg)	Aerial(mg/kg)	Root (mg/kg)	Mean mass (g/plant)	references
Sunflower	Cu	3.334-19.8	1.2-79.38	1.8-450	17.87	[110], [111], [112], [125], [130], [172], [173], [174]
	Zn	3.58-715	7-214.4	0.04-217.62		
	Pb	17.4-230	1.74-74	2.35-104.81		
	Ni	27-68	1.4-11.5	4.87-34.1		
	As	6.693	0.49	0.48		
	Cd	1.12-28.17	0.2395-17.12	0.1024-10.7		
	Cr	12.8	4.85	4.74		
	Co	7.9	1.095	1.01		
Mustard	Cd	1.44-191.4	1.37-83.1	1.69-134	1.092	[107], [109], [124], [163]
	Pb	80-2211.66	2.9-1072	1.97-1815.7		
	Cu	100-492.69	96.5-165.4	200-299.3		
	As	7889.83	363.8	398		
	Cr	456.9	99.2	135.6		
Bamboo	Cu	12.76–195	18–212.2	60–810	319 g/plant	[101], [138], [139], [165], [175]
	Zn	28.74-2980	1625-2400	2400-6500		
	Cd	5-14.5	3.45-41.61	5-40.8		
	Cr	180-300	237.1-860	490.9-1310		
	Pb	132.5	482	4283		

Table 2.5: Mean Metal Concentration in Initial Soil, Roots, and Aerial Parts of Plants, and Percentage of Mean Concentration in Roots and Aerial Parts

Plants	Metals (C)	Mean C soil (mg/kg)	Mean C shoot (mg/kg)	Mean C root (mg/kg)	%shoot	%root
sunflower	Cu	915.752	23.136	151.73	2.526	16.569
	Zn	191.81	118.67	93.7	61.869	48.850
	Pb	102.47	42.96	59.93	41.924	58.485
	Ni	48.67	6.32	19.485	12.985	40.035
	As	6.693	0.49	0.48	7.321	7.172
	Cd	14.645	8.68	5.4	59.269	36.873
	Cr	12.8	4.85	4.74	37.891	37.031
	Co	7.9	1.095	1.01	13.861	12.785
mustard	Cu	296.345	130.95	240.65	44.188	81.206
	Pb	805.09	372.37	631.22	46.252	78.404
	Cd	96.42	42.235	67.845	43.803	70.364
	As	7889.83	363.8	398	4.611	5.044
	Cr	456.9	99.2	135.6	21.712	29.678
bamboo	Cu	77.43	109.42	372.11	141.315	480.576
	Zn	176.74	1897.23	4450	1073.458	2517.82
	Pb	132	482	4283	365.152	3244.7
	Cd	8.63	16.7	22.9	193.511	265.353
	Cr	240	548.55	900.45	228.56	375.188